The interaction of DPPC and hyaluronan

Dissertation

zur Erlangung des Doktorgrades an der Fakultät für Mathematik,
Informatik und Naturwissenschaften
Fachbereich Physik
der Universität Hamburg

vorgelegt von Thomas Zander
Hamburg, 25. Mai 2016

Gutachter:

Prof. Dr. Andreas Schreyer
Prof. Dr. Regine Willumeit-Römer

Datum Disputation: 25. Juli 2016

Eidesstattliche Erklärung

Hiermit erkläre ich an Eides statt, dass ich die vorliegende Dissertation selbst verfasst und keine anderen als die angegebenen Quellen und Hilfsmittel genutzt habe.

Hamburg, 25. Mai 2016

Thomas Zander

Liste der aus der Arbeit hervorgegangenen Publikationen

T. Zander, D.C.F. Wieland, A. Raj, M. Wang, B. Nowak, C. Krywka, A. Dedinaite, P.M. Claesson, V.M. Garamus, A. Schreyer, R. Willumeit-Romer
The influence of hyaluronan on the structure of a DPPC-bilayer under high pressures
Colloids and Surfaces B: Biointerfaces, 142: 230-238, 2016
DOI: 10.1016/j.colsurfb.2016.02.040

M. Wang, T. Zander, X. Liu, C. Liu, A. Raj, D.C.F. Wieland, V.M. Garamus, R. Willumeit-Römer, P.M. Claesson, A. Dedinaite
The effect of temperature on supported dipalmitoylphosphatidylcholine (DPPC) bilayers: Structure and lubrication performance
Journal of colloid and interface science, 445: 84-92, 2015
DOI: 10.1016/j.jcis.2014.12.042

Zusammenfassung

Die synovialen Gelenke zeigen herausragende Schmiereigenschaften. Die Reibungskoeffizienten sind selbst unter hoher Last und bei verschiedenen Scherraten die niedrigsten, die in der Natur beobachtet werden können. Gleichzeitig ist der Verschleiß durch Abnutzung minimal. Verantwortlich für die fast reibungslose Bewegung der Gelenke ist die Synovialflüssigkeit, die die Bewegung von zwei Knorpelgegenstücken schmiert. Die Synovialflüssigkeit ist eine komplexe Mischung aus Proteinen, Hyaluron (HA) und Phospholipiden. Allgemein wird angenommen, dass das Zusammenspiel dieser verschiedenen Komponenten für die niedrigen Reibungskoeffizienten in den synovialen Gelenken verantwortlich ist. Die genauen Mechanismen und Funktionen des Zusammenspiels sind aber noch nicht hinreichend untersucht.

Um die grundlegenden molekularen Interaktionen besser zu verstehen, wurde ein Modellsystem bestehend aus HA und dem Phospholipid DPPC untersucht.Es wird angenommen, dass beide Bestandteile einen großen Einfluss auf die Schmiereigenschaften der synovialen Gelenke haben. Zwei experimentelle Designs wurden für die Untersuchungen genutzt: (i) DPPC-Vesikel in einer HA-Lösung, um das Verhalten in Lösung zu untersuchen (ii) DPPC auf Silizium-Wafern mit adsorbiertem HA, um Informationen über die Strukturen zu bekommen, die sich auf den Knorpelgrenzflächen bilden können. Im Rahmen der Experimente wurden sowohl das Molekulargewicht von HA als auch die Lösungsbedingungen (der Effekt von $CaCl_2$) systematisch untersucht, um deren Einfluss auf die Interaktion von DPPC und HA zu ergründen. Des Weiteren wurde der Effekt von hohen Lasten, wie er auch während ganz alltäglicher Tätigkeiten vorkommt, untersucht. Zu diesem Zweck wurden hoher hydrostatischer Druck auf die Proben auf den Silizium-Wafern aufgebracht.

Um ein möglichst vollständiges Bild der sich formenden Strukturen und der Interaktionen zwischen den beiden Komponenten zu bekommen, wurden, DPPC-Vesikel in HA-Lösung mittels DSC, DLS und SAXS untersucht. Die Proben auf Silizium-Wafern wurden mit XRR und Fluoreszenzmikroskopie untersucht, um Informationen über die horizontale und die vertikale Struktur zu bekommen.

Die Untersuchungen zeigen, dass HA vorrangig in der Region der Kopfgruppen der Lipide adsorbiert. Da HA mit niedrigem Molekulargewicht einen höheren Einfluss auf die Doppelschichtstruktur von DPPC hat als HA mit einem hohem Molekulargewicht, kann davon ausgegangen werden, dass HA mit niedrigerem Gewicht stärker

mit DPPC interagiert. Messungen in Lösungen mit $CaCl_2$ machen deutlich, dass die Anwesenheit von Ca^{2+}-Ionen die Interaktion deutlich verstärkt. Dieses Ergebnis lässt darauf schließen, dass die Interaktion von elektrostatischen Kräften dominiert wird. Die Untersuchungen bei hohem hydrostatischen Druck zeigen, dass sowohl HA als auch $CaCl_2$ in vielen Fällen zu einer Stabilisierung der Proben, die auf Silizium-Wafern aufgebracht sind, führen.

Abstract

Synovial joints show outstanding lubrication properties. Even under high load or at different shear conditions the friction coefficients are the lowest found in nature. At the same time they show a very high wear resistance. The almost frictionless motion is provided by the synovial fluid mediating the motion of two cartilage counterparts. The synovial fluid is a complex entity of different proteins, hyaluronan (HA) and phospholipids. It is assumed that the complex interaction of these molecules is responsible for the fantastic lubrication properties. However, the interplay of the molecules and its functions are not fully understood yet.

To shed light on the molecular interplay responsible for low friction, a model system was investigated to study basic aspects of the molecular interactions. The model was composed of HA and the phospholipid DPPC. Both are supposed to have a major influence on the lubrication properties of the synovial joint. Two different experimental designs were chosen: (i) DPPC vesicles in a solution containing HA to study the behavior in bulk and (ii) Si supported DPPC bilayers with adsorbed HA to reveal the structures forming at the cartilage surface. During the course of this study the molecular weight of HA and the solution condition (effect of $CaCl_2$) were systematical varied to investigate their influence on the interaction of DPPC and HA. Further, the effect of high loads as they occur during every day activity was simulated. For this purpose high hydrostatic pressure (up to 2000 bar) was applied to the Si supported samples.

DPPC vesicles in HA solution were studied using DSC, DLS and SAXS to obtain a comprehensive picture of the formed structures and interactions. Si supported samples were studied using XRR and fluorescent microscopy to examine the vertical structure of the sample and the lateral arrangement, respectively.

The measurements show that HA adsorbs to the headgroup region of DPPC bilayers. Furthermore, they show that low molecular weight HA interacts stronger with DPPC bilayers than high molecular weight HA as the bilayer structure of DPPC was stronger affected by low molecular weight HA. Measurements in a solution containing $CaCl_2$ reveal a strongly enhanced interaction due to the presence of Ca^{2+} ions. Thus, it can be assumed that the interaction is mainly driven by electrostatic forces. Studies at high hydrostatic pressure reveal that HA and $CaCl_2$ in many cases lead to a stabilization of the Si supported DPPC bilayer at high hydrostatic pressure.

Contents

Chapter 1

Introduction

Evolution created biological materials and complex systems with extraordinary properties: like the tensile strength of spider silk, the adaption of bone to changed external stress by remodeling, the adhesion ability of gecko feet and many more. Understanding the principles of such systems opens possibilities for versatile applications from clinical or medical applications to new engineering solutions. One of these very interesting systems is the synovial joint (e.g. the knee), which allows an almost frictionless movement of our limbs. In synovial joints two cartilage counterparts slide upon each other, lubricated by the synovial fluid. This system provides exceptional good lubrication properties even under harsh conditions and has been in the focus of scientific interest for about 80 years [1]. However, the lubrication mechanisms are still not completely understood. A deeper insight into the lubrication mechanisms would be of huge interest for medical applications, like synthetic lubricants for artificial joints (e.g. after hip replacements) or the development of new therapies for patients suffering from arthritis. Further, new approaches for lubrication are also of high interest for technical applications. Lower friction would lead to tremendous savings in energy consumption. 28 % of the fuel energy in cars is for example needed to overcome friction losses [2]. Another important point is that lubricants which are effective in aqueous solutions would provide wide-ranging environmental benefits compared to oil-based lubrication systems. Finally the synovial joint is a very flexible lubrication system. Thus, it is favorable for technical applications, as it works for example very well under high and low loads and shear forces.

Friction coefficients found in the synovial joint are lowest in nature with values between 0.01 and 0.001 [3–5]. Most remarkable, these friction coefficients are maintained at very different conditions, like different shear rates ranging from stagnant

up to values of $\approx 10^6 - 10^7 s^{-1}$ [3] and under very high loads (loads up to five times the body weight have been reported [5]). A sketch of the structure of a synovial joint can be found in figure 1.1. The synovial joints consist of two articulated bone plates which are covered with cartilage. Between the two cartilage covered bone plates the synovial cavity can be found. It is surrounded by a fibrous capsule [6]. The main function of the bone plates and the cartilage cover is to absorb and

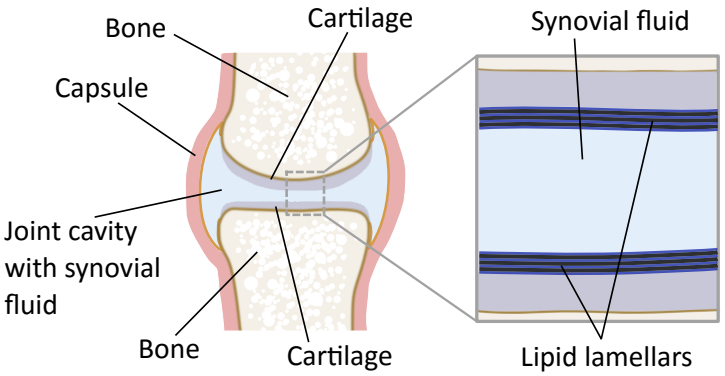

Figure 1.1: *Sketch of the structure of a synovial joint. The inset on the right shows a magnification of the gap between the two cartilage covered bone counterparts.*

transfer the load on the joints to the underlying bones. Cartilage is a soft tissue and consists mainly of water, collagen and proteoglycants. Therefore, it can easily deform under load conditions and thereby absorb these loads up to a certain degree [6, 7]. High loads, as they occur even during normal every day activity (e.g. during walking, climbing of stairs etc.), lead to a pressurization within the synovial capsule, as the two cartilage counterparts get squeezed together. On top of the cartilage of the hip joint pressures up to 180 *bar* were reported for everyday movements [8, 9]. The cartilage is covered with olligolamellar lipid structures, which consist mainly of three different lipid types: phosphatidylcholine (41 %), phosphatidylethanolamine (27 %) and sphingomyelin (32 %) [10]. The space between the two cartilage counterparts, i.e. the synovial cavity, is filled with the synovial fluid, which is a very efficient lubricant. The synovial fluid is a complex mixture of various macromolecules in an aqueous solution. It is assumed that proteins like lubricin, albumin, globulin and hyaluronan (HA) are responsible for the lubrication properties of the synovial fluid [3]. HA is very important for the viscoleastic properties of the synovial fluid [11, 12]. As it alleviates pain after being injected into the synovial joint, it is claimed to be one of the key factors in joint lubrication [7]. The concentrations of the most important proteins and HA were summarized in a review by Ghosh et al. 2014 [13]: albumin ($12 - 13\ mg/mL$),

globulin ($7 - 8\ mg/mL$), lubricin ($0.05 - 0.35\ mg/mL$) and HA ($1 - 4\ mg/mL$). Most likely, the interplay of lamellar lipid structures on top of the cartilage [14, 15] and the synovial fluid [13] is responsible for the actual low lubrication coefficients. Several studies have shown that lamellar structures, as well as single components of the synovial fluid are able to reduce friction on there own. Liu et al. 2012 [16] showed that the friction coefficient between two Si supported lipid bilayers was close to the ones found in the real synovial joints. Further, Murakami et al. 2014 [17] measured friction coefficients between two cartilage in an aqueous solution and reached values below 0.01 if HA was added to the solution. Also albumin and lubricin have the ability to act as lubricants at boundaries [18, 19]. However, non of these single components is able to reach the lubrication properties (friction coefficient under various conditions and wear resistance) of the whole system. Therefore it is assumed that complex interaction of the different components and synergistic effects are responsible for the lubrication properties. Murakami et al. 2013 [20] discovered that different mixtures of the four components HA, globulin, albumin and DPPC showed a wide variety of different friction coefficients. Moreover, the wear resistance depended strongly on the actual mixture. Best results were obtained by mixing all four components. Also the composition seems to be very important as for example the concentration of the different proteins were found to be different in the synovial fluid of healthy people and people suffering from osteoarthritis [13]. Further, the molecular weight of the HA seems to be an important factor as it is decreased in joints of patients suffering from arthritis compared to healthy patients [21, 22]. Also higher molecular weight HA seems to be more efficient in terms of wear reduction [23].

There is not only a single lubrication mechanism, which is responsible for the lubrication properties but a synergistic combination of different lubrication modes depending on load and cartilage separation [17]. However, it is assumed that boundary lubrication at the cartilage surface plays a major role especially under high load and low shear rates. In this situation the two cartilage counterparts are almost in contact with each other and only separated by a thin fluid film [10, 14, 24, 25]. Therefore, the abilities of lipid layers to reduce friction has raised attention and it could be shown that solid supported lipid bilayers prepared of DPPC enable very low friction coefficients [26, 27], which even come close to friction coefficients in the synovial joint. The question how DPPC bilayer structures interact with the synovial fluid and how this changes the friction forces was addressed by Liu et al. 2012 [16] and Wang et al. 2013 [28]. Here QCM (quartz crystal microbalance) and friction force measurements were used to study how the properties of DPPC get

altered in the presence of HA, which is claimed to be one of the key components in the synovial fluid and especially determines the viscosity of the synovial fluid [13]. QCM revealed that HA adsorbs to solid supported DPPC bilayers. These solid supported DPPC bilayers with adsorbed HA show very low friction coefficients, although the friction coefficients are slightly higher than those of sole DPPC [16, 28]. All of the above cited studies focus almost exclusively on the lubrication properties or they are clinical studies, investigating solely the composition of the synovial fluid. Only little focus was put on experiments studying the molecular structure of complexes formed by the interaction at ambient conditions, but most important no studies under simulated load conditions have been done. Deeper insight into the behavior of the synovial fluid and the structures at the cartilage surface is absolutely necessary to understand the molecular mechanisms. Therefore it is the aim of this work to look into these properties, to contribute to a understanding and to help closing the gap at this point.

For this study a simple model system containing of two of the important components responsible for lubrication in the synovial joint - DPPC and HA - was chosen. DPPC (1,2-dipalmitoyl-sn-glycero-3-phosphocholine) is a typical phospholipid. Phospholipids play an import role in biology since they are essential for the formation of membranes, e.g. in cell walls. They are amphipillic molecules with a hydrophilic and polar group (usually revered as 'head group') and a hydrophobic group ('tail group'), as illustrated in figure 1.2a. The head group is zwitterionic, with a positivity and a negatively charged part. Due to this molecular structure of

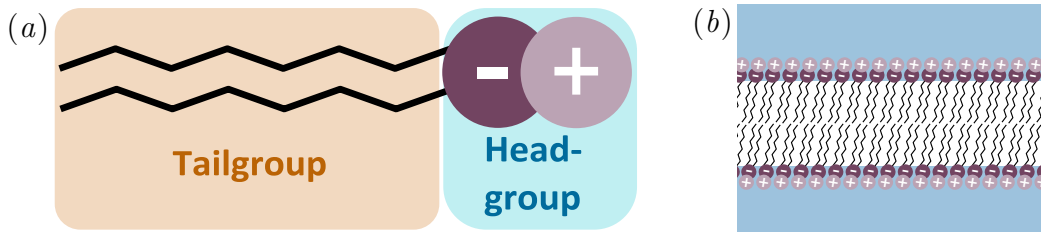

Figure 1.2: *(a) Sketch of a single phospholipid. (b) Sketch of phospholipid bilayer in water.*

the phospholipids they self assemble in water to minimize their free energy. The simplest structures are bilayers where the lipids organize into large 2D layers, which can be seen in figure 1.2b. The layers are organized in such a way that the tails (black lines in fig 1.2) point to each other. Thereby, they form a hydrophobic region. The lipid heads (blue circles) are in contact with water. Stacked on each other such bilayers form multilamellar structures. In water the layers are curved and form closed hollow spheres (lipid vesicles), whereas at solid liquid interfaces flat

layers are found. In the synovial joint lipid layers can be found in both conditions. In the synovial liquid lipid vesicles are present and flat lamellar lipid structures can be found at the cartilage - synovial fluid interface.
The phospholipid DPPC (which is used for this work) is a very abundant lipid in the synovial joint [10, 24] and it is also well characterized in literature [29–32]. It belongs to the group of saturated diacyl phosphatidlcholines, i.e. DPPC molecules have two symmetric saturated hydrocarbon chains as tails and a phosphocholine

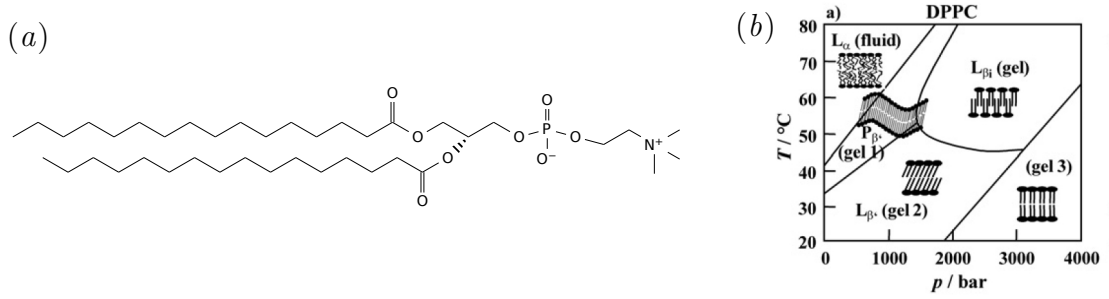

Figure 1.3: *(a) Drawing of a DPPC molecule. (b) Temperature - pressure phase diagram of DPPC in water. Reproduced from [32] with permission of The Royal Society of Chemistry.*

head group. In figure 1.3a the chemical structure is shown. The two hydrocarbon chains are build up of 16 carbon atoms each and connected by a glyceride group to the head group. The head group itself consists of two basic building blocks: a negatively charged PO_4-group and a positively charged choline group.
Layered DPPC structures show usually three different phases depending on pressure and temperature: fluid phase (L_α), rippled phase ($P_{\beta'}$) and gel phase ($L_{\beta'}$). At ambient pressure DPPC undergoes the phase transition from the gel to the ripple phase at around 34 °C and a transition from the ripple to the fluid phase at around 41 °C [30]. The phase transitions can be induced by pressure as well. [32] Increasing the pressures leads to a transition from the fluid phase to the ripple phase to gel phase (see figure 1.3b). In the gel phase the fatty acid chains of the lipids are in an all-trans configuration, whereas in the fluid phase the chains are molten, i.e. they have a random conformation [30]. Due to the random conformation of the lipid chains in the fluid phase the bilayer thickness is lower than in the gel phase. At the same time DPPC molecules in the fluid phase occupy a bigger area (parallel to the bilayer) than molecules in the gel phase [33]. The ripple phase is more complicated and its structure has just recently been better understood [34]. In general in the rippled phase the bilayer is partly molten. The melting occurs along straight lines with a fixed distance. The different thicknesses of the bilayer in the molten lines

and in between leads than to the formation of ripples with a certain periodicity. Former studies demonstrated that solid supported lipids do not form a ripple phase [35, 36], but there are still studies claiming the existence of a ripple phase for solid supported bilayer [37, 38]. The second component of the used model system is HA, which is a very common molecule in the human body. It can be found e.g. in the extracellular matrix, the eye vitreous humor, the intercellular space of the epidermis and in the synovial fluid, where it fulfills very different functions from the maintenance of the elastoviscosity of liquid connective tissue up to playing a receptor-mediated role in inflammation processes [39–41]. Especially its viscoelastic properties are important in the synovial joint. HA shows very unusual rheological properties with a very high viscosity that decreases with increasing shear force. It is extraordinary hydrophilic and can trap large amounts of water (up to 1000 times of its own weight) [40].

HA is a linear polysaccharide, consisting of repeating disaccharides units of β1-4 D-glucuronic acid and β1-3 N-acetyl-D-glucosamine [42]. The chemical structure of the repeat unit is shown in figure 1.4. HA has one carboxyl group per repeat

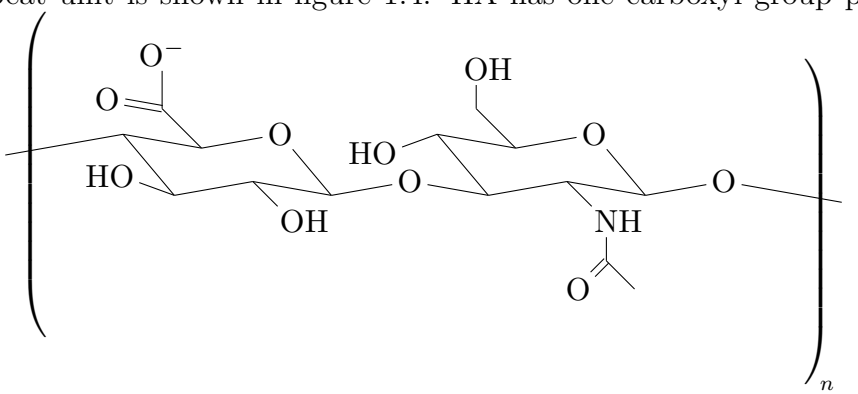

Figure 1.4: *Basic disaccharide repeat unit of the HA molecules (left: β1-4 D-glucuronic acid, right: β1-3 N-acetyl-D-glucosamine).*

unit which makes it a polyelectrolyte that is a negatively charged at physiological pH values. Each repeat unit has a length of approximatly 1 nm and a weight of $\approx 400\ Da$ [40]. Since HA molecules could consist of up to 10.000 disaccharides a molecule could extend up to 10 μm.

The structural conformation of HA is a matter of debate, which is mainly due to the fact that conformation strongly depends on the environment (ions, pH, etc.). Solid state fibre investigations of HA and HA in aqueous solution claimed left-handed helix structures with two, three and four disaccharide unites per turn [41]. Double helices have been found as well [43, 44] e.g. in the presence of Ca^{2+} [42]. A combined NMR (nuclear magnetic resonance) and computer simulation study stated that a left handed 4-fold helix (see fig. 1.5, PDB code 2BVK) is the av-

erage conformation of HA in aqueous solution [45]. Different groups also claim

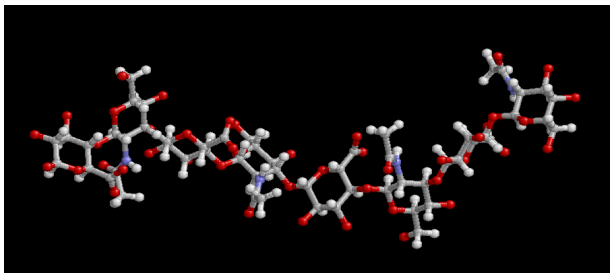

Figure 1.5: *Strucutre of HA in aqueaus solution. From PDB 2BVK [45].*

that the structure of HA is stabilized by hydrogen bonds [40, 46], whereas others claim that these hydrogen bonds are rather weak and show a rapid interchange with the solvent [45]. But it is widely agreed that HA (especially high molecular HA) forms expanded random coiled structures in aqueous solution [39–42, 46]. HA with low molecular weight (oligosaccharides) instead, tend to be in more rod like conformation [39]. For persistence length of HA values between 4 and 9 nm can be found in literature [41, 42, 47].
Despite being in general extremely hydrophillic it is believed that HA form hydrophobic patches [42, 46]. This combination would makes HA an amphiphilic molecule (like DPPC).
HA solutions are very viscous and some groups believed that the HA chains form stable networks [11, 44, 48]. Recent studies argue that HA does not form networks (at least not at physiological NaCl conditions), but that the viscous properties arise only from entanglements of the single chains [40–42]. This could also explain the non newtonian behavior of HA solutions.

Objective

As the full system would be to complex, simple model systems were studied to get a better understanding of the molecular mechanisms which are responsible for the good lubrication properties of the synovial joint. A special focus was put on the effect of high loads. As mentioned before, two of the important components responsible for lubrication in the synovial joint are DPPC and HA. They were chosen as model system. For these systems information about the friction characteristics was gathered by other groups [16, 28]. Further, HA of different molecular weight was used as a low molecular weight of HA has been related to joint diseases like arthritis [12, 21, 49].
The aim of the present work is to approach the following questions:

1. What structures are formed by interaction of DPPC bilayers and HA?
2. What structures might form at the cartilage interface?
3. How does the molecular weight of HA influence these structures?
4. How does the solution composition change the interaction?
5. How are these structure affected by high loads?

To answer these different questions two experimental arrangements were chosen and studied with different methods. For the first setup DPPC vesicles with HA were used and studied with small angel X-ray scattering (SAXS), dynamic light scattering (DLS) and differential scanning calorimetry (DSC). This setup and the used methods are well suited to obtain information about the structures formed by DPPC and HA (question 1) and how these structures are influenced by the molecular weight of HA and the solution composition (question 3 and 4). Using SAXS and DLS structural information on different length scales can be obtained. DSC provides information about the phase behavior. To study which structures might form at the cartilage interface (question 2) and how these structures are affected by high loads (question 5) a second setup was used: Si supported DPPC bilayers with HA. The influence of high loads was probed by applying high hydrostatic pressures to the sample. Structural changes of the molecular arrangement were studied in situ using X-ray reflectivity, which is a surface sensitive technique. Further, the influence of the molecular weight of HA and the solution conditions (question 3 and 4) were investigated. Information about the lateral organization of this sample system was gathered by fluorescent microscopy.

Chapter 2

Materials and methods

In this chapter first the sample preparation will be explained and afterwards the theory behind the different measurement techniques will be presented together with a description of the actual measurements and the data evaluation.

2.1 Sample preparation

In this section the preparation of the different samples will be described. In general two different kinds of experiments have been carried out: (i) investigation of the interaction of DPPC vesicles and HA and (ii) investigation of Si supported DPPC/HA at different hydrostatic pressures. The preparation of the samples for the first kind of experiments are described in the section 2.1.1 whereas the preparation of the samples for the latter kind of experiment is described in section 2.1.2. Table 2.1 shows an overview of the used materials. All chemicals were used as received, without further purification.

Table 2.1: *List of the used chemicals and the corresponding suppliers.*

Name	Short Name	Supplier	Order No
1,2-dipalmitoyl-sn-glycero-3-phosphocholine	DPPC	Avanti Polar Lipids Inc. (Alabaster, USA)	850355P
1-palmitoyl-2-12-[(7-nitro-2-1,3-benzoxadiazol-4-yl)amino]dodecanoyl-sn-glycero-3-phosphocholine	NBD-DPPC	Avanti Polar Lipids Inc.	810131C

Name	Short Name	Supplier	Order No
Hyaluronan ($M_w = 1500\ kDa$) with 5/6-carboxy-tetramethyl-rhodamine	-	Creative PEGWorks (Chapel Hill, USA)	HA-704
Hyaluronan ($M_w = 10\ kDa$) with 5/6-carboxy-tetramethyl-rhodamine	-	Creative PEGWorks	HA-705
Hyaluronan $M_w = 10\ kD$a	HA10	Creative PEGWorks	HA-101
Hyaluronan $M_w = 250\ kD$a	HA250	Creative PEGWorks	HA-103
Hyaluronan $M_w = 750\ kD$a	HA750	Creative PEGWorks	HA-104
Hyaluronan $M_w = 1500\ kDa$	HA1500	Creative PEGWorks	HA-106
Hyaluronan $M_w = 2500\ kDa$	HA2500	Creative PEGWorks	HA-107
Calcium chloride dihydrate	$CaCl_2$	Carl Roth (Karlsruhe, Germany)	5239
4-(2-Hydroxyethyl)-1-piperazineethanesulfonic acid	HEPES	Sigma-Aldrich (St. Louis, USA)	54457
Sodium chloride	NaCl	Sigma-Aldrich	31434
Trichloromethane	Chloroform	Sigma-Aldrich	C2432
28% Ammonium hydroxide solution	NH_4OH	Sigma-Aldrich	338818
'ultrapure' water of 'Typ 1' quality (ISO 3696)	Milli-Q	EMD Millipore (Billerica, USA)	
30% hydrogen peroxide	H_2O_2	EMD Millipore	1072980250

2.1.1 Vesicle solutions with hyaluronan

To prepare DPPC vesicles in solution with homogenous well defined size three steps had to be followed: 1. dissolving of the lipids in chloroform 2. formation of multilamellar vesicles with a random size distribution 3. creation of almost unilamellar vesicles with well defined size. For this study two different buffer solutions were used. One containing NaCl only ($c_{NaCl} = 150\ mM$) and another one containing NaCl ($c_{NaCl} = 150\ mM$) and $CaCl_2$ ($c_{CaCl_2} = 10\ mM$). The solutions were prepared by dissolving the needed amount of salt in Milli-Q water, followed by five minutes sonication.

In a first step the needed amount of DPPC was dissolved in chloroform in a small

glass vial. Afterwards the solvent was evaporated under a constant stream of nitrogen and as a result a lipid film formed on the walls of the glass vial. To remove any residual chloroform, which might be caught in the multilamellar structures, the vials were placed in a vacuum oven at 55 °C and 0.1 $mbar$ for several hours.
After removing the vials from the oven buffer solution was added and the solution was heated to 55 °C. The mixtures have then been vortexed for 1 min leaving a turbid solution of multilamellar vesicles with a random size distribution. To ensure a complete hydration of the lipids the solution was kept at 55 °C and a mixing rate of 350 rpm for about $2-3$ h using a thermomixer (BioShake Series, Analytik Jena, Jena, Germany) just interrupted 2-3 times by vortexing.
In the last step the multilamellar vesicles were extruded and thus almost unilamellar vesicles with defined size were obtained. The solution had been extruded 35 times through a membrane with 0.2 μm pore size (Nuclepore Track-Etched Polycarbonate Hydrophilic Membranes, GE Healthcare Life Science, Little Chalfont, UK) making use of the Avanti Mini-Extruder (Avanti Polar Lipids Inc., Alabaster, USA) in order to form large almost unilamellar vesicles [50]. Extrusion was done at 55 °C and the solution was kept at 55 °C until it was used.
For DPPC-vesicle/HA samples a HA solution was prepared by adding HA to the buffer and stirring the solution until the HA was completely dissolved. The mass concentration of HA in the solution was set to be equal to the mass concentration of DPPC. Finally HA solution was mixed with the vesicles solution in ratio of 1:1 at 55 °C and was kept at this temperature until usage.

2.1.2 Silicon supported samples

Solid supported samples composed of DPPC and DPPC/HA were used for XRR measurements. They were prepared on silicon wafers with a surface area of 7.5×7.5 mm^2 in a stepwise adsorption approach at a temperature of 55 °C. Before usage the wafers were cleaned following the RCA-1 cleaning protocol [51, 52]. They were first immersed into a hot (70 °C) solution containing 5 parts purified water, 1 part 27% NH_4OH and 1 part 30% H_2O_2, for 15 min. Afterwards the wafers were rinsed with large amounts of Milli-Q water. To prepare the samples buffer solution, DPPC solution (0.5 mg/mL) and HA solution (0.5 mg/mL), all prepared as described in section 2.1.1, were used.
The preparation procedure for sole DPPC samples is shown in the upper part of figure 2.1. During the preparation process it has been ensured that the wafers remained covered with liquid. The samples were prepared in a solutions containing

NaCl ($c_{NaCl} = 150\ mM$). Additional samples were prepared in a solution containing $CaCl_2$ ($c_{CaCl_2} = 10\ mM$) as well. To prepare the samples cleaned wafers were immersed into the vesicle solution (step 2 in fig. 2.1) and kept there for 10 *min* (step 3). During that time the vesicles in the solution adsorbed and subsequently burst at the Si-surface and thereby formed a bilayer. This so called vesicle fusion process has already been described in former studies [53, 54]. Afterwards wafers were rinsed with buffer solution and the DPPC covered wafers could be used for experiments (step 4).

To prepare DPPC/HA samples additional steps, which are shown in the bottom

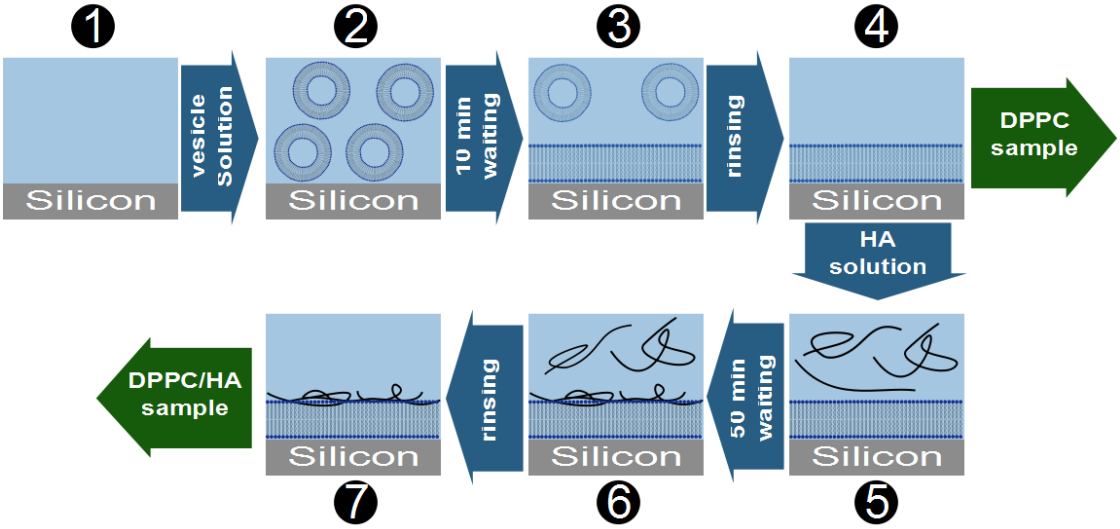

Figure 2.1: *Sketch of the preparation procedure for Si supported DPPC and DPPC/HA samples.*

part of figure 2.1, were appended after step 4. In step 5 the wafers were immersed into a buffer solution containing 0.5 mg/mL HA (either HA with a MW of 10kDa or 1500kDa) and kept there for 50 *min* to let the HA adsorb (step 6). Afterwards the wafers were rinsed with buffer solution (step 7) and the wafers could be used for experiments.

2.2 Methods

2.2.1 Small angle X-ray scattering

Small angle X-ray scattering (SAXS) is a powerful technique to study the structure of particles with a typical size of several *nm* in solution, like proteins, lamellar

structure (e.g. lipid bilayers), polymers or nanoparticles. Therefore SAXS was well suited to study the interaction of lipid bilayers and HA in solution. In the following the necessary theory, the experimental set up and the measurements itself as well as the evaluation of the obtained data will be described.

Theory

If an incoming X-ray wave (wave vector $\boldsymbol{k}_i$) hits a scattering center (electrons) it might get scattered, which results in a change of the direction of the wave vector of the outgoing wave ($\boldsymbol{k}_o$). This is illustrated in figure 2.2. The wavelength of

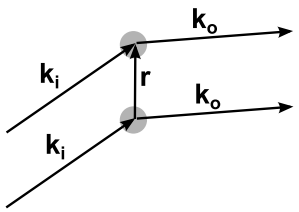

Figure 2.2: *Scheme of the scattering of X-rays on two single electrons (gray circles).* $\boldsymbol{k}_i$, $\boldsymbol{k}_o$ *are the wave vectors of the incoming and outgoing wave respectively.* $\boldsymbol{r}$ *is the position vector.*

the incoming and the outgoing wave shall be the same ($k = |\boldsymbol{k}_i| = |\boldsymbol{k}_o|$), i.e. the scattering shall be elastic. Additionally multiple scattering events are negligible, meaning that the outgoing wave won't get scattered themselves. This assumption is valid for diluted samples of low electron density. If the incoming wave hits not only one, but many scattering centers, each will be the source of an outgoing wave (see figure 2.2). The different outgoing waves have all the same wavelength and they only differ by their phases ϕ, which is due to their different positions in space. [55, p.114] ϕ can be expressed like follows:

$$\phi = (\boldsymbol{k} - \boldsymbol{k}_0) \cdot \boldsymbol{r} = \boldsymbol{q} \cdot \boldsymbol{r} \tag{2.1}$$

$\boldsymbol{r}$ is the position vector and $\boldsymbol{q}$ is the so called scattering vector. The amplitude of the summation of all the single outgoing waves $F(\boldsymbol{q})$ can be described as:

$$F(\boldsymbol{q}) = \sum_j b_j e^{-i\phi_j} = \sum_j b_j e^{-i\boldsymbol{q}\boldsymbol{r}_j} \tag{2.2}$$

b_j is here the scattering length of the single scattering center. Since the number of scattering centers is usually very high and their position can not be exactly determined the sum over the position of single scattering centers (eq. 2.2) get

replaced by an integral over the scattering length density ($\sum b_j = \rho(\boldsymbol{r})dV$) in a certain volume element dV: [56, p.19]

$$F(\boldsymbol{q}) = \int\int\int dV \cdot \rho(\boldsymbol{r}) e^{-i\boldsymbol{q}\boldsymbol{r}} \tag{2.3}$$

$F(\boldsymbol{q})$ can also be described as the Fourier transform of scattering length density of the investigated object. The intensity of the scattered wave is the conjugate complex of F and is usually expressed in such a way:

$$I(\boldsymbol{q}) = FF^* \tag{2.4}$$

This equation is for example valid for a dilute solution of particles, i.e. there is no long range order of the particles. As soon as the assumption of a dilute solution does not hold anymore and the particles start to affect each other a structure factor $S(q)$ has to be introduced that accounts for this.

$$I(\boldsymbol{q}) = |F(\boldsymbol{q})|^2 \cdot S(\boldsymbol{q}) \tag{2.5}$$

For special cases different approximations and simplifications can be made. In the case of two dimensional structures, where the structure is much larger in two directions than in in the third, which are isotropically distributed in the irradiated volume the intensity I can be expressed as $I(q) \propto q^{-2} I_{2D}$ [56, p.35]. I_{2D} could be described as a 'thickness-factor'. with the following amplitude F_{2D} [57]:

$$F_{2D}(q) = \int dz \cdot \rho(z) e^{iqz} \tag{2.6}$$

z denotes the direction of the small dimension of the structure. Such two dimensional structures could for example be lipid bilayers. In the case that the two dimensional objects arrange into new complex structure (e.g. lamellar structures) I_{2D} can not only be described by $F_{2D}(q)$ but a structure factor describing the inter lamellar organization has to be introduced. The intensity can then be written as: [58]

$$I(q) \propto \frac{1}{q^2} \cdot |F(q)|^2 S(q) \tag{2.7}$$

Measurements

The small angle scattering (SAS) measurements were been carried out at designated small angle X-ray scattering beamlines. For the measurements a typical

SAS-setup has been utilized, which is illustrated in figure 2.3. The incoming beam gets collimated to define the beam size and shape before it hits the sample. Behind the sample in large distance (from 1 m up to several 10 m) the detector is placed to detect the scattered beam waves. Parts of the X-rays hitting the sample are not

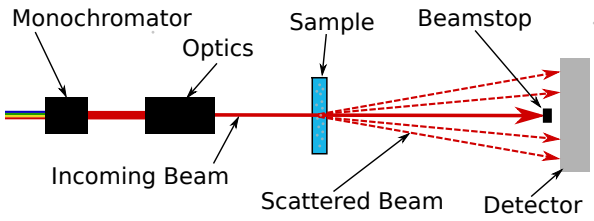

Figure 2.3: *Sketch of a SAS setup. The beamstop blocks the transmitted beam to avoid a damage of the detector.*

scattered by it and get just transmitted. This part is usually blocked by a beamstop to avoid a damage of the detector due to the large intensity of the transmitted beam.

Small angle X-ray scattering (SAXS) measurements were done at the BioSAXS beamline [59] (P12, Petra III, Hamburg, Germany) at energies of 10 keV. The samples were usually measured in glass capillaries with a diameter of 1 mm (0.01 mm wall thickness). To measure at different temperatures a temperature controlled sample stage from Linkam (Tadworth, UK) was used.

DPPC and DPPC/HA samples were studied with SAXS in two buffer solutions (150 mM NaCl and 150 mM NaCl with 10 mM $CaCl_2$). The concentration of DPPC and HA was 4 mg/mL, respectively and HA with a molecular weight of 250 kDa was used. Measurements were performed at three different temperatures: 25 °C, 37 °C and 55 °C.

Evaluation

To evaluate the measured data of the SAXS experiments, in a first step, the recorded 2D images were converted into 1D function of the scattered intensity as a functions of the length of the scattering vector transfer q. To obtain the 1D scattering curve all pixels of the images, which have the same radial distance to the beam center were binned. In the last step the background (measurement of the buffer without DPPC and HA) gets subtracted.

To fit the obtained SAXS data sets the equations 2.6 and 2.7 were used. A model electron density profile (a function describing the electron density $\rho(z)$ perpendicular to the lamellar surface) was build and the resulting theoretical scattering

intensity was compared to the data sets of the samples. The scattering curves of the DPPC-vesicles usually show two characteristic kinks or humps at $q \approx 1\ nm^{-1}$ and $q \approx 1.8\ nm^{-1}$, which are clear signs for the existence of 'multi' (≥ 2) lamellar structures. Therefor a combination of form factors was used to fit the scattering curves of the samples, to account for the simultaneous presence of 'multi' and single bilayer structures. Different electron density profiles were used for the form factors. For the form factor of single bilayer structures (F_S) the density profile ρ_S and for

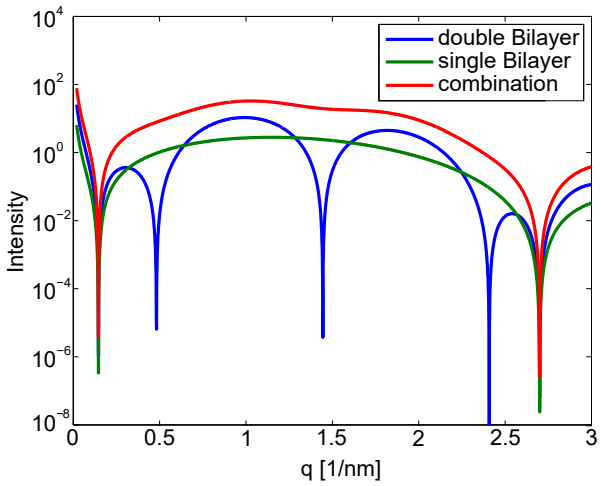

Figure 2.4: *Theoretical scattering curves of a single bilayer structure (green) a double bilayer structure (blue) and a combination of both (red).*

double bilayer structures (F_D) the density profile ρ_D were used. The effect of the combination of the two different form factors is illustrated in figure 2.4. Single bilayer structures give rise to a very broad oscillation whereas the oscillations of the double bilayer structure is much shorter. After combining the form factors one obtains a broad oscillation with two characteristic humps, which are also present in the measured data (see fig. 3.3a and b). A similar approach of combining multi bilayer and single bilayer structures was also applied by Pabst et al. 2003 [58]. To describe a single bilayer structure a combination of three Gaussian curves with two curves for the head and one curve for the tails was used:

$$\begin{aligned}\rho_S(z) = \rho_{Water} + \Delta\rho_H \exp\left(-\frac{(z-z_H)^2}{2\sigma_H^2}\right)\dots \\ +\Delta\rho_T \exp\left(-\frac{(z)^2}{2\sigma_T^2}\right) + \Delta\rho_H \exp\left(-\frac{(z+z_H)^2}{2\sigma_H^2}\right)\end{aligned} \tag{2.8}$$

The resulting electron density profile is symmetric with its center of symmetry set to $z = 0$. z_H gives the distance of the headgroup to the center (see figure

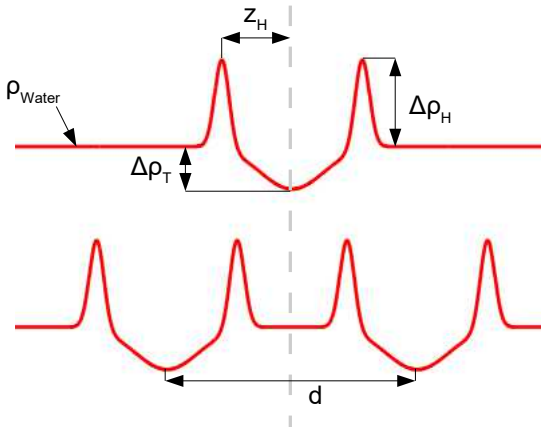

Figure 2.5: *Schematic drawing of the used electron density profile.*

2.5) and σ_H and σ_T describe the width of the Gaussian curves for the headgroup and tail group, respectively. $\Delta\rho_H$ and $\Delta\rho_T$ are defined as difference between the electron density of the headgroups and the tail group to the electron density of water ($\Delta\rho_{H/T} = \rho_{H/T} - \rho_{Water}$), as it is illustrated in figure 2.5. As a constant electron density does not give a scattering pattern (see eq. 2.3) the term ρ_{Water} in equation 2.8 can be skipped [56, p.21]. For a further reduction of the parameters space $\rho_S(z)$ is normalized by $\Delta\rho_H$, which leaves only one parameter (ρ_r) describing the ratio of the electron densities of the headgroups and tails:

$$\rho_r = \frac{|\rho_{Tails} - \rho_{Water}|}{|\rho_{Heads} - \rho_{Water}|} \tag{2.9}$$

Thus, $\rho_S(z)$ can now be written as [58]:

$$\rho_S(z) \quad = \exp\left(-\tfrac{(z-z_H)^2}{2\sigma_H^2}\right) - \rho_r \exp\left(-\tfrac{(z)^2}{2\sigma_T^2}\right) + \exp\left(-\tfrac{(z+z_H)^2}{2\sigma_H^2}\right) \tag{2.10}$$

For the electron density profile of the double bilayer structure ρ_D the structure of the single bilayer was doubled and an additional parameter d (see fig. 2.5) has been introduced, which determines the distance of the centers of the bilayers to each other:

$$\begin{aligned}\rho_D(z) = &\exp\left(-\frac{(z - z_H - \frac{d}{2})^2}{2\sigma_H^2}\right) - \rho_r \exp\left(-\frac{(z - \frac{d}{2})^2}{2\sigma_T^2}\right) + \exp\left(-\frac{(z + z_H - \frac{d}{2})^2}{2\sigma_H^2}\right) \dots \\ &+ \exp\left(-\frac{(z - z_H + \frac{d}{2})^2}{2\sigma_H^2}\right) - \rho_r \exp\left(-\frac{(z + \frac{d}{2})^2}{2\sigma_T^2}\right) + \exp\left(-\frac{(z + z_H + \frac{d}{2})^2}{2\sigma_H^2}\right)\end{aligned} \tag{2.11}$$

To calculate the scattering intensity of mixtures of single and double lamellar structures the following formula is used:

$$I(q) = A \cdot \frac{1}{q^2} \cdot \left(|F_D|^2 + n|F_S|^2)\right) + BG \tag{2.12}$$

A is a scaling factor and with BG a constant incoherent background is taken into account. The factor n scales the amount single bilayer and double bilayer structures. The model can easily be extended for mixtures with vesicles that having an arbitrary number (x) of maximum layers, by introducing new form factors:

$$I(q) = A \cdot \frac{1}{q^2} \cdot \left(n|F_S|^2 + \sum_{a=2}^{x} |F_a|^2\right) + BG \tag{2.13}$$

As the scattering from single, double, triple, etc. lamellar structures is calculated by single form factors for each structure, no structure factor is needed to account for multilamellar structures. Additionally it is assumed that the measured solution is very dilute, so that the particles are not affected by each other. Thus, in this case no structure factor is needed to calculate the scattering intensity. For mixtures with a maximum number of x layers the ratio of unilamellar to multilamellar vesicles (R_{UM}) can be calculated as follows:

$$R_{UM} = \frac{n}{x-1} \tag{2.14}$$

The approach to use a combination of two form factors for the double bilayer (or more for multi bilayers) instead of a structure factor has the big advantage that it is easily possible to add extra layers to account for the adsorption of for example HA. Since vesicles were used for the study additional substances can only adsorb to one side of the bilayer structure. A sketch of such a case is shown in figure 2.6. The adsorbed layer (HA) was also described by a Gaussian curve and added to the $\rho(z)$ profiles from equation 2.10 and 2.11:

$$\rho_{S-HA}(z) \quad = \rho_S(z) + \rho_{rHA} \cdot \exp\left(-\tfrac{(z-z_{HA})^2}{2\sigma_{HA}^2}\right) \tag{2.15}$$

$$\rho_{D-HA}(z) \quad = \rho_D(z) + \rho_{rHA} \cdot \exp\left(-\tfrac{(z-z_{HA}-\frac{d}{2})^2}{2\sigma_{HA}^2}\right) \tag{2.16}$$

with ρ_{rHA} being defined similar to ρ_r (eq. 2.9):

$$\rho_{rHA} = \frac{\rho_{HA} - \rho_{Water}}{\rho_{Heads} - \rho_{Water}} \tag{2.17}$$

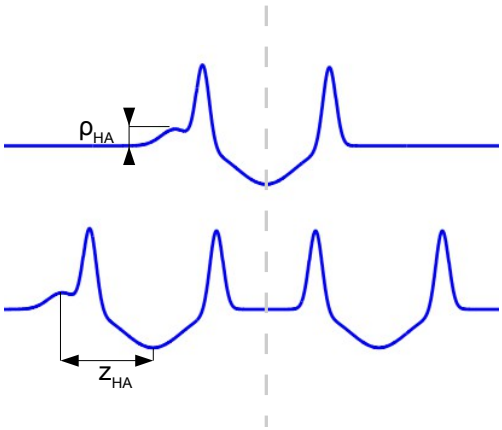

Figure 2.6: *Electron density profile of single and double bilayer vesicles with an adsorbed layer on one side.*

The fitting was done with MATLAB (MATLAB version 8.2, MathWorks, Natick, USA) making use of the non-linear curve-fitting routine 'lsqcurvefit' (part of the MATLAB Optimization Toolbox), which uses a least-square method [60, 61].

2.2.2 Dynamic light scattering

Dynamic Light Scattering (DLS) is a very commonly used to obtain information about the size of particles in solution. Therefore it has been used to examine the interaction of lipid vesicles and HA by studying how the size of the vesicles changes due to the presence of HA. In the following the theory of DLS will be summarized and afterwards the measurements and data evaluation will be described.

Theory

DLS is a well suited technique to determine the hydrodynamic properties of particles, like the diffusion coefficient which is, correlated to the size and shape of the particle. In DLS light from a laser hits the sample solution and gets partially scattered by the particles in the solution. The intensity of the scattered light (I)

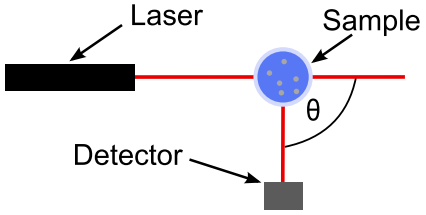

Figure 2.7: *DLS setup.*

gets measured under certain angle θ. A sketch of a typical set up is shown in figure 2.7. The light scattered from particles at different positions causes interference patterns. As the particles are in constant motion, caused by the Brownian motion of the molecules of the solution, these patterns and thus the intensity of the scattered light fluctuates with time. Fluctuations arising from small particles have a low amplitude and a high frequency, whereas large particles cause fluctuations with a higher amplitude and low frequency. The intensity fluctuations under a certain angle are measured and transformed into a time correlation function of the intensity of the scattered light [62–64]:

$$C(q,\tau) = \frac{\langle I(q,t)I(q,t+\tau)\rangle}{\langle I(q,t)\rangle^2} = 1 + \gamma[g^{(1)}(\tau)]^2 \tag{2.18}$$

γ is a setup constant and in an ideal case $\gamma = 1$ and $g^{(1)}(\tau)$ is the normalized first order autocorrelation function.

$$g^{(1)}(\tau) = \exp(-q^2 D\tau) \tag{2.19}$$

D is the so called translational diffusion coefficient. It is directly connected to the hydrodynamic radius R_h of the particles [65]:

$$D = \frac{k_B T}{6\pi\eta R_h} \tag{2.20}$$

where k_B, T and η denote Boltzmann's constant, the absolute temperature and the viscosity of the fluid, respectively. The hydrodynamic radius is not the real radius of the particle, it is the radius of a sphere that would migrate with the same speed in the fluid as the examined particle. This radius does not only depend on the size and shape of the particle itself, but also on the thickness of the so called hydration shell around the particle and further on the thickness of the electrical double layer formed around charged particles by ions the solution. Both, the hydration shell and the double layer increase the effective size of the particle and, thus, the hydrodynamic radius. The thickness of the double layer depends on the Debye length in the solution. Therefore a high ionic strength reduces the thickness of the double layer.

Measurements

Measurements were performed using the SpectroSize 300 (Xtal concepts GmbH, Hamburg, Germany). It is equipped with a laser with a wavelength of 660 nm. The scattering angle was set to 90° and measurements were performed at room

temperature. The sample solutions were all measured in the same quartz cuvette. Usually every sample has been measured 10 times for 20 s. Six different sample (DPPC, DPPC/HA10, DPPC/HA250, DPPC/HA250, DPPC/HA1500, DPPC/HA2500)have been measured at two different solution conditions (150 mM NaCl and 150 mM NaCl with 10 mM $CaCl_2$). The concentration of DPPC and HA was 1 mg/mL, respectively.

Evaluation

Data evaluation was done using the instrument software. An evaluation was done for every measurements separately. At first the evaluation routine transforms the measured intensity over time function into a so called auto-correlation function and does a fit of this function using equation 2.18 to obtain the diffusion coefficient and with that the hydrodynamic radius. The routine also accounts polydispersity and particles with different sizes. The resulting ten size distribution functions per sample were then averaged using MATLAB.
For the interpretation of the results it has to be taken into account that the intensity of scattered light from large particles is much bigger as from small particles. Depending on the size of the particles and the wavelength vesicles with a ten times higher radius can have a 10^6 times higher intensity.

2.2.3 Differential scanning calorimetry

Differential Scanning Calorimetry (DSC) is a well suited method to study the phase transitions materials. It has been used to investigate how the presence of HA changes the phase behavior of DPPC-bilayers. In the following first the theory behind this method will explained. Afterwards the experimental procedures and the evaluation of the data will be described.

Theory

In DSC the heat capacity difference of two solutions, sample solution and reference, gets measured, where the sample solution contains a substance of interest in a solvent and the reference contains only the solvent. The measured difference is then the heat capacity function C_P of the substance of interest. In contrast to liquids like water organic matter has in most cases a very low heat capacity, i.e. the amount of heat it can take up without changing its temperature. [66] This changes when the organic matter (e.g. proteins or other biomolecules) undergoes a

change in their structure. A molecule might have two structural states (A and B) within a certain temperature range, where B is the state with the higher enthalpy. The equation of the standard Gibbs free energy change ΔG of such a system is [66, 67]

$$\Delta G^0 = \Delta H^0 + T\Delta S^0 = -RT \ln K \tag{2.21}$$

where ΔH^0 is the change of enthalpy and ΔS is the change of entropy between system A and B, T is the absolute temperature and R the gas constant. K is an equilibrium constant defined as the ratio of the fractional occupancies of state A and B ($K = [B]/[A]$). [68] The system is in equilibrium if $[A] = [B]$ and therefore $\Delta G^0 = 0$. The temperature for this is the equilibrium temperature $T_m = \Delta H^0/\Delta S^0$.

All important parameters defining the thermodynamical behavior of the system

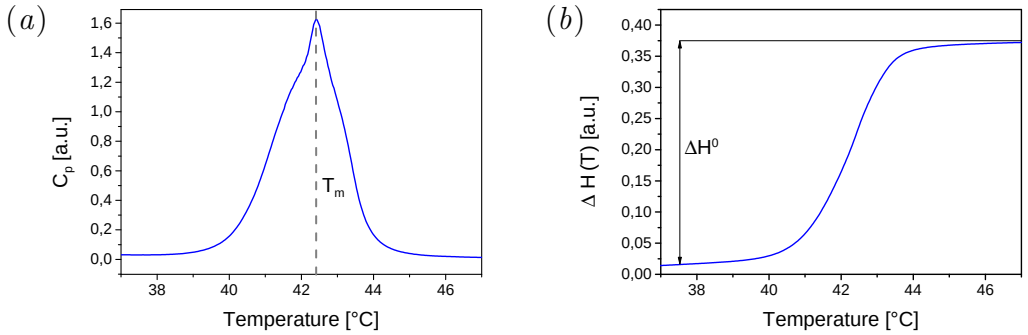

Figure 2.8: *(a) Heat capacity function of DPPC lipids. The position of the maximum is approximately T_m. (b) Integrated heat capacity function.*

can be derived from the heat capacity function (the change of enthalpy with time) measured by the DSC [67]

$$C_p(T) = \eta \frac{d\,\langle \Delta H(T) \rangle}{dT} = \eta \frac{K}{(1+K)^2} \frac{\Delta H^{0\,2}}{RT^2} \tag{2.22}$$

with $\langle \Delta H(T) \rangle = \Delta H^0 \cdot K/(1+K)$ and η being a factor to normalize on the concentration of the sample. A typical heat capacity curve for lipid vesicles is shown in figure 2.8 a. The integral under the curve of C_p gives the enthalpy change (ΔH^0) between the two states A and B (see fig. 2.8 b) and the position of the maximum is roughly the equilibrium temperature (see fig. 2.8 a). From these two parameters also the entropy change ΔS^0 can be determined.

Measurement

For the measurements a VP-DSC MicroCalorimeter (MicroCal, Northhampton, USA) was used. The instrument is equipped with two Tantaloy 61 ™ cells (one for the sample and one for the reference). Every sample was scanned 5 times from low to high and five times from high to low temperatures. The scanning rate was 20 K/h for all measurements with a waiting time of 15 min between each scan. The temperature range was usually $20 - 55°C$. Care has been take to avoid air bubbles and to have the same volume ($\approx 0.5\ mL$)in the sample as well as in the reference cell. Before measurement all solutions have been degased.
Samples composed of DPPC vesicles and DPPC vesicles with HA of different molecular weights (10 kDa, 250 kDa, 750 kDa, 1500 kDa and 2500 kDa) were probed in to different buffers solution (150 mM NaCL and 150 mM NaCL with 10 mM $CaCl_2$). The concentration of the samples was 1 mg/mL for each, HA and DPPC vesicles.

Evaluation

Data recorded with the DSC were processed with a specific instance of Origin developed to visualize data generated by the DSC (MicroCal's Origin). From the recorded raw data a water-water measurement was subtracted. For the water-water measurement both cells have been filled with ultra pure water. In theory the result of such a measurement should be a line at zero since both cells are filled with the same material and therefore there should be no measurable difference of the heat capacity of between the two curves. However due to instrumental effects the measured curve is not flat and not zero. To eliminate these instrumental effects the data of the water-water measurement was subtracted from the sample measurements. Even after subtracting the water-water measurement the DSC curve is usually not zero on either side of the peak, as the heat capacity of the sample is, even in the absence of a phase transition, temperature depended. Therefore a baseline correction was done for a proper evaluation.
In a second step a background subtraction of constant backgrounds was done. These backgrounds do not contain information about the reaction and have to be removed in order to determine the change of enthalpy (ΔH^0) between state A and B of the system, in this case between the gel and the fluid phase of the DPPC lipids.
From the final curves it was possible to calculate the enthalpy change between the gel state and the fluid state of the lipids and the transition temperature (or equi-

librium temperature). The heat capacity functions of DPPC show usually a small peak before the main transion, which is due to the pre-transition from gel to ripple phase (as explained in chapter 1). To obtain ΔH^0 an integration over the whole measured temperature interval (including the pre-transition) was done.

2.2.4 X-ray reflectivity

X-ray reflectivity measurements have been performed to study the structure of silicon supported DPPC and DPPC/HA samples as it is an excellent tool for this task. It allows to resolve the electron density of the samples with a very high resolution (in the Ångström range). The measurements have been performed at different hydrostatic pressures of up to 2 *kbar* to study how the pressure changes the structural arrangement of the samples. In the following the theory behind X-ray reflectivity will be explained, followed by a description of the measurements and a description of the data evaluation.

Theory

The basic principles of X-Ray Reflectivity (XRR), like Snell's law and the Fresnel equations, are already well known from classical optical physics. If a plane wave

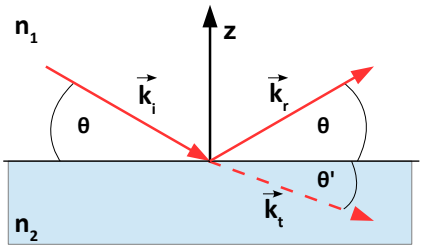

Figure 2.9: *Scattering geometry for reflectivity and transmission at the interface between the two media with the refraction coefficients n_1 and n_2. $\boldsymbol{k}_i$, $\boldsymbol{k}_r$ and $\boldsymbol{k}_t$ are the wavevectors of the incoming, reflected and transmitted waves respectively. θ denotes the scattering angle of the incoming and reflected wave and θ' denotes the scattering angle of the transmitted wave.*

Ψ_i in a medium with the refractive index n_1 hits the interface to a second medium with a refractive index n_2 a part of the wave gets reflected Ψ_r and the other part transmits into the second medium Ψ_t (see figure 2.9). A plane wave can be described by:

$$\Psi_x = A_x e^{i\boldsymbol{k}_x \cdot \boldsymbol{r}} \tag{2.23}$$

A denotes the amplitude of the wave and $\boldsymbol{k}$ is the wavevector. From the continuity equations of these three waves at the interface:

$$\text{Continuity } \Psi: \qquad A_t = A_i + A_r \tag{2.24}$$

$$\text{Continuity } \nabla\Psi: \qquad A_t\boldsymbol{k}_t = A_i\boldsymbol{k}_i + A_r\boldsymbol{k}_r \tag{2.25}$$

Snell's law can be derived [69]:

$$n_1 \cos(\theta) = n_2 \cos(\theta') \tag{2.26}$$

where θ is the angle between the wavevector of the incident and reflected wave and the surface between the two media and θ' is the angle between the wavevector of the transmitted wave and the surface. The refractive index n for X-rays is smaller than unity and can be described as follows:

$$n = 1 - \delta + i\beta \tag{2.27}$$

where β (the absorption coefficient) is much smaller than δ and δ is a function the electron density ρ, the absolute value of the wavevector $k = \frac{2\pi}{\lambda}$ and the scattering length of an electron r_0: [55, p. 71]

$$\delta = \frac{2\pi\rho r_0}{k^2} \tag{2.28}$$

For X-rays, at sufficiently small angles total external reflection can be observed. Setting n_1 to unity the critical angle of total reflection θ_c can be calculated from equation 2.26 (with $\theta' = 0$) and 2.27. Using the fact that $\delta << 1$ and assuming that β is negligible θ_c can be approximated by: [70, p. 6]

$$\theta_c = \sqrt{2\delta} \tag{2.29}$$

The reflectivity coefficient r for a perfectly flat surface is given by the well known Fresnel equation:

$$r = \frac{k_{i,z} - k_{t,z}}{k_{i,z} + k_{t,z}} \tag{2.30}$$

$k_{i,z}$ and $k_{t,z}$, are components of the respective wavevector perpendicular to the surface: $k_{i,z} = n_1 k \sin\theta$ and $k_{t,z} = n_2 k \sin\theta'$. The actual reflectivity R is the modulus square of the reflectivity coefficient: $R = |r|^2$. Using the equations 2.26 and 2.27 together with 2.30 and assuming the simple case of $n_1 = 1$ the reflectivity

can be written as: [71, p. 91f]

$$R(\theta) = \left| \frac{\theta - \sqrt{\theta^2 - \theta_c^2 - 2i\beta}}{\theta + \sqrt{\theta^2 - \theta_c^2 - 2i\beta}} \right|^2 \tag{2.31}$$

Since $R(\theta)$ changes with the wavelength of the used radiation, it makes sense to rewrite R as a function of the wave vector transfer q, with $q = \frac{4\pi \sin\theta}{\lambda}$:

$$R(q) = \left| \frac{q - \sqrt{q^2 - q_c^2 - \frac{32i\pi^2\beta}{\lambda^2}}}{q - \sqrt{q^2 - q_c^2 - \frac{32i\pi^2\beta}{\lambda^2}}} \right|^2 \tag{2.32}$$

In the following I will refer to R (eq. 2.32) as Fresnel reflectivity (R_F). For large q ($q \geq 3q_c$) R_F is proportional to q^{-4}. [71, p. 92]
Adding a slab with a different refractive index and a finite thickness to the surface between a medium 0 and a substrate leads to extra reflections at the additional surfaces (see fig. 2.10). The different path lengths of the waves lead to oscillation

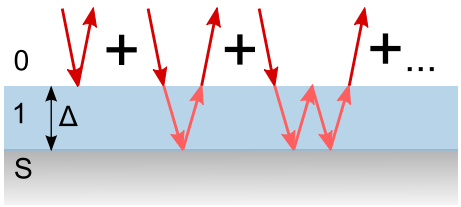

Figure 2.10: *Sketch reflections occurring at the interfaces of a single slab (1) of the thickness Δ on top of a substrate (S).*

of the intensity of the specular beam, the so called Kiessig fringes [55, p. 83]. It is assumed that the substrate is semi infinite and that therefore waves which are transmitted into the substrate will be completely absorbed. For this simple case the reflection coefficient (r_{slab}) can be written as: [55, p.83]

$$r_{slab} = \frac{r_{01} + r_{1S}e^{iq_1\Delta}}{1 - r_{01}r_{1S}e^{iq_1\Delta}} \tag{2.33}$$

r_{01} and r_{1S} denote the reflection coefficient at the interface between medium 0 and 1 and between medium 1 and the substrate (S), respectively. Δ is the thickness of the slab (medium 1). Extending this model by adding a second slabs of finite thickness and a certain thickness Δ_2 would lead the following expression for the

reflection coefficient r [71, p. 105]:

$$r = \frac{r_{01} + r_{12}e^{iq_1\Delta_1} + r_{2S}e^{i(q_1\Delta_1+q_2\Delta_2)} + r_{01}r_{12}r_{2S}e^{iq_2\Delta_2}}{1 + r_{01}r_{12}e^{iq_1\Delta_1} + r_{12}r_{2S}e^{iq_2\Delta_2} + r_{2S}r_{01}e^{i(q_1\Delta_1+q_2\Delta_2)}} \tag{2.34}$$

By extenting the equation in a recursive approach ([72]) to N layers it is possible to describe any possible layered system.
In the frame of the Kinematic theory, which neglects for example multiple scattering, a much simpler expression for the reflection coefficient can be described: [71, p. 107ff]

$$r(q) = \sqrt{R_F}\frac{1}{\rho_n}\int_{-\infty}^{\infty}\frac{d\rho(z)}{dz}e^{iqz}dz \tag{2.35}$$

z is as illustrated in figure 2.9 the position perpendicular to the surface and $\rho(z)$ is the average electron density perpendicular to the surface. ρ_n is a normalization constant equal to electron density at very large z: $\rho_n = \rho(z \to \infty)$.
The above described equations for an exact analytical calculation of the reflectivity coefficient (eq. 2.34) are only valid for sharp interfaces which do not occur in reality. Real systems always show a certain interfacial roughness σ. In general roughnesses lead to a decrease of the reflected intensity especially in the high q region. If the roughness is much smaller than the thickness of the respective layer ($\sigma_i << \Delta_i$) the roughness can easily be incorporated into the existing equations by replacing the reflectivity coefficient for sharp roughness ($r_{j,j+1}$) by coefficients for rough interfaces ($\tilde{r}_{j,j+1}$). [70, p. 16] To derive these new reflectivity coefficients it is assumed that the interface can be found at slightly different position around a certain value, which are weighted with an probability function. The specific expression of $\tilde{r}_{j,j+1}$ depends on the used probability function. For a gaussion distribution the following expression can be found: [70, p. 16]

$$\tilde{r}_{j,j+1} = r_{j,j+1}\exp\left(-2k_{z,j}k_{z,j+1}\sigma_j^2\right) \tag{2.36}$$

Another possibility to account for interfacial roughness is the so called 'effective density model'. This model is especially interesting if the assumption $\sigma_i << \Delta_i$ does not hold anymore. For this model a very different approach is followed to account for interfacial roughnesses. Instead of assuming that there are fixed interfaces between two media with certain values for the dispersion, δ_j, the real dispersion profile $\delta(z)$, with $\delta(z) = \int\int dxdy\ \delta(x, y, z)$, is used [70, pp. 26-31]. To calculate the reflectivity from such a continuous profile with the exact Parrat algorithm, the dispersion function gets sliced into very thin sections of equal thickness, with

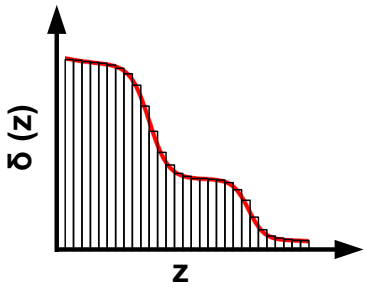

Figure 2.11: *Schetch of the principle of the 'effective density model'.*

a constant dispersion and sharp interfaces (see fig. 2.11). In the past the big disadvantage of this model was that it needs a lot computational power.

Measurements

A reflectivity setup which allows applying hydrostatic pressure up to 5 *kbar* [73] was used for the measurement. The setup consist of a cell housing the sample and a high pressure hand pump (SITEC-Sieber Engineering AG, Switzerland) which was connected with a tubing to the sample cell (see fig. 2.12 c). The tubing was filled with water to generate high pressures within the cell. Additionally a refrigerated-

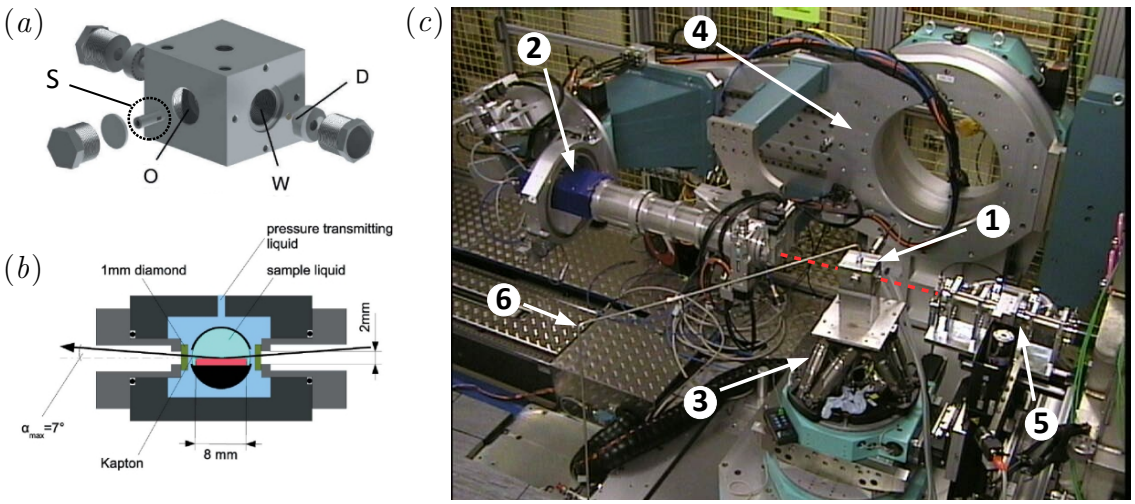

Figure 2.12: *(a) Sketch of the Sample Cell. S: inner cell compartment O: opening to place the inner cell compartment in the sample cell W: diamond windows D: cylinders to keep the windows in place (b) Drawing of the scattering geometry. Both adapted from Wirkert et al 2014 [73] with permission of the IUCr. (c) Photo of the sample cell installed at beamline I07, Diamond. The red broken line indicate the path of the beam. 1: Sample cell 2: Detector 3: Hexapod to align the cell 4: Diffractometer 5: Beam defining slits 6: High pressure connecting tubing.*

heating circulating bath was connected to the sample cell, allowing very accurate

control of the sample temperature ($\pm$ 0.2 K). The samples cell has been developed especially for X-ray reflectivity measurements at the solid-liquid interface by TU-Dortmund. A sketch of the cell can be seen in figure 2.12 a and b. The Si supported sample itself was placed in a closed inner cell which was filled with buffer solution. Thereby it was ensured that the sample did not came in direct contact with the pressure transmitting medium. The inner cell allowed a maximum size of the wafers of 7.5x7.5 mm^2. A membrane at the end of the inner cell prevent a contamination of the sample with and ensured the transfer of pressure from the medium into the inner cell. The cell design made it necessary to measure at high energies with high intensities to obtain a sufficient scattering signal. In the course of this experiments were performed at the following sources: (1) Bl9, Delta, Germany [74] at 27 keV with a beamsize of 100 $\times$ 1000 μm (2) I07, Diamond, UK [75]at 30 keV with a beam size of 150 $\times$ 300 μm (3) X04SA, SLS, Switzerland [76] at 27 $keV$with a beam size of 50 $\times$ 100 μm (4) ID15, ESRF, France, at 70 keV with a beam size of 1 $\times$ 50 μm. All beamelines were equipped with a diffractometer. A typical setup of the sample cell in the beamline is shown in figure 2.12 c.

A more schematic picture of the arrangement of the whole set up with the sample

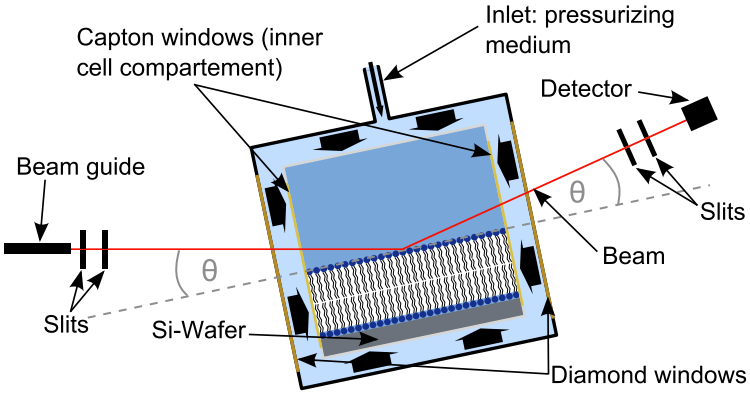

Figure 2.13: *Sketch of the geometry of the measurement set up with the sample and sample cell.*

and the sample cell within the beamline is shown in figure 2.13. The sample was prepared on top of the silicon wafer, which was mounted into the buffer filled inner sample compartment. First, the X-ray beam passed the buffer and then hit the sample and the Si-wafer. The intensity of the reflected beam was detected by a detector as a function of the scattering angle 2θ.

Three different samples composition on Si-wafers were measured: DPPC, DPPC with HA10 and DPPC with HA1500. They were measured in 150 mM NaCl at 25 °C, 39 °C and 55 °C and in 150 mM NaCl with 10 mM $CaCl_2$ at 39 °C and

55 °C. Pressures up to 2000 *bar* were applied to the samples.
Since the shape of the reflectivity curves (sample structures) does not differ significantly between 1 *bar* and 60 *bar* (see appendix A.4), we preferably measured at 60 *bar*. This experimental procedure was chosen to avoid artifacts like bubble formation, which may occur especially after decreasing the pressure to ambient values. At 60 *bar* the air is solved in the liquid phase. In the following the measurements performed at higher pressures will be presented.

Evaluation

To evaluate the data, theoretical scattering curves were fitted to the experimental data using the Paratt algorithm [72]. For the fits electron density profiles consisting of 6-7 layers have been used. A sketch of the layer system is shown in figure 2.14. The layers represent the different sections of the sample in the following order

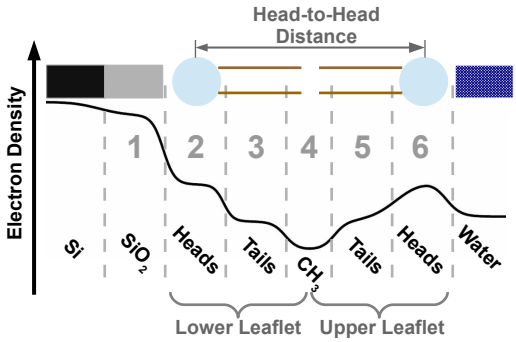

Figure 2.14: *Electron density of DPPC sample together with a sketch of a Si supported DPPC-bilayer to illustrate how the six layer model was built.*

starting from silicon on the very far left (see figure 2.14): silicon dioxide, headgroup, tailgroup, CH_3 terminal group, tailgroup, headgroup, HA (for DPPC/HA samples). The thickness of the silicon dioxide layer was determined from measurements using the bare Si-wafer before building the DPPC bilayer (with or without adsorbed HA) in order to minimize the number of fitting parameters and ambiguities in the fitting process. The electron densities of Si and water were calculated, where the mass density of water at different pressures and temperatures was taken from [77]. All other parameters were determined from the fitting. Since biological system, like lipid bilayers, show high interfacial roughnesses classical box models could not be used. These models only allow roughnesses, which are small compared to the thickness of the box. Instead the effective-density model has been applied to account for high roughnesses [70, pp. 26-31]. As a consequence of the effective

density model the layer thickness could not be determined with a reasonable accuracy, therefore the head to head distance is as a measure for the bilayer thickness. The reflectivity curves were always plotted as so called 'Fresnel normalized' curves, i.e. the curves were normalized by the Fresnel reflectivity R_F (see eq. 2.32). Fresnel normalized curve have the advantage that the oscillations of the curves become amplyfied, which is shown in figure 2.15.

2.2.5 Fluorescence microscopy

Fluorescence microscopy provides information about the distribution of molecules on the micrometer scale. This method has been used to investigate the distribution of DPPC and HA of Si supported DPPC and DPPC/HA samples. First the method will be explained in more detail and afterwards the measurements and data evaluation will be described

Theory

Using a fluorescence microscope it is possible to localize certain specific elements of a sample by labeling them with fluorescent dyes. These dyes absorb light of a well defined wavelength and get excited. Consequently they emit light with a wavelength that is higher than the wavelength for the excitation. By implying different sets of two bandpass filters into a microscope it is possible to visualize only the specific dyes. The first bandpass (Filter 1 in figure 2.16) determines the excitation energy by only allowing light with the wanted wavelength to pass and reach the sample. The second bandpass (Filter 2 in figure 2.16) determines the wavelength of the light that reaches the ocular lens of the microscope and the detector.

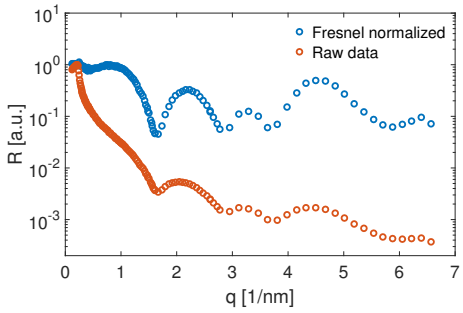

Figure 2.15: *Comparison of a Fresnel normalized curve and a non normalized curve.*

Measurements

The Nikon Eclipse Ni-E (Nikon Corporation, Tokyo, Japan) fluorescence microscope (resolution: 0.23 $\mu m/pixel$), was used to take images of Si supported DPPC and DPPC/HA samples in 155 mM NaCl and 155 mM NaCl / 10 mM $CaCl_2$ solution. DPPC was labeled with a fluorescent dye called [(7-nitro-2-1,3-benzoxadiazol-4-yl)amino]dodecanoyl (NBD), which was incorporated to the fatty acids of DPPC. For the measurements labeled DPPC was mixed with conventional DPPC (1 $w\%$ of labeled DPPC), to keep the phase behavior close to that of pure DPPC [78]. The excitation wavelength of NBD is 460 nm and the wavelength of the emitted light is 534 nm. HA was labeled with 5/6-carboxy-tetramethyl-rhodamine (Rhodamine, degree of substitution: 5mol % dye labeling). It was used as received and not mixed with conventional HA. The excitation wavelength of NBD is 552 nm and the wavelength of the emitted light is 575 nm. Two filter blocks from Semrock Inc (Rochester, USA) were used to visualize the fluorescent markers: i) for NBD-DPPC a filter block which emits blue and detect green light (FITC-3540C) was used and ii) for rhodamine labeled HA a filter block emitting green and detecting red light (TXRED-4040C) was used. The measurements were performed at room temperature with an immersion (or dipping) objective to be able to measure in water.

The images were recorded at room temperature and the samples were measured in petri dishes filled with ether a NaCl or a NaCl/ $CaCl_2$ solution. To attach the wafers to the bottom of the petri dish, the bottom was covered with agarose before use. Unfortunately the agarose layer was not completely homogenous, which caused a tilt of the wafer. Therefore not the complete field of view was in the focal plane.

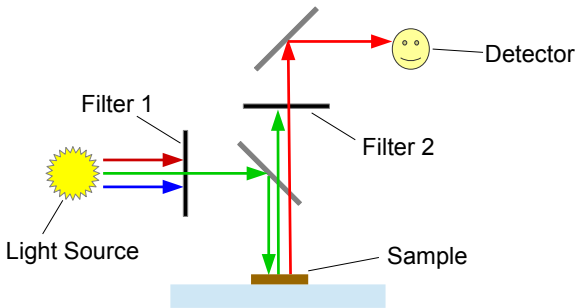

Figure 2.16: *Sketch of the filter arrangement in a fluorescence microscope.*

Evaluation

After recording the microscopy images were further processed using the program ImageJ [79]. The images show spots with strongly increased intensity, showing an accumulation of material. To evaluate the size and number of these structures, the 'Particle Analysis' plug-in of ImageJ was used. Before the evaluation the structures were defined by setting a threshold value to the intensity. All parts with an intensity above this value belong areas of accumulated material. After these spot were defined the 'Particle Analysis' plug-in determined size and number of the spots. The estimated error of the size of the structures is around 10 %, as the definition threshold yield a certain inaccuracy.

Chapter 3

Results and discussion

In the framework of this thesis the interaction of HA and DPPC phospholipids was examined. In the synovial joint DPPC multilayers can be found in the synovial fluid (unbound) and on top of the cartilage (supported). To account for both cases two different experimental designs were chosen: (i) mixtures of DPPC vesicles with HA and (ii) DPPC bilayers, prepared on Si wafers with adsorbed HA. Further simplification of the system was made by only investigating bilayers, which are the basic building blocks of multilayer structure. DPPC vesicles with HA were analyzed by different comprehensive methods (DSC, DLS, SAXS). The interaction of Si supported DPPC bilayers and HA was studied using XRR and fluorescent microscopy. Further, the scenario of a joint under load was addressed, by evaluating the influence of pressure on Si-supported DPPC/HA composites.
In the course of the experiments the solution conditions and the molecular weight of the used HA were systematically varied. Molecular weights of HA from $M_W = 10\ kDa$ up to $M_W = 1500\ kDa$ were used. Different studies claimed that the molecular weight of the HA in joints of patients suffering form arthritis was significantly reduced compared to healthy patients [21, 22]. Therefore it is very interesting to study if and how the molecular weight of HA has an influence on the interaction of DPPC and HA. For the experiments with different molecular weights, HA solutions were always prepared with the same mass concentration of HA. This ensured that for all experiments the same number of disaccharide units and with that the same number of charged groups were present in the solution. All samples were studied under two different solution conditions. The first solution contained only sodium chloride at a physiological concentration ($c_{NaCl} = 150\ mM$), as found in synovial joints. For the second solution condition calcium chloride was added in a low concentration ($c_{CaCl_2} = 10\ mM$). With the addition of $CaCl_2$ the influence

of divalent ion Ca^{2+} should examined. Calcium can be found in low concentration ($1.2 - 2.4\ mM/L$) in the synovial fluid [80, 81] and it is well known that $CaCl_2$ is able to alter the structure of DPPC bilayers [53, 82–87] and the charge density of HA [88]. The $CaCl_2$ concentration was chosen to be higher to obtain a stronger and clearer effect.
In the following first the results obtained from studies of DPPC vesicles and HA and afterwards the results from Si-supported DPPC bilayers with HA will be presented.

3.1 Interaction of DPPC vesicles and hyaluronan

This chapter will cover the result from studies of DPPC vesicles and HA solution. This experimental design was chosen to mimic the condition in the synovial fluid, were DPPC is the most abundant phospholipid [89] and interacts with HA under bulk conditions.

DPPC vesicles were studied extensively over the last decades. Therefore they are well understood, which makes them very well suited to study how HA effects structures formed by phospholipids. To obtain a complete picture of the interaction three comprehensive methods have been chosen, covering a broad range of accessible length scales from the sub-nanometer (SAXS) to sub-micrometer (DLS) range and information about the phase behavior of the sample system (DSC). Using this very simple model system it might be possible to derive information about the basic interaction between the two components DPPC and HA. HA with five different molecular weights was probed to study the influence of the chain length of HA on the structures forming. The results from the two different solutions conditions can be found in two separate sections: (i) sodium chlorid ($c_{NaCl} = 155\ mM$) in section 3.1.1 (ii) sodium chloride ($c_{NaCl} = 155\ mM$) with calcium chloride ($c_{CaCl_2} = 10\ mM$) in section 3.1.2.

In table 3.1 a summary of all probed samples can be found, with the respective examination method. The preparation of the samples was done as explained in section 2.1.1. Vesicles were prepared via the extrusion method and mixed with HA. For DLS and DSC concentration of 1 mg/mL was chosen for DPPC and HA. For SAXS a higher concentration of 4 mg/mL each was necessary for a sufficient scattering signal.

Table 3.1: *Collection of all samples compositions and the respective methods with which they were studied.*

	DSC		DLS		SAXS	
	NaCl	NaCl/ $CaCl_2$	NaCl	NaCl/ $CaCl_2$	NaCl	NaCl/ $CaCl_2$
DPPC	x	x	x	x	x	x
DPPC + HA10	x	x	x	x		
DPPC + HA250	x	x	x	x	x	x
DPPC + HA800	x	x	x	x		
DPPC + HA1500	x	x	x	x		
DPPC + HA2500	x	x	x	x		

3.1.1 Interaction in sodium chloride solution

3.1.1.1 Differential scanning calorimetry

Using DSC it was possible to study how the phase behavior of DPPC was changed in the presence of HA with different molecular weights. Five scan with a scanning speed of 20 K/h were performed for every sample. Shape and position of the two phase transition (pretransition and main transition) peaks were evaluated. Pretransition denotes the transition from the $L_{\beta'}$ (gel) to the $P_{\beta'}$ (ripple) phase and main transition denotes the transition from $P_{\beta'}$ (ripple) to L_α (fluid). HA did not show a phase transition visible in the DSC curve in the studied temperature range, therefore DSC measurements were only sensible to the signal from DPPC. As a control sample sole DPPC in 150 mM $CaCl_2$ was measured. The DSC curves of all samples along with a magnification of the pretransition (transition from $L_{\beta'}$ to $P_{\beta'}$) region can be found in Figure 3.1a. Two transitions can easily be identified for all samples: the pretransition around 32 °C − 34 °C and the main transition (transition from $P_{\beta'}$ to L_α) slightly below 42 °C. In general, no strong changes of the DSC profiles, like vanishing of transition peaks or strong shifts of the peak positions, can be observed. However, a small change is observed for the shape of the main transition. While the profile for pure DPPC is symmetric, the profiles becomes asymmetric for mixtures of DPPC and HA. Additionally the profiles show a shoulder on the left side. Both observations hint at changed transition dynamics. The main transition temperature is calculated by averaging the maxima of the five main transition peaks and the standard deviation is used as error.The values for the main transition temperatures are collected in figure 3.1b. For sole DPPC the temperature of the main transition is 41.83 ± 0.02 °C and does not change significantly in the presence of HA. T The pretransition of the samples (see inset in fig. 3.1a) is not very distinct and it seemed as if there were two broad peaks, with the peak at higher temperatures being the dominant one. Sole DPPC showed the maxima at 31.7 ± 0.1 °C and 34.1 ± 0.5 °C. For DPPC with HA the position of the first peak changed to values between between 31.1 ± 0.1 °C and 31.5 ± 0.1 °C and the second maximum could be found between 33.8 ± 0.5 °C and 34.1 ± 0.5 °C. From the area under the complete DSC curve the enthalpy of the phase transition of DPPC ($L_{\beta'}$ to L_α) was calculated. The results (average of the five scans) are collected in figure 3.1c. For the errors the standard deviation was used. The enthalpy for sole DPPC was 1.17 ± 0.01 mJ and HA lead to a decrease of the enthalpy. The decrease was stronger for HA with a higher molecular weight.

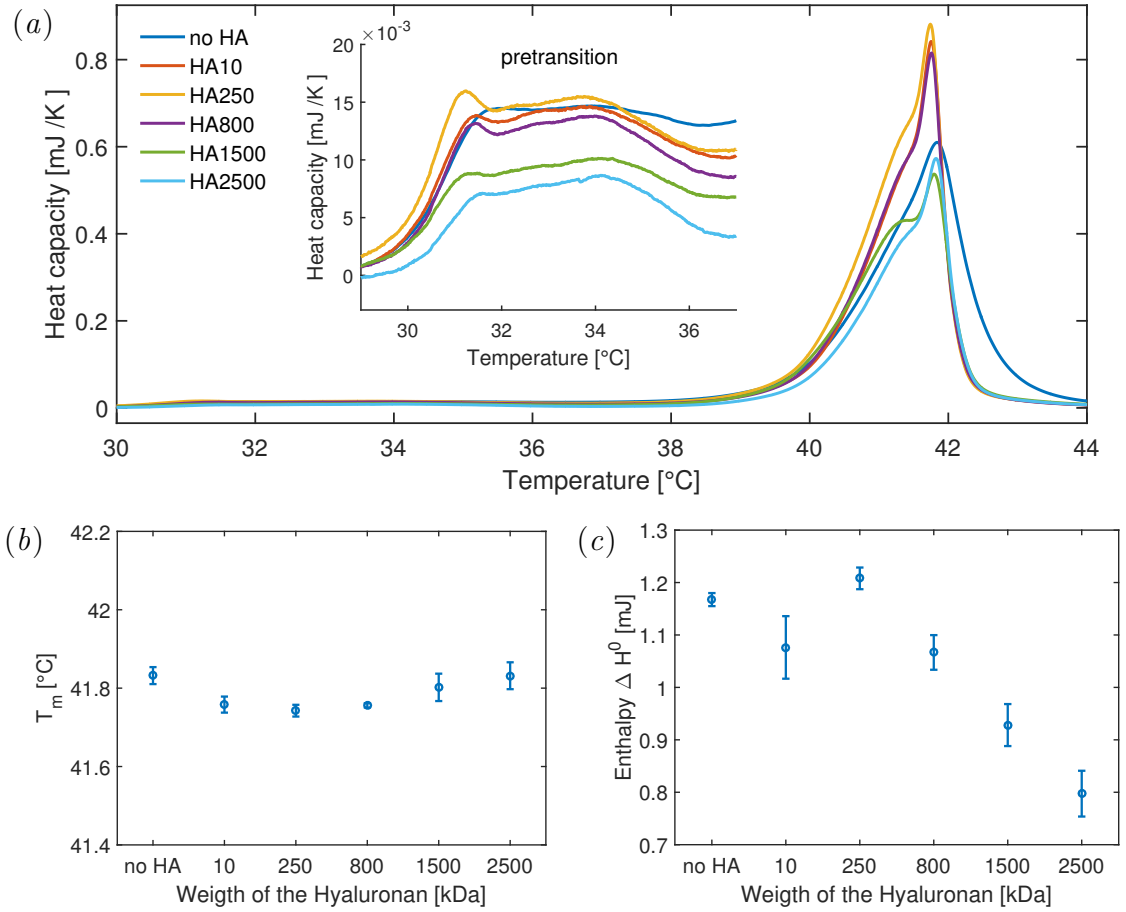

Figure 3.1: *Results of the DSC measurements of DPPC and DPPC with HA of different molecular weights. (a) DSC curves of all samples. The inset shows a magnification of pretransition area. (b) Transition temperature (c) Enthalpy of the transition process*

3.1.1.2 Dynamic light scattering

DLS measurements have been performed to investigate the influence of HA on the hydrodynamic radius of DPPC vesicles. Measurements were performed at 25 °C. The intensity over radius curves of all samples are presented in figure 3.2a. They show two peaks: one at roughly 100 *nm* and the second one in the micrometer region (see fig. 3.2a). It shows that two size populations of particles had developed in the solution. The population with a radius of around 100 *nm* represented probably single vesicles, since the vesicles were formed by extrusion through membranes with a pore size of 200 *nm*, which results in a radius of 100 *nm* for the formed vesicles. The second population (micrometer region) is probably caused by aggregation of vesicles. It has to be noted that, although the area under peaks of the smaller particles is lower than the area under the peak of the bigger particles, the number of particles belonging to the population with the smaller radius is much higher

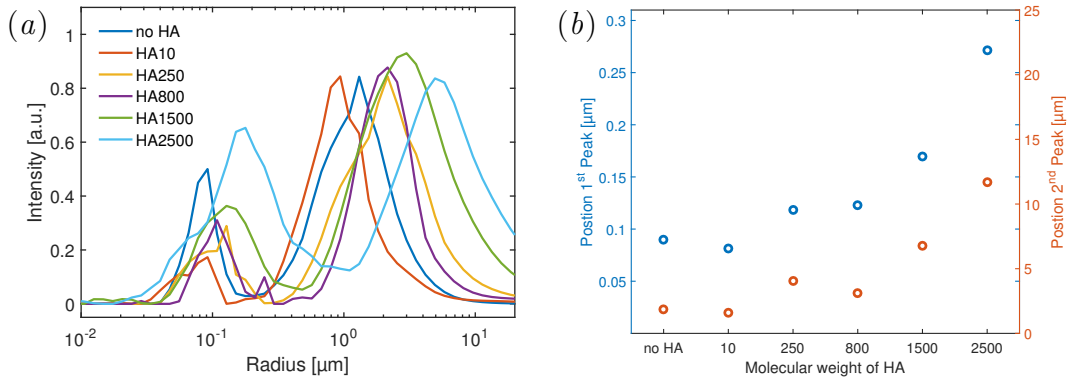

Figure 3.2: *Results from DLS measurements on DPPC and DPPC with HA of different molecular weight. (a) DLS intensity of radii curves. (b) Center of mass of the first and second peak in the DLS curve for the different samples.*

than the number belonging the to other population. This is due to the fact that light gets scattered much stronger by larger particles.
The addition of HA led to a change of the area and the position of the two peaks as a function of the molecular weight of the HA, indicating a major role of the molecular weight. In figure 3.2b the positions of the center of mass of the two peaks are collected for the different samples. For both peaks the value increases with an increasing molecular weight of the HA. Sole DPPC vesicles and vesicles with HA10 show the lowest values. Looking at the curves in figure 3.2a it can easily detected, that the area under the curve of the first peak changes also as function of the molecular weight. The addition of HA10 to the vesicle solution lead to an decrease of the area under the peak. With increasing molecular weight of the HA the area increases again. Also the width of that peak depends on the molecular weight of the HA. For HA with a molecular weight of $M_W = 1500\ kDa$ and $M_W = 2500\ kDa$ the width is considerably increased compared to the other samples.

3.1.1.3 Small Angle X-Ray Scattering

Information about the bilayer structure of DPPC vesicles in NaCl solution ($c_{NaCl} = 150\ mM$) with or without added HA were obtained from SAXS measurements. HA with a molecular weight of 250 kDa was used and measurements of DPPC, HA and DPPC with HA were performed at three different temperatures to get information about the bilayer structure of the vesicles in all three DPPC phases: 25 °C (DPPC in $L_{\beta'}$ phase), 37 °C (DPPC in $P_{\beta'}$ phase) and 50 °C (DPPC in L_α phase).

The scattering curves of sole DPPC vesicles at the three different temperatures, which are shown in figure 3.3a, are clearly dominated by a broad oscillation reach-

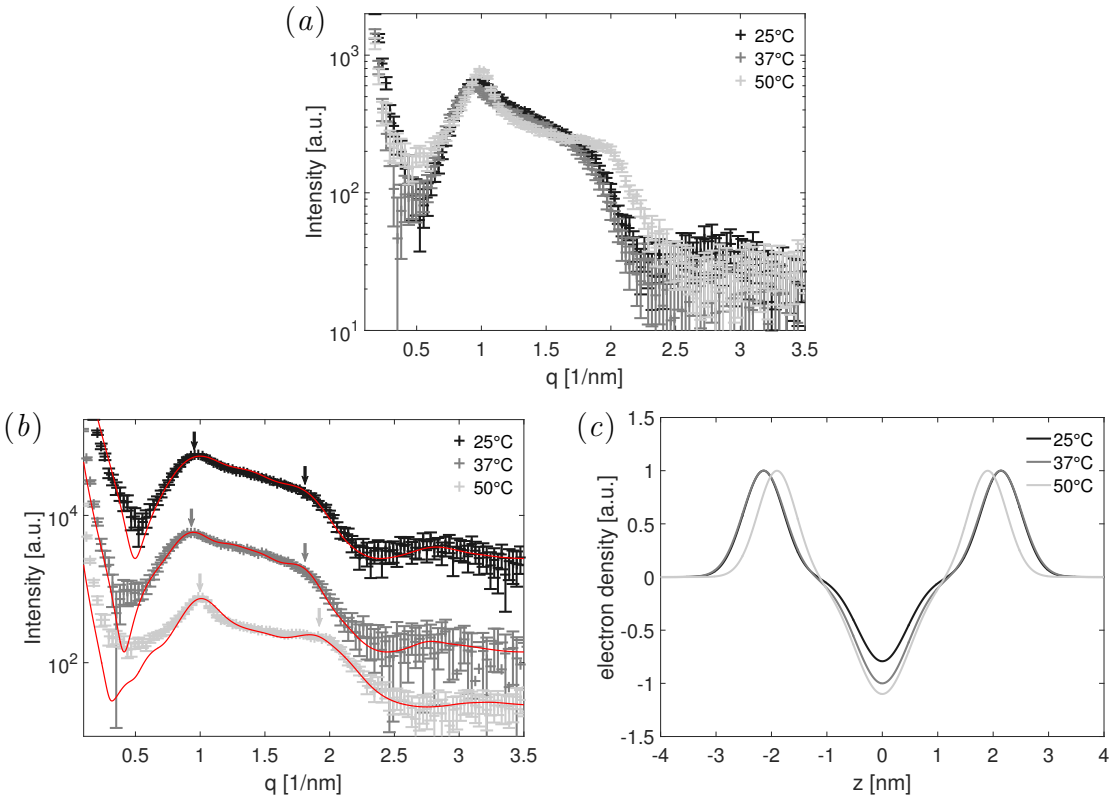

Figure 3.3: *Results from SAXS measurements of DPPC vesicles at three different temperatures. (a) Scattering curves. (b) Scattering curves with fits. Arrows indicate the positions of multilamellar peaks. Vertical offset is for clarity. (c) Relative electron density profiles of the bilayer at the three temperatures, calculated from fits of the scattering curves.*

ing from around 0.5 nm^{-1} to 2 nm^{-1}, which stemmed from the scattering of single bilayers. However the oscillation is superposed by two peaks that are narrower. The position of the peaks is indicated by an arrow in figure 3.3b. The first of these peaks can be found at around 1 nm^{-1}, which fits to the d-spacing (bilayer thickness plus width of the water layer between two bilayer) of DPPC multilayers [33]. Already from these observation it could be concluded, that the studied vesicles are a mixture of unilamellar and a smaller amount of multilamellar (> 1 lamellar) vesicles. In general the curves at 25 °C and 37 °C look quite similar. The width of the oscillation is a little bit smaller for the sample measured at 37 °C compared to the sample measured at 37 °C, hinting at a slightly increased bilayer thickness. Further the multilamellar peak is shifted to a lower q-value (from 0.99 ± 0.02 nm^{-1} for 25 °C to 0.94 ± 0.02 for 37 °C) for this samples and it can be concluded that the d-spacing is increased. The curve of the measurement at 50 °C shows a much broader oscillation than the other two curves, showing that the bilayer thickness decreased. Also the d-spacing from the multilamellar vesicles is decreased, which

can be concluded from the shift of the multilamellar peak position to higher q-values (1.01 ± 0.02). The multilamellar peak was also much more distinct at 50 °C, which could hint at a higher amount of multilamellar vesicles.
In order to obtain more quantitative information about the bilayer structure a model, given by equation 2.12 was fitted to the data sets. The model is described in detail in section 2.2.1. It uses a combination of the scattering from unilamellar and multilamellar vesicles. The electron density of a bilayer was described by three Gaussians, to account for two head group regions and the tail group region. In figure 3.3c the electron density profiles for the DPPC vesicles measured at 25 °C, 37 °C and 50 °C are shown, which were obtained from the fitting procedure. The fits itself are presented in in figure 3.3b and the fitting parameters are collected in a table 3.2. In the region below $q \approx 0.8\ nm^{-1}$ deviation between the fit and the experimental data can be observed. These deviation are attributed to the use of new glass capillaries for every sample. As the capillaries show small differences of their dimensions (diameter and wall thickness) they cause differences in the scattering signal, especially in the low q region However, the fits confirm the conclusion,

Table 3.2: *Parameters of the fits of DPPC vesicles. $\sigma_{H/T}$ gives the half width of the Gaussian curve for the head -/ tail group, z_H describes the distance of the headgroup to the bilayer center, ρ_r give the relative electron density of the tail group, d is the d-spacing, n is a measure for the amount of unilamellar structures, A a scaling factor and BG the background level*

	25 °C	37 °C	50 °C
$\sigma_H\ [nm]$	0.36 ± 0.02	0.38 ± 0.02	0.35 ± 0.03
$\sigma_T\ [nm]$	0.45 ± 0.02	0.48 ± 0.03	0.50 ± 0.04
$z_H\ [nm]$	2.14 ± 0.04	2.14 ± 0.04	1.90 ± 0.08
ρ_r	0.79 ± 0.04	1.00 ± 0.06	1.10 ± 0.07
$d\ [nm]$	6.7 ± 0.2	6.9 ± 0.2	6.3 ± 0.2
n	20 ± 1	45 ± 4	18 ± 2
A	6.5 ± 0.5	2.1 ± 0.1	4.1 ± 0.3
BG	26 ± 3	14 ± 1	25 ± 3
no. of layers	3	4	5

which were already drawn from the scattering curves. From 25 °C to 37 °C a very small increase of the bilayer thickness can be observed (see fig. 3.3b). However, the head-to-head distance stays constant (see parameter z_H in tab. 3.2, which is half of the head-to-head distance). The small increase of the bilayer thickness (head-to-head distance plus the width of the head groups) of $\approx 0.05\ nm$ is caused by a higher width of the head groups at 37 °C (see σ_H in tab. 3.2). It is below the uncertainties. Further, the d-spacing increases slightly from 6.7 nm to 6.9 nm

(see tab. 3.2). A further increase of the temperature to 50 °C leads to a strong decrease of the head-to-head distance (0.5 nm) as well as the d-spacing (0.6 nm). Beside a change in thickness of the bilayer, changes of the electron density could be observed. With increasing temperature the parameter ρ_r increases. ρ_r describes the ratio between the electron density of the head group and the tail group. This change could be caused by a decrease of the absolute electron density of the tail group or a decrease of the absolute electron density of the head groups. Since the relative electron density of the head group in this model is equal to unity (eq. 2.9), an increase of ρ_r causes a decrease of the relative electron density of the tail group region. Using equation 2.14 the ratio of unilamellar to multilamellar vesicles can be calculated. It is 3.6 : 1 at 50 °C and was above 10 : 1 for lower temperatures. Also the number of maximum layers is higher at 50 °C (see tab. 3.2). Thus the tendency to form multilamellar vesicles is higher at 50 °C. This was already suspected from the scattering curves in figure 3.3a.

After the measurements of sole DPPC-vesicles have been presented, the measurements of DPPC vesicles with HA will be introduced to investigate how the structure of DPPC vesicles is changed in the presence of HA. The scattering curves of DPPC with HA showed a superposition of the scattering from vesicles and free HA (see appendix A.1). Due to the low concentration of DPPC, vesicle occupy only a small fraction of the sample volume. Therefore it can be assumed that a large fraction of the HA is not in contact with the vesicles and, thus, can be regarded as free HA. To use the same model for fitting as for sole DPPC the scattering of the free HA had to be subtracted first, so that only the scattering from the vesicles and bound HA was left over. The resulting scattering curves (measured at 25 °C, 37 °C and 50 °C) are shown in figure 3.4a. Additionally the scattering curves of sole HA at the three different temperatures are shown in figure 3.4b. Since the curve of HA are almost identically it can be supposed that the structure of free HA does not change as a function of the temperature. Comparing the scattering curves of DPPC with HA (fig. 3.4a) to the curves of sole DPPC (fig. 3.4a) it can be seen that the addition of HA does not cause strong effects. However, small differences are present, so that the fits that were used for the measurements of sole DPPC do not match the DPPC/HA very well as it is shown in figure 3.5. From the results of the DLS measurements, it was suspected that these changes result from HA adsorbed to the outside of the vesicles. To account for such an adsorption the model used for fitting has been adapted as described in section 2.2.1. An extra layer was added to the model used to fit the curves of sole DPPC vesicles. To minimize the parameter space the parameters for DPPC bilayer/ multilayer was not changed in

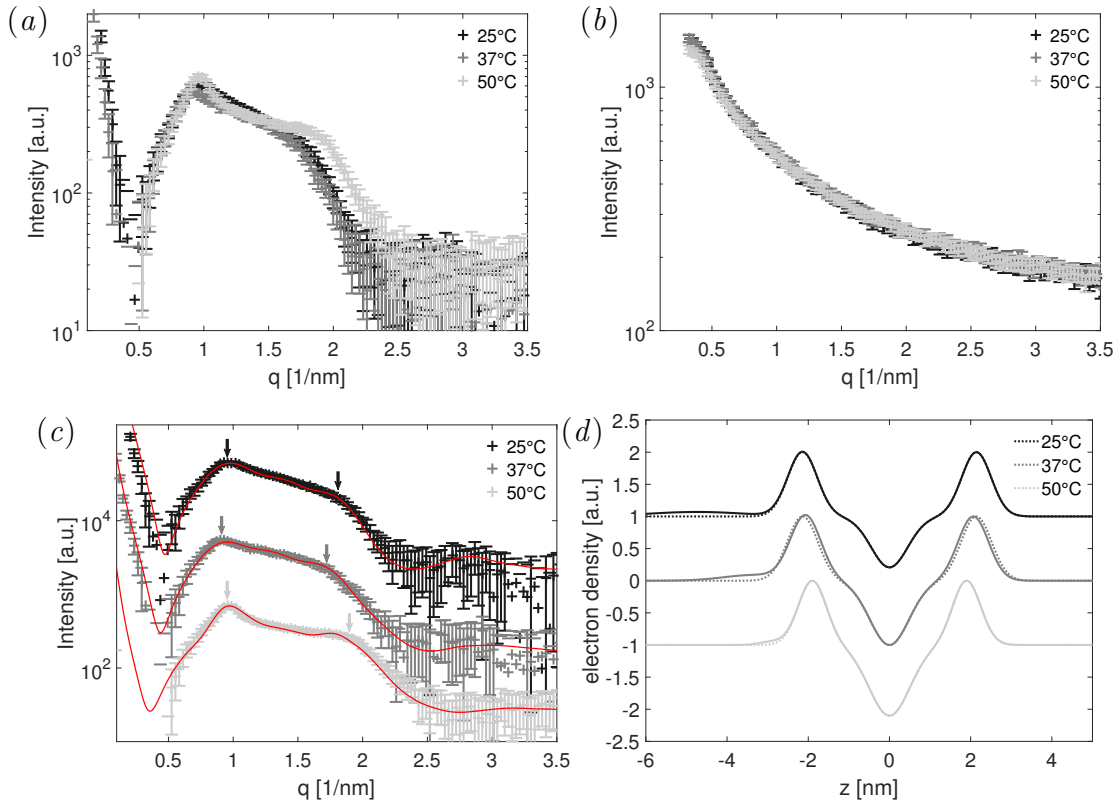

Figure 3.4: *Results from SAXS measurements of DPPC vesicles with HA and sole HA at three different temperatures. (a) Scattering curves of DPPC with HA. The scattering of free HA has already been subtracted. (b) Scattering of HA. (c) Scattering curves of DPPC with HA with fits of the data. Arrows indicate the position of multilamellar peaks. The offset is for clarity. (d) Relative electron density profiles of the bilayer at the three temperatures, calculated from fits of the scattering curves (solid lines). Additionally the relative electron density profiles of a sole DPPC bilayer is shown (broken lines)*

a first step. Only if necessary to achieve a sufficient fit the parameters for z_H and the d-spacing were changed. Fits of the scattering curve are shown in figure 3.4c and the obtained fitting parameters can be found in table 3.3. The relative electron density profiles in figure 3.4d show a small additional layer on the left side of the bilayer. It has to be noted, that the shape of the additional layer is restricted to a Gaussian curve. It could be observed that the center of this extra layer moved with increasing temperature closer to the bilayer, while the thickness of the layer decreased. The electron density reached its maximum at 37 °C. In general it seems as if the layer is most pronounced at 37 °C. Furthermore changes of the bilayer thickness and the d-spacing were observed (see tab. 3.3). The d-spacing of the vesicles with HA at 37 °C (7.1 ± 0.3 nm) and 50 °C (6.6 ± 0.2 nm) was slightly increased compared to DPPC vesicles without HA (6.9 ± 0.2 nm at 37 °C and

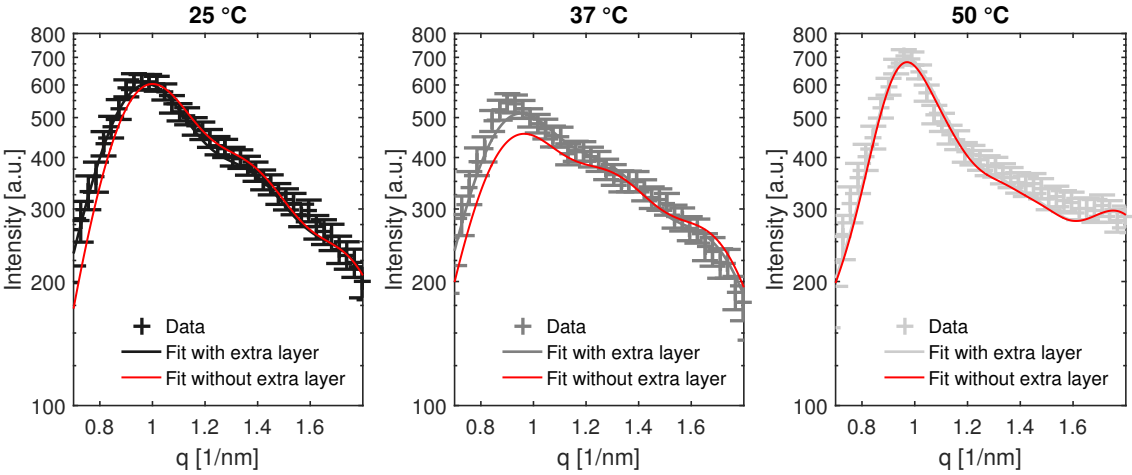

Figure 3.5: *Segment of the scattering data of DPPC vesicles with HA at three different temperatures, together with the calculated scattering from two model (solid lines). The gray scaled line show the fits of the data calculated with the described bilayer model with an added layer for HA. Red lines show the scattering of the same model without the extra layer.*

6.3 ± 0.2 *nm* at 50 °C). At the same time the head-to-head distance of the bilayer with HA at 37 °C is a little bit smaller than the head-to-head distance of a bilayer without HA.

The obtained differences between sole DPPC vesicles and DPPC vesicles with

Table 3.3: *Parameters of the fits of DPPC vesicles with HA. $\sigma_{H/T/HA}$ gives the half width of the Gaussian curve for the head -/ tail group / HA layer, $z_{H/HA}$ describes the distance of the headgroup/ HA layer to the bilayer center, $\rho_{r/HA}$ give the relative electron density of the tail group/ HA layer, d is the d-spacing, n is a measure for the amount of unilamellar structures, A a scaling factor and BG the background level*

	25 °C	37 °C	50 °C
σ_H $[nm]$	0.36 ± 0.01	0.38 ± 0.02	0.35 ± 0.03
σ_T $[nm]$	0.45 ± 0.03	0.48 ± 0.02	0.50 ± 0.03
z_H $[nm]$	2.14 ± 0.04	2.06 ± 0.03	1.90 ± 0.05
ρ_r	0.79 ± 0.03	1.00 ± 0.04	1.10 ± 0.05
d $[nm]$	6.7 ± 0.2	7.1 ± 0.3	6.6 ± 0.2
n	19 ± 2	29 ± 2	29 ± 2
A	6.2 ± 0.3	3.1 ± 0.1	3.2 ± 0.2
BG	22 ± 3	17 ± 2	25 ± 3
no. of layers	3	3	5
ρ_{HA}	0.07 ± 0.02	0.09 ± 0.03	0.05 ± 0.03
z_{HA} $[nm]$	2.6 ± 0.9	1.3 ± 0.5	1.0 ± 0.05
σ_{HA} $[nm]$	1.2 ± 0.6	0.8 0.4	0.30 ± 0.1

HA are quite small (especially for 50 °C) and special care has to be taken when interpreting the electron density profiles. As the quality of the data is not very high and the used model restricts the shape of the added layer there are some uncertainties in the electron density profile are existing, which is reflected in the high relative errors for the HA layer (see tab. 3.3).

3.1.1.4 Discussion

In this section the interaction of DPPC vesicles with HA will be discussed on the basis of the presented results. The three applied methods allowed to obtain a comprehensive picture of the interaction as they probe different length scales and different properties. Together, the results of the three methods convincingly show that HA adsorbs to DPPC vesicles and that the molecular weight of the used HA influences the interaction. It seems reasonable to divide the used HA into two groups when describing the interaction: low molecular weight ($\leq$ 800 kDa) and high molecular weight ($\geq$ 1500 kDa).
First the result from DSC will be discussed, which give insight into the phase behavior of the samples systems. Measurements of DPPC showed the two characteristic peaks for the pretransition ($L_{\beta'}$ to $P_{\beta'}$) at around 34.1 ± 0.5 °C and for the main transition at around 41.83 ± 0.02 °C. The results are in agreement with literature with respect to the transition temperatures of DPPC [30, 67]. Koynova et al. [30] report in their review a value of 34.4 ± 2.5 °C for the pretransition and 41.3 ± 1.8 °C for the main transition. The division of the pretransition into two peaks might be due to small impurities, as the pretransition is known to be very sensitive to any kind of contamination [67]. For the mixed system of HA and DPPC vesicles changes in the DSC signal are observed. The temperature of the main transition did not change considerably, but a shoulder evolved on the lower temperature side of the main transition. The development of a shoulder while the transition temperature is relative unaffected was already well described by McElhaney et al. 1982 [90] for the interaction of small molecules with phospholipid membranes. It was claimed that this behavior is a sign for molecules which interact mainly with the glycerol backbone at the hydrophobic-hydrophilic interface of the membrane. Such an interaction scenario is possible for HA as it was reported that HA has hydrophobic patches which can bind to lipids [41, 44]. For HA with low molecular weight the assumption of a small molecule might be valid, but for HA with a high molecular weight the assumption gets very questionable, especially since the transition enthalpy decreases. It seems therefore reasonable that the interaction

mechanisms for high molecular weight HA differ slightly from those of HA with a small molecular weight. However it can be excluded that HA interacts considerably with the alkyl chains of the lipids. Molecules that are present in this region, like for example cholesterol [91], cause a change of the main transition temperature and an increase of the width of the main transition [90]. Further it is known that even small amounts of contamination lead to a disappearance of the pretransition [92].
DLS measurements showed the existence of two different populations of vesicles, as two intensity peaks at two different positions were found. One at around 1 μm and one at around 100 nm. It seems reasonable that the peak at ≈ 1 μm stems from aggregated vesicles. As a membrane with a pore size of 200 μm was used for the extrusion of the vesicles it can be assumed that the peak at around 100 nm belongs to non aggregated vesicles. Two different trends could be observed, after adding HA of different molecular weight to the solution: i) an increase of the hydrodynamic radius of the vesicles as a function of the molecular weight ii) a decrease of the amount of non aggregated vesicles with a stronger decrease for HA of low molecular weight HA.
An increased hydrodynamic radius for DPPC vesicles with HA has already been reported by Wang et al. 2013 [28], who used HA with a molecular weight of 620 kDa. The HA induced change of the hydrodynamic radius is comparable with the here presented results. From the increase of the hydrodynamic radius it could be concluded that HA adsorbs to the DPPC vesicles, which fits to the here presented results obtained from SAXS where an additional layer at the outside of the vesicles was supposed. The increase of the hydrodynamic radius as a function of the HA can be explained by the different conformations of HA with a low and high M_W. At very low molecular weights (e.g. 10 kDa) HA can be regarded as a stiff rod, while high molecular weight HA in aqueous solution has a random coil conformation with a radius of gyration, that increases as a function of the molecular weight [93]. A HA coil with a larger radius of gyration adsorbing to a DPPC vesicle will lead to large increase of the hydrodynamic radius.
The second trend implied that HA promoted the formation of aggregates, which can be deduced from the decreased intensity of the peak at around 100 nm for samples with HA. This hints at formation of supramolecular HA-DPPC structures, as illustrated in figure 3.6i. Such a formation has already been claimed by Crescenzi et al. 2004 [94], who visualized the aggregates with electron microscopy. The effect got weaker for HA with a higher molecular weight, which hints at an increased interaction strength of HA with low molecular weight. High and low molecular weight HA have the chemical structure and the number of charged carboxyl groups

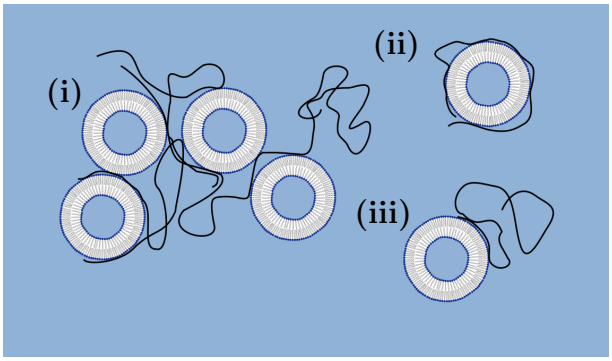

Figure 3.6: *Sketch illustrating the possible structure of DPPC/HA aggregates (i) and possible structures of single DPPC vesicles enveloped by HA (ii) or with attached HA chains (iii).*

in the solution is the same as the same mass concentration was used for all molecular weights of HA. Thus, the reason for the increased interaction is most likely the changed conformation (rod vs. random coil). HA of a higher molecular weight, has, due to its coiled structure, a high amount of mass that is excluded from an interaction with the vesicles since it is situated within the coil. Like the results from DSC, DLS measurements imply an interaction of DPPC vesicles with HA.
For the SAXS measurements DPPC vesicles were mixed with HA ($M_W = 250\ kDa$) and measured at three different temperatures (25 °C, 37 °C and 50 °C). The temperatures correspond to the three bilayer phases: gel phase ($L_{\beta'}$), rippled phase ($P_{\beta'}$) and fluid phase (L_α) [30]. This was also confirmed by the DSC measurements presented here. As the different phases go along with different structural conformations of the lipids the structure of the bilayer changes, while the lipids undergo a phase transition [30]. This is most obvious for the changed d-spacings and head-to-head distances, which were higher in the $P_{\beta'}$ and $L_{\beta'}$ phase than in the L_α phase. The head-to-head distance of 4.3 nm and 3.8 nm for the $L_{\beta'}$ L_α, fit well to the values reported by Nagle et al. 1996 [95]. In contrast to that the results for the d-spacing do not match those reported in literature [95]. A reason for this might be the different preparation methods. The vesicles used for the studies in literature are large multilamellar vesicles, while the here presented results stem from small vesicles with a low number of lamellar. They are called pauci-lamellar vesicles and are well known for PC vesicles prepared by extrusion with membranes of a pore size of 200 nm [96]. The smaller vesicle size induces higher stresses due to the high curvature, which could have a strong effect on the d-spacing. Another effect that is observed during the phase transition is the changed electron density ρ_r. This effect can be explained by an increased volume per DPPC molecule, which

could be the result of higher degree of disorder, due the molten alkyl chains after the phase transitions. An increased volume per molecule for the L_α and $P_{\beta'}$ phase compared to the $L_{\beta'}$ phase has already been reported [31].The addition of HA did not change the scattering profiles considerably, which shows that the bilayer structure did not change much. It could be observed that the d-spacing for the $P_{\beta'}$ and the L_α was increased by HA. A possible explanation could be that HA moved between the bilayers and thereby increases the d-spacing as it was suggested in a study by Kreuzer et al. 2012 [97]. The question arises, how HA should enter the space between two lamellae, as vesicles consist of closed shells of lipids and the presented results do not imply a strong interaction between the HA and DPPC. Thus, an induced disruption of the DPPC bilayers seems very unlikely. Also a penetration through the bilayers is not very likely as the electron density profiles and especially the DSC measurements rule this out. Also Kreuzer et al 2012 [97] did not find an evidence for such kind of interaction. In general some parts of the multilamellar structure could arise from aggregated vesicles, where it is easily possible for the HA to accumulate. The electron density profiles showed a diffuse layer of HA with low electron density. At 37 °C the layer seemed to be most compact. At this temperature the bilayer was in the $P_{\beta'}$ phase which should give the HA chains a better possibility to interact with DPPC molecules, due to its rippled structure. However, it is difficult to give a detailed information about the formed structures as the shape of the layer in the used model is restricted to a Gaussian form and the limited q-range restricts the resolution of the density profile.

The combination of the three methods could confirm that HA and DPPC vesicles do interact with each other, although the interaction is not very strong. In general the interaction of HA and DPPC could be facilitated by two different mechanisms. First, by an electrostatic interaction of the negatively charged carboxyl groups of HA with the positively charged part of the zwitterionic headgroup of DPPC (as indicated by the sketch in fig. 3.7a) and, second, the hydrophobic patches of HA might enable the interaction with the alkyl chains in the inner part of bilayer. The here presented SAXS measurements showed only a diffuse layer on top of the bilayer and no changes of the inner bilayer (tail group region) structure. Further, the results from DSC measurements do not hint at an interaction of HA with the alkyl chains. Thus an adsorption of HA at the headgroup water interface seems very likely. It can be presumed that the positive charge of the NH^+ group, which is located directly at the vesicle interface (see fig. 3.7b), binds to the negative carboxyl group of HA, i.e. the interaction is dominated by electrostatic forces. This is in agreement with result from recent other works that claimed that HA adsorbs

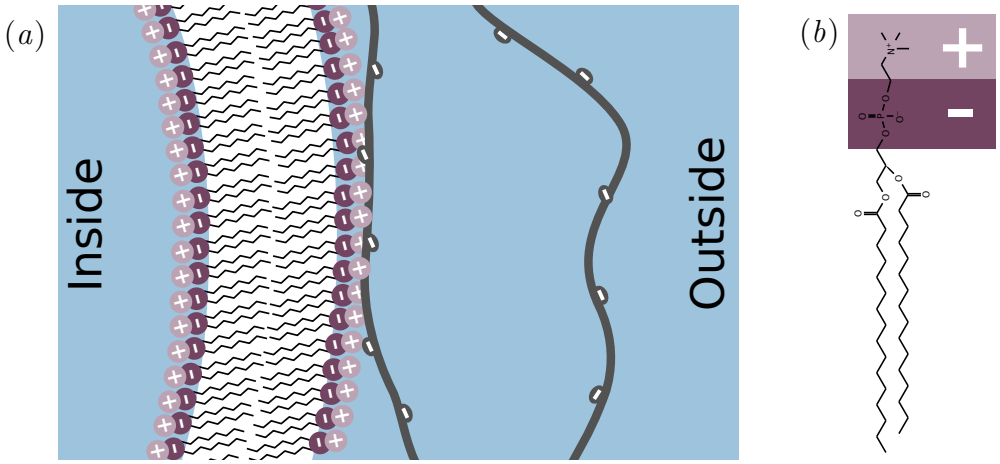

Figure 3.7: *(a) Sketch of a DPPC vesicle in HA solution. (b) Sketch illustrating the charge distribution in the headgroup of a lipid.*

to the headgroup region [97, 98]. However DSC results hint also at a low amount of HA at the glycerol - headgroup interface. The sketch in figure 3.7a summarizes the results, where HA binds to the interface of the vesicles via its charged groups. The measurements with different HA show that the molecular weight has a significant influence on the interaction of the two components. It is already known from several other studies that the molecular weight plays an important role in the synovial joint. It has been claimed that high molecular weight HA shows a better wear resistance [23] and that the molecular weight plays an important role in arthritis [22, 49]. While it is difficult to interpret the result from the DSC measurements which show a somehow stronger effect of the high molecular weight HA on the phase behavior of DPPC, the results from DLS hint at a stronger interaction of low molecular weight HA with DPPC. Also in the literature the important question, if high or low molecular weight HA has a different effect on the bilayer is a matter of discussion [98, 99]. Since, up to now, there are no studies, investigating the effect of the molecular weight on the lubrication properties of DPPC/HA mixtures it is hard to conclude from the presented results if a stronger interaction between HA and DPPC is beneficial or not. Only indirect information about the effect of the molecular weight is available as the molecular weight of HA in the synovial fluid of arthritic joints was found to be lower compared to healthy joints [21, 22].

3.1.2 Interaction in sodium chloride solution with calcium chloride

3.1.2.1 Differential scanning calorimetry

DSC measurements of DPPC and DPPC/HA (using HA with different molecular weights) in a solution containing sodium chloride ($c_{NaCl} = 150\ mM$) and calcium chloride ($c_{CaCl_2} = 10\ mM$) have been performed to evaluate how divalent Ca^{2+} ions change the phase behavior of DPPC vesicles with HA.
The DSC profiles of the six samples are shown in figure 3.8a. An inset in this figure shows a magnification of the pretransition region. The data shows two typical peaks, which belong to two phase transitions of DPPC: the pretransition ($L_{\beta'}$ to $P_{\beta'}$ phase) at around $34 - 35$ °C and the main transition ($P_{\beta'}$ to L_α phase) at around 42 °C. For the calculation of the main transition temperature the average position of the peak maximum of five scans is used and the standard deviation is given as error. The temperature of the main transition of DPPC in sodium chloride with calcium chloride is determined to be 42.72 ± 0.02 °C, which is around $1\ K$ higher than for DPPC in sole NaCl. Adding HA leads to a decrease of the transition temperature, as it can be seen in figure 3.8b, depicting the transition temperature as a function of the molecular weight of the HA. As seen in chapter 3.1.1.1, in a solution without $CaCl_2$ no significant change of the main transition temperature is detected. In the presence of $CaCl_2$ HA10 has the strongest effect on the transition temperature and decreases it by 0.7 °C. The transition temperature increases with increasing molecular weight until it reached a maximum temperature of 42.29 ± 0.02 °C for a molecular weight of 800 kDa and then stays constant. The shape of the profiles of the main transition shows deviations which are caused by the molecular weight of the HA. In general all profiles are asymmetric (with or without HA). In the presence of HA with a molecular weight lower 800 kDA the main transition shows two distinct peaks, which can be seen in figure 3.8a. The second peak vanishes for higher molecular weight HA ($> 800\ kDa$). In contrast to the main transition temperature the temperature of the pretransition of DPPC increases in the presence of HA (see fig. 3.8a). Sole DPPC has a pretransition temperature of 35.3 ± 0.1 °C, whereas the addition of HA leads to an increase of the temperature by 1.2 °C for HA10 and by 1.7 °C for HA2500. In figure 3.8c the enthalpy of the transition for the lipids from the $L_{\beta'}$ phase to the L_α phase is plotted as a function of the molecular weight of the added HA. In general the enthalpy is increased in the presence of HA, but the effect is very small for HA with high molecular weight ($\geq 1500\ kDa$).

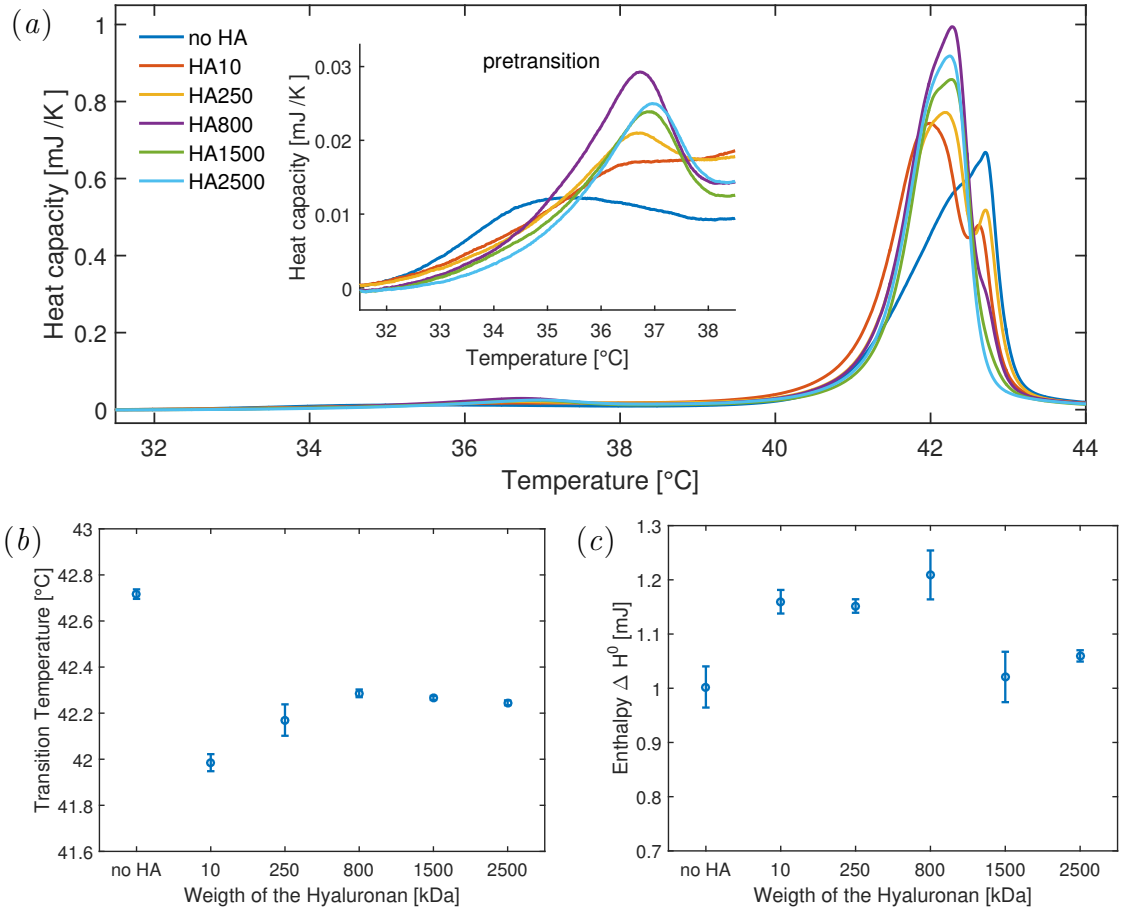

Figure 3.8: *Results of the DSC measurements of DPPC and DPPC with HA of different molecular weights. (a) DSC curves of all samples. The inset shows a magnification of pretransition area. (b) Transition temperature (c) Enthalpy of the transition process*

The results show that HA in the presence of $CaCl_2$ modifies the phase behavior of DPPC. Furthermore it can be observed that the effect on the phase transition depends on the molecular weight of HA.

3.1.2.2 Dynamic light scattering

DLS measurements of DPPC vesicles with HA in aqueous solution (containing 150 mM NaCl and 10 mM $CaCl_2$) were performed to obtain information about the formed structure on micrometer range. The measurements were performed at 25 °C.

The size distribution functions of sole DPPC vesicles and DPPC vesicles with HA, which were obtained from the DLS measurements, are shown in figure 3.9a. The addition of $CaCl_2$ causes strong differences between sole DPPC samples and samples with HA. DPPC vesicles in a solution containing $CaCl_2$ only show a single

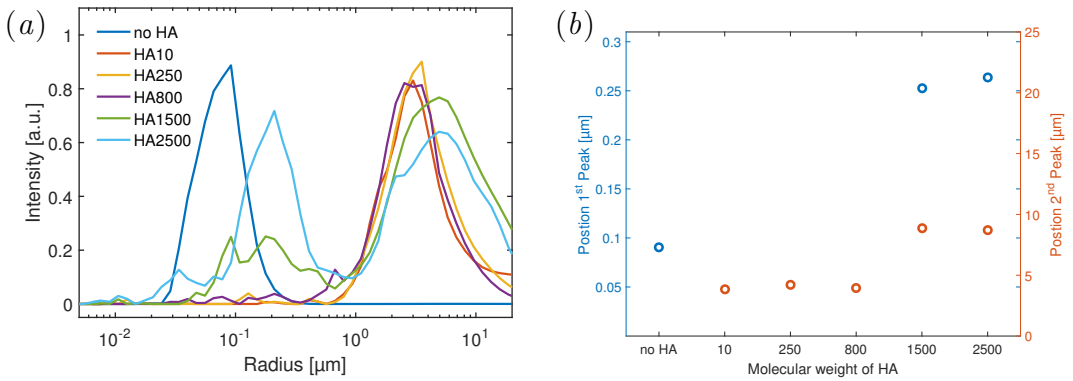

Figure 3.9: *Results from DLS measurements of DPPC and DPPC with HA of different molecular weight in NaCl with $CaCl_2$. (a) DLS intensity of radii curves. (b) Center of mass of the first peak in the DLS curve for the different samples.*

peak at a radius of around 100 nm, which corresponds well with the pore size of the membrane used for the vesicle preparation. No peak is visible at larger radii which hint at an absence of aggregates of the single vesicles. The addition of HA results in a drastic change of the curves (see fig. 3.9a). For all used molecular weights of HA a peak in the micrometer range is visible. Further, a large difference in the curves can be recognized between samples with HA of a high molecular weight ($\geq$ 1500 kDa) and HA with low molecular weight ($\leq$ 800 kDa). $CaCl_2$ causes a vanishing of the peak at around 100 nm for HA with lower molecular weight. For the sample with HA1500 the peak reappears and increases its amplitude for the sample with HA2500. Comparing the position of the center of mass of the peak around 100 nm (for those samples where the peak was observed) it could be recognized that HA leads to an increase of the hydrodynamic radius (see fig. 3.9b). No conclusion can be drawn about a possible change of the peak position with increasing molecular weight of the HA, since no peak can be observed for samples with HA of low molecular weight. Also the position of the peak in the micrometer range is different for samples with HA of low and high molecular weight. While the peaks show very similar shapes and do not change its positions significantly for samples with low molecular weight HA, the peak position shifts to higher values for samples with HA1500 and HA2500.

3.1.2.3 Small angle X-ray scattering

So far DSC and DLS experiments have been discussed. As these methods do not provide detailed information about the bilayer structure, SAXS experiments were performed to resolve how $CaCl_2$ changes the bilayer structure of DPPC vesicles with HA. The samples were probed in three different phases of DPPC: $L_{\beta'}$ (25 °C),

$P_{\beta'}$ (37 °C) and L_α (50 °C).

The scattering of DPPC vesicles at the three different temperatures, which are shown in figure 3.10a, are strongly dominated by a broad oscillation reaching from around 0.5 nm^{-1} to 2 nm^{-1}. Such oszillations are typical for unilamellar vesi-

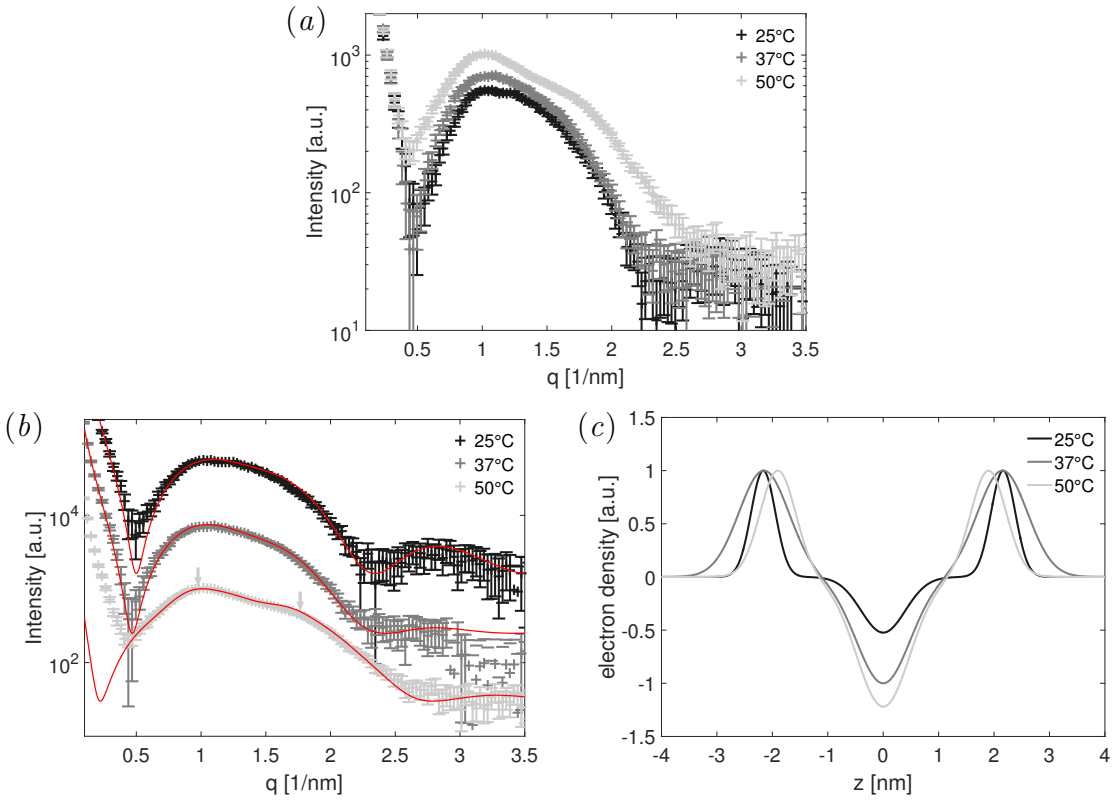

Figure 3.10: *Results from SAXS measurements of DPPC vesicles in a solution containing* 150 *mM NaCl and* 10 *mM*$CaCl_2$ *at three different temperatures. (a) Scattering curves of DPPC with HA. The scattering of free HA has already been subtracted. (b) Scattering curves with fits. Arrows indicate the positions of multilamellar peaks. Vertical offset is for clarity. (c) Relative electron density profiles of the bilayer at the three temperatures, calculated from fits of the scattering curves.*

cles. In contrast to the scattering curve for vesicles at 25 °C and 37 °C the curve measured at 50 °C shows in addition to the oscillation a distinct peak at around 1 nm^{-1} and a second less pronounced peak at 1.8 nm^{-1} (marked by the arrows in fig. 3.10b), indicating multilamellar($\geq$ 2 lamellae) structures. Such peaks are characteristic for multilamellar vesicles, therefore it can be assumed, that the vesicles at 50 °C are partially multilamellar. The oscillation width of the measurements at 25 °C and 37 °C do not show strong difference, while the width increases strongly from 37 °C to 50 °C. This hints at an decreased bilayer thickness for the vesicles at 50 °C. Although the oscillation width of the scattering curve at 25 °C and 37 °C are similar, clear differences of the oscillation shape are visible. Around $q = 1nm^{-1}$

the intensity of the curve measured at 37 °C is significantly higher than the intensity of the curve measured at 25 °C, which might be due to changes in the bilayer structure.

For an quantitative analysis the model described in section 2.2.1 was fitted to the data. The model for the bilayer was build up by three Gaussian curves (eq. 2.10)

Table 3.4: *Parameters of the fits of DPPC vesicles. $\sigma_{H/T}$ gives the half width of the Gaussian curve for the head -/ tail group, z_H describes the distance of the headgroup to the bilayer center, ρ_r give the relative electron density of the tail group, d is the d-spacing, n is a measure for the amount of unilamellar structures, A a scaling factor and BG the background level*

	25 °C	37 °C	50 °C
σ_H $[nm]$	0.22 ± 0.01	0.45 ± 0.04	0.32 ± 0.02
σ_T $[nm]$	0.40 ± 0.03	0.48 ± 0.03	0.48 ± 0.04
z_H $[nm]$	2.16 ± 0.05	2.15 ± 0.05	1.90 ± 0.04
ρ_r	0.52 ± 0.04	1.00 ± 0.07	1.22 ± 0.04
d $[nm]$	-	-	6.0 ± 0.2
n	20 ± 2	19 ± 2	17 ± 2
A	19 ± 2	6.5 ± 0.5	12 ± 1
BG	16 ± 2	25 ± 5	30 ± 4
no. of layers	1	1	3

and to account for multilamellar vesicles the scattering of uni- and multilamellar models was combined (eq. 2.13). All fits together with the data are shown in figure 3.10b and the fitting parameters can be found in table 3.4. For 50 °C deviations between the fit and the experimental data are observed. The reason for this might be found in the use of different capillaries for the samples, which makes a background subtraction very difficult. Especially the low q region is strongly affected by scattering from the glass capillaries. In figure 3.10c the resulting model electron densities are shown. While the DPPC vesicles at 25 °C and 37 °C were fitted with a exclusively unilamellar model, the model for the vesicles at 50 °C contained also a multilamellar fraction. The fits show a head-to-head distance of 4.3 nm (double of z_H, see tab. 3.4) for the bilayers at 25 °C and at 37 °C. However the bilayer appears to have a higher thickness at 37 °C compared to 25 °C (see fig. 3.10c), which is mainly caused by an increase of the width of head group (see parameter σ_H in tab. 3.4). Also the tail group region shows strong structural differences between 25 °C and 37 °C. The parameter ρ_r, which is a measure for the ratio between the absolute electron density of the head groups and the tail groups (see eq. 2.9) increases considerably from 25 °C to 37 °C. This indicates that either the electron density of the head group and/or the tail group decreases. However,

due to the definition of ρ_r as relative electron density, which is normalized to the head group density, no absolute statements can be made. A further increase of the temperature to 50 °C leads to a clear change of the vesicle structure (see parameters in tab. 3.4). The head-to-head distance decreases to 3.8 nm, a certain fraction multilamellar structure develops with a d-spacing of 6 nm and the value of ρ_r increased further.

The scattering curves of DPPC vesicles with HA are a superposition of the scattering of DPPC vesicles and the scattering of free HA. To determine the structure of the vesicles with bound HA, it was necessary to seperate the scattering of free HA. Therefore, measurements of HA in a solution containing NaCl and $CaCl_2$ were performed. The resulting scattering profiles were subtracted from the curves obtained for DPPC vesicles with HA. The scattering curves of sole HA can be found in figure 3.11b. They do not show any significant differences. The resulting scattering curves of the DPPC vesicles in the presence of HA are shown in figure 3.11a. They have a completely different shape than the curves of sole DPPC vesicles (see fig. 3.10a). At all temperatures the curves are a superposition of a broad oscillation from 0.5 nm^{-1} to around 2 nm^{-1} and two peaks at roughly 1 nm^{-1} and 1.8 nm^{-1} (marked by arrows in fig. 3.10). These peaks are a sign for multilamellar structures. The shape of these multilamellar peaks found for the DPPC/HA samples in NaCl/$CaCl_2$ solution differs strongly from those found for DPPC/HA sample in sole NaCl solution (see fig. 3.4a). Compared to the multilamellar peaks of the samples in sole NaCl solution the peaks of the samples in figure 3.11a show higher width and are better defined, which hint at a lower number of lamellae and a higher ratio of multilamellar to unilamellar vesicles, respectively. The position of the first peak varies slightly for the different temperatures. It shifts from $0.96 \pm 0.02 nm^{-1}$ to $0.93 \pm 0.02 nm^{-1}$ for samples at 25 °C and 37 °C. Further heating to 50 °C leads to shift of the first peak to $0.99 \pm 0.02 nm^{-1}$. From these shifts it can be concluded that the d-spacing reaches its lowest value at 50 °C and its highest value at 37 °C. While the width of the bilayer oscillation does not show a strong difference between the measurements for 25 °C and 37 °C, it shows a strong increase after heating the samples from 37 °C to 50 °C and thus the bilayer thickness decreases.

To fit the scattering curves the model described in section 2.2.1 was used. To improve the fitting results the model for the bilayer was complemented by an extra layer (eq. 2.16) that should account for adsorbed HA. The parameters of the model DPPC bilayer from the fitting of sole DPPC vesicles were in a first step not changed and only the parameters of the additional layer were changed. In a second step also the parameters of the bilayer were changed, if necessary. To show that

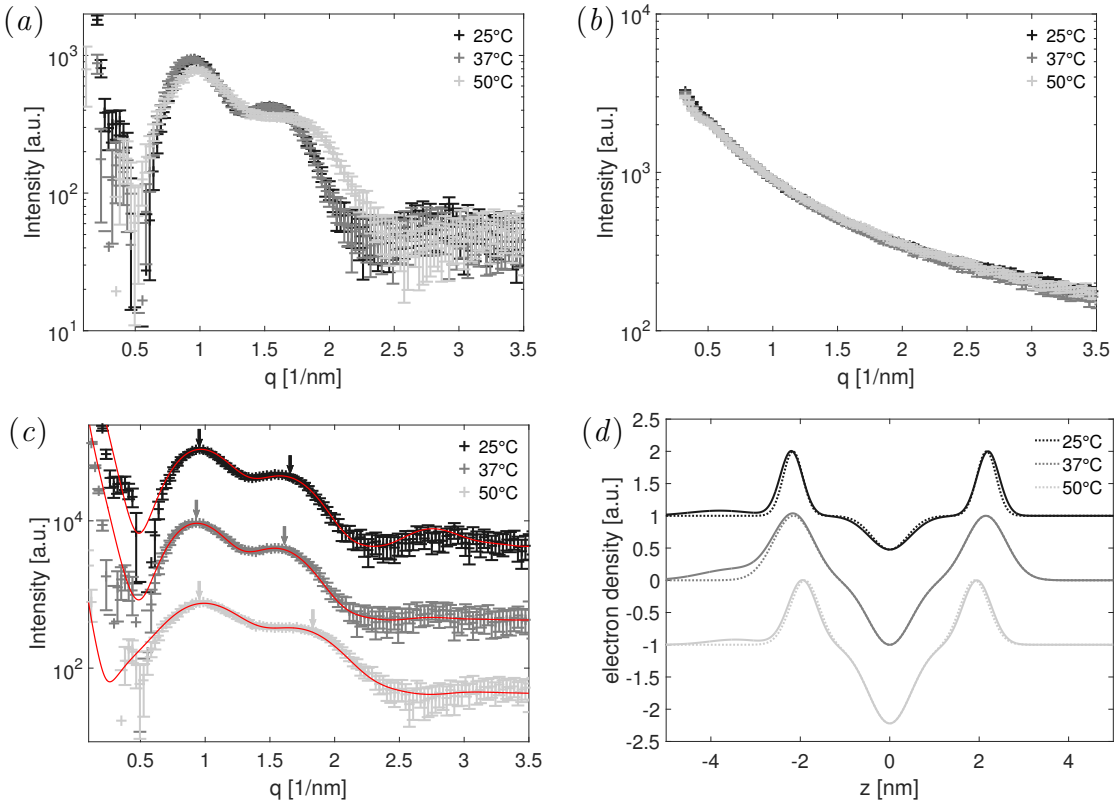

Figure 3.11: *Results from SAXS measurements of DPPC vesicles with HA (M_W = 250 kDA) in a solution containing NaCl and $CaCl_2$ at three different temperatures. (a) Scattering curves of DPPC with HA. The scattering of free HA has already been subtracted. (b) Scattering curves of HA. (c) Scattering curves of the samples with fits. The arrows indicate the position of multilamellar peaks. Vertical offset for clarity. (d) Relative electron density profiles of the bilayer at the three temperatures, calculated from fits of the scattering curves (solid lines) and relative electron density profiles of sole DPPC vesicles from figure 3.10b (broken lines).*

a modification of the model was necessary, the calculated scattering curves from two different models (bilayer with additional layer and bilayer) are compared to the scattering data of DPPC/HA samples at the three different temperatures in figure 3.12. The figure shows only the parts of the scattering curves where a significant difference between the two models can be observed. The first model is the model that was used to fit the DPPC/HA data, a bilayer plus an extra HA layer. For the second model (red lines in fig. 3.12) the extra layer has been removed. Thus the model is very similar to the model that was used to fit the data of sole DPPC. The only difference between the models is the combination of unilamellar and bilamellar vesicles. It can be clearly seen that the model without the extra layer for HA shows a lower intensity than the measured data in the q-range from around $0.7 - 1.3\ nm^{-1}$. For $q > 1.3\ nm^{-1}$ the model fits the data almost as good

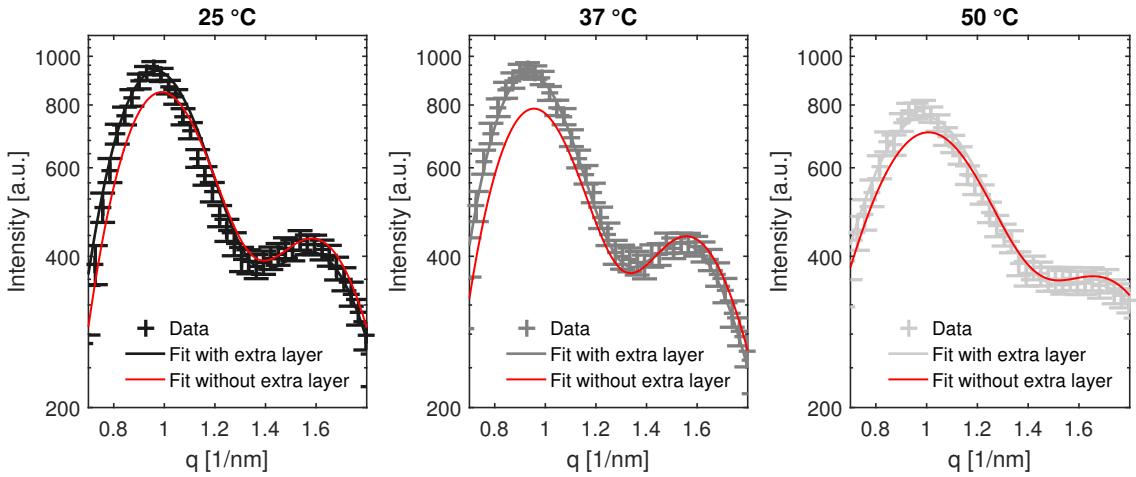

Figure 3.12: *Segment of the scattering data of DPPC vesicles with HA at three different temperatures, together with the calculated scattering from two model (solid lines). The gray scaled line show the fits of the data calculated with the described bilayer model with an added layer for HA. Red lines show the scattering of the same model without the extra layer.*

as the more complex model with the extra layer. This comparison shows that a modification of the model was necessary, but it cannot be excluded that other modification of the model might work as well. The chosen model with an additional Gaussian shaped layer is the most reasonable choice for a modification, as it allows to simulate the adsorption of a HA layer to the vesicle with a low amount of extra parameters. It has to be noted that it is not possible to distinguish if the HA is at the outside of a bilamellar lipid or between the two bilayers.

The fits together with the data are shown in figure 3.11c and all fitting parameters can be found in table 3.5. In figure 3.11d the calculated relative electron density profiles are shown together with the profiles of figure 3.10b. Obviously the structure of the bilayer itself does not change dramatically by adding HA, although the curves of scattering intensity of DPPC vesicles and DPPC vesicles with HA do look very different. The difference between the sample arises mainly from a transformation of unilamellar to multilamellar systems. Interestingly the curves can be fitted with a model that combines exclusively unilamellar and bilamellar vesicles. The fits also reveal that the amount of bilamellar vesicles is quite high (compared to the amount of multilamellar vesicles in a solution containing sole NaCl). For samples at 25 °C and 37 °C the ratio of unilamellar to bilamellar vesicles is 3 : 1 and for samples at 50 °C it is 5 : 1 (calculated by eq. 2.14 with values from tab. 3.5). The head-to-head distance is comparable to the samples of sole DPPC, around 4.4 nm at 25 °C and 4.3 nm at 37 °C. It decreases to 3.9 nm as the samples was heated up

Table 3.5: *Parameters of the fits of the DPPC vesicles and DPPC vesicles with HA. $\sigma_{H/T/HA}$ gives the half width of the Gaussian curve for the head -/ tail group / HA layer, $z_{H/HA}$ describes the distance of the headgroup/ HA layer to the bilayer center, $\rho_{r/HA}$ give the relative electron density of the tail group/ HA layer, d is the d-spacing, n is a measure for the amount of unilamellar structures, A a scaling factor and BG the background level*

	25 °C	37 °C	50 °C
σ_H $[nm]$	0.25 ± 0.02	0.45 ± 0.04	0.32 ± 0.03
σ_T $[nm]$	0.46 ± 0.04	0.48 ± 0.04	0.48 ± 0.04
z_H $[nm]$	2.20 ± 0.06	2.15 ± 0.05	1.95 ± 0.07
ρ_r	0.52 ± 0.05	1.00 ± 0.07	1.22 ± 0.06
d $[nm]$	7.0 ± 0.2	7.3 ± 0.2	6.6 ± 0.2
n	3.0 ± 0.4	2.9 ± 0.3	5.0 ± 0.5
A	78 ± 6	25 ± 2	21 ± 2
BG	45 ± 5	45 ± 5	44 ± 4
no. of layers	2	2	2
ρ_{HA}	0.08 ± 0.04	0.18 ± 0.05	0.08 ± 0.04
z_{HA} $[nm]$	1.6 ± 0.6	1.3 ± 0.4	1.5 ± 0.6
σ_{HA} $[nm]$	0.7 ± 0.3	0.7 ± 0.2	0.6 ± 0.3

to 50 °C. In contrast the values found for the d-spacing are considerably higher for DPPC in the presence of HA than for sole DPPC. The lowest value can be found at 50 °C, while the highest is found at 37 °C (see tab. 3.5).
On the left side of the bilayers in figure 3.11d the extra layer of HA can be observed. It is most distinct at 37 °C, while at 25 °C and 50 °C it is much weaker. The parameter for the relative electron density of the HA layer ρ_{HA} is highest at 37 °C and the distance to the bilayer center z_h is lowest at 37 °C, while the layer width does not change considerably. At 25 °C and 50 °C ρ_{HA} as well as z_H have similar values. From the figure it seems that the extra layer is hardly connected to the bilayer at 25 °C and 50 °C, but this might be an artifact as the shape of the layer is restricted to be Gaussian like. In general it is necessary to be careful when evaluating the results, since the data quality is not perfect and the evaluable q-range is small. Particularly in the low q-region the fit quality is low. One reason is probably that every sample was measured in a different glass capillary, which have slightly different inner diameters and wall thicknesses. Therefor every capillary has a different scattering signal, especially in the low q-region.

3.1.2.4 Discussion

Besides Na^+ and Cl^- also a variety of other ions can be found in the synovial fluid, like the divalent Ca^{2+}. Such multivalent ions can have a strong influence on the structure and interaction of molecules. Therefore a small amount of $CaCl_2$ ($c_{CaCl_2} = 10\ mM$) was added to the sample solution to study the influence of divalent ions on the interaction of DPPC vesicles and HA. The amount of $CaCl_2$ is higher, but in the range of what can be found in the synovial joint [81]. Again DSC, DLS and SAXS studies were performed to obtain a comprehensive picture about the formed structures and interactions. The overall parameters of the experiment (temperature, sample and ion concentrations, molecular weight of HA) were the same as for studies in sole NaCl solution to have a good comparability. Nevertheless, even the addition of low amounts of $CaCl_2$ (10 mM) induces strong changes to the sample system.

The phase behavior of DPPC with and without HA was changed significantly by $CaCl_2$. First of all, pure DPPC shows an increase of the main and the pretransition of to 0.89 K and 1.2 K, respectively. The increase fits in general to results reported in literature, where an increase of the main transition of DPPC of 3.5 K was reported for 1 M $CaCl_2$ [30]. An increase of the temperature of the pretransition for low $CaCl_2$ concentration was described by Hayashi et al. 2005 [100]. Since such strong changes of the phase behavior between DPPC in NaCl and DPPC in NaCl with $CaCl_2$ could be detected it is obvious that Ca^{2+} ions bind to the membrane of DPPC. The addition of HA leads to a strong decrease of the pre- and main transition temperature, while the transition enthalpy is increased. Interestingly the effect on the phase behavior is much stronger for HA of low molecular weight ($< 800\ kDa$) than for HA of high molecular weight ($> 800\ kDa$). Wieland et al. 2016 [98] also observed a stronger influence of low molecular weight HA on phase behavior of DPPC monolayers. A decreased main transition temperature of lipids, as induced by the HA, is usually regarded as a sign for an impurity that distracts the lipid packing [67]. The shape of the main transition is strongly altered, especially in the presence of low molecular weight HA. For HA with low molecular weight a second peak at higher temperature could be observed, that disappeared with increasing molecular weight. According to McElhaney et al.1982 [90] the development of a second separate peak might be the result of a molecule interacting with the head group of the lipids. The peak of the pretransition becomes more distinct for high molecular weight HA, while it is very weak for HA with $M_W = 10\ kDa$, which also implies that high molecular weight HA has a weaker effect on the tail group region.

DLS results for sole DPPC show only particles with a radius of 100 nm which fits very well to the size that was expected for vesicles. The absence of a peak in the micrometer range denotes an absences of aggregates, as they were detected for DPPC vesicles in sole NaCl. The reason for this behavior is probably that the Ca^{2+} ions that have been adsorbed to the membrane and lead to a positive charging of the vesicles [87], so that there is a repulsion force between the vesicles. The addition of HA changes the DLS curves dramatically. For low molecular weight HA the peak at 100 nm vanishes and reappears for high molecular weight HA. Further, a peak in the micrometer range appears, indicating an aggregation of vesicles. For sole NaCl solution such a strong aggregation is not observed, but this can be explained by a stronger attraction between the negatively charged HA chains and the DPPC bilayer, which might be positively charged. Due to their divalent nature Ca^{2+} ions can bridge two negatively charges and, thus, work as 'cross-linkers' as it is indicated in figure 3.13. The reason for the stronger interaction of low molecular weight HA with the vesicles might be found in the different conformation of HA. Low molecular weight HA (e.g. $M_W = 10\ kDa$) is assumed to be more rod-like while HA with a high molecular weight has in aqueous solution the structure of a semiflexible random coil [39, 40]. It might be more difficult for coiled structure to interact with the membranes, since most of the chain volume is not exposed to the membrane surface. At least for DPPC vesilces with HA of $M_W = 1500\ kDa$ and $M_W = 2500\ kDa$ the radii of the not aggregated particles could be compared to those of sole DPPC vesicle. HA causes an increase of the radius, as it has already been shown in the previous section 3.1.1 and reported in literature [28] for DPPC vesicles and HA in pure NaCl solution. The increase is comparable to these earlier results and also a dependence of the particle size from the molecular weight of the HA could be detected. This dependence is probably caused by the increase of the radius of the coil as a function of the molecular weight [93].

The scattering curves show that at 25 °C and 37 °C only unilamellar vesicles can be found as it was reported by Uhrikova et al. 2008 [87]. This effect is well described for PC vesicles which are doped with charged lipids (like PS lipids) [96]. Ca^{2+} ions seem to have a similar effect, i.e. they lead to a charging of the membrane. Only at 50 °C oligolamellar structures can be detected, which is in contrast to the findings from Uhrikova et al. 2008 [87]. A reason for this might be that the here presented results were recorded in solution containing a high concentration of NaCl which screen [101] the Ca^{2+} induced charging of the membrane. Such a screening of Ca^{2+} ions adsorbed to DPPC membranes was also reported by Lis et al. 1981 [85]. This and a higher thermal fluctuation at 50 °C might explain the different

results. Besides promoting the formation of unilamellar vesicles the addition of Ca^{2+} has also a strong effect on the electron density in the tail group region. The profile of the sample at 25 °C shows a much higher electron density level as profile of a DPPC bilayer in sole NaCl. The higher level of the electron density in the tail group region is probably due to closer packing of the alkyl chains induced by Ca^{2+} ions, as it was already suggested by Kataoka et al. 1985 [83] and Aruga et al. 1985 [82].

To probe the samples at different phases, measurements were performed at different temperatures. They reveal the typical phase induced structural changes of a bilayer. At 25 °C and 37 °C the head-to-head distance has the same value. It decreases when the sample was heated up to 50 °C. This change is due to a phase transition of the bilayer to fluid (L_α) phase [30, 87, 95]. The head-to-head distance of the DPPC bilayer in NaCl with $CaCl_2$, showed the same values as the bilayers in sole NaCl. This is only partially consistent whith the results reported by Uhrikova et al. 2008 [87]. They report a $CaCl_2$ induced increase of the bilayer thickness in the L_α phase of about 0.2 nm. Unfortunately, a comparison of the values for the bilayer thickness is not possible, as they used a different model. The increase was claimed to be due to a changed arrangement of the lipids which was caused by a long range electrostatic potential of the adsorbed Ca^{2+} ions [86]. However, there are also studies claiming that Ca^{2+} ions don't have an impact on the bilayer thickness [85]. Further, the electron density level of the tail group region changes as a function of the temperature. At 25 °C the relative electron density profile shows a very defined structure and a high electron density level in the tail group region, which differs very much from the profiles at elevated temperatures in the $P_{\beta'}$ and L_α phase, where the packing density seems to be decreased by molten chains.

Instead of exclusively unilamellar vesicles a mixture of unilamellar and bilamellar structures is found for DPPC vesicles with HA, indicating a strong interaction. It has to be noted, that the maximum number of lamellae is only two and that the amount of bilamellar structures is quite high. The question arises if the bilamellar structures are the result of a disruption and reorganization of the vesicles due to the presence of HA, or if the HA causes an aggregation of the vesicles leading to a favorable distance of the vesicles to each other. A strong aggregation of the vesicles is also seen in the DLS data. A disruption of the vesicles would hint at very a strong interaction between the HA and the vesicles with a considerably strong interaction with the alkyl chains. DSC measurements do not hint at a interaction with the alkyl chains. Also the SAXS measurements do not hint at a strong interaction of HA with the tail group region. The electron density profiles do not show

strong differences of the bilayer structure between vesicles with and without HA. Furthermore, after a disruption the lipids would form new vesicles by self assembly, which would probably lead to vesicles with more than just two layers.
The bilayer structure itself does not change dramatically due to the addition of HA, but the bilayer model used to fit sole DPPC had to be adapted slightly. An extra layer was added on top of one side of the bilayer to account for the differences. The layer is most pronounced at 37 °C, where the rippled structure of the bilayer would lead to an increase surface area [34]. This might improve the possibility of the HA chains to interact with the bilayer. In general, the extra layer seems to

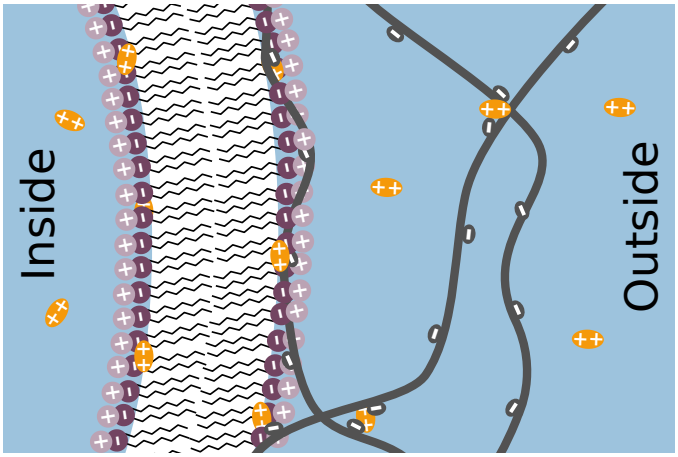

Figure 3.13: *Sketch of a DPPC vesicle in HA solution with $CaCl_2$ (orange circles).*

be a little bit more compact as for the measurements of DPPC and HA in sole NaCl solution. This could be due to stronger bonds between the single HA chains, caused by a cross-linking through the Ca^{2+} ions. This is also illustrated in figure 3.13. As for the results for DPPC and HA in sole NaCl care has to be taken in the interpretation of the results, since the shape of the layer is restricted to Gaussian like and the possible resolution is limited.
DSC and SAXS measurements show that the structure and phase behavior of the DPPC vesicles change due to the addition of $CaCl_2$ which is a sign for an adsorption of Ca^{2+} ions. It seems reasonable that the ions are bond via coulomb attractions to the negatively charged phosphate groups of the lipids [82, 83, 87]. It has even been claimed that the concentration of Ca^{2+} in the plane of the lipid head group is strongly increased compared to the concentration in in bulk solution [86]. The adsorption of a Ca^{2+} ion to the phosphate group leads to a charge inversion from -1 to $+1$ and, thus, changes the originally zwitterionic nature of the lipid to be cation ionic (double positive). Such positively charged lipids will strongly attract the negatively charged HA chains and will bind them to the lipid bilayer, which is

illustrated in figure 3.13. The binding between HA and DPPC vesicles is probably also responsible for the observed aggregation of the vesicles. Furthermore, the Ca^{2+} ions could cause an inter-chain cross-link of the HA molecules, which could lead to more compact layer of HA on top of the DPPC vesicle. The obtained results from DSC, DLS and SAXS show a much stronger interaction of DPPC and HA in the solution with $CaCl_2$ than without $CaCl_2$. To obtain a more detailed picture of the actual supramolecular structures that have formed other techniques (e.g. cryo-TEM) and sample systems could be helpful.

3.1.3 Summary

Studies on the interaction of DPPC vesicles and HA in two different solution condition (NaCl and NaCl/$CaCl_2$), which were presented and discussed in the last chapter can be summarized in the following four main findings:

- $CaCl_2$ has a strong influence on the phase behavior and structure of the DPPC vesicles. The transition temperatures are increased and the formation of unilamellar vesicles is promoted. These effects are very likely induced by Ca^{2+} ions binding to the phosphate group of DPPC and, thus, induce a charge inversion. Thereby the packing and attraction of the lipids in the vesicle bilayer are changed, which influences the phase behavior, and the bilayer get a positive overall charge, which causes repulsion force between single bilayers.

- In a solution containing only NaCl HA and DPPC vesicles show only a weak interaction. Results from DSC, DLS and SAXS hint at an adsorption of HA at the headgroup region, but DSC and SAXS show that the bilayer structure is not strongly altered by the HA. The interaction is probably driven by electrostatic interaction between the negatively charged carboxyl groups of HA and the positively charged NH_3^+ group of the lipid heads.

- After $CaCl_2$ is added to the solution the interaction of HA with the DPPC vesicles becomes much stronger. A considerable change of the phase transition temperature is observed and a strong tendency of the vesicles to aggregate. The enhanced interaction is claimed to be due to a bridging of the Ca^{2+} ions between the HA chains and the DPPC bilayer.

- It can be observed that HA of low molecular weight ($< 800\ kDa$) generally showed a stronger interaction with the DPPC vesicles. Its effect on the transition temperature is larger and a stronger aggregation can be seen.

3.2 Interaction of DPPC and hyaluronan at the solid liquid interface

In the synovial joint lipid bilayers can not only be found unbound in the synovial fluid but also in large quantities at the cartilage surface. It is assumed that these bilayers play a major role for the boundary lubrication. As these bilayers have to be regarded as supported bilayers and not as unbound bilayers another experimental scheme was chosen to study the organization of DPPC with HA at interfaces: Si supported DPPC/HA layers. Of special interest was how the system reacts to high hydrostatic pressure, as it occurs at high loads at the cartilage surface [5, 8, 9]. The sample system was studied in two different solutions. First the results obtained for sample systems in 155 mM NaCl solution will be presented. This concentration of NaCl matches the physiological NaCl concentration quite well. In the synovial joint also divalent Ca^{2+} ions can be found in low concentration. To study their effect on the structure, the DPPC/HA samples were also investigated in a solution containing 150 mM NaCl and 10 mM $CaCl_2$. To study the influence of the molecular weight of HA on the interaction two different molecular weights were used. Results from measurements of DPPC vesicles and HA (section 3.1) indicated a strong difference between HA with a low molecular weight and HA with high molecular weight. Thus, short HA chains with $M_W = 10\ kDa$ and long HA chains with $M_W = 1500\ kDa$ were used for the experiments. The sample system was investigated using fluorescent microscopy and XRR. Using XRR it was possible to apply high hydrostatic pressures (up to 3 $kbar$) to the samples and to measure at different temperatures, to study the response of the layers to the varying conditions.

3.2.1 Silicon supported DPPC with hyaluronan in sodium chloride solution

As the the distribution of the lipids at the cartilage surface probably has a strong influence on the lubrication properties, fluorescent microscopy was used to obtain results about the lateral structure of the DPPC and DPPC/HA layers on the micro meter scale. These images will be presented first and afterwards the vertical structure of sole DPPC on the nanometer scale will be described at different pressures and temperatures. After the evaluation of the sole DPPC structure the influence of HA will be discussed. To ensured that all physiological relevant phases of the DPPC bilayer ($L_{\beta'}$, $P_{\beta'}$, L_α) were studied, samples were probed at three different

temperatures: 25 °C, 39 °C and 55 °C. Additionally, it was studied how the layers behave under extreme outer conditions. Therefore hydrostatic pressures up to 2000 *bar* (180 *bar* are reported for every day activity [8, 9]), which should be well above the phase transition of DPPC at 55 °C (see fig. 1.3b) were applied during the measurements. Measurements were preferable done at 60 *bar* instead of 1 *bar* to avoid air bubbles in the XRR sample cell and it has been shown before (see appendix fig. A.4) that the sample did not change between 1 *bar* and 60 *bar*.

3.2.1.1 Lateral structure on the micro meter scale

Images of Si supported DPPC and DPPC/HA samples in 150 mM NaCl, recorded with a fluorescence microscope are shown in figure 3.14. The samples were prepared as described in section 2.1.2 and according to the used fluorescent labels DPPC appears green in the microscope images and HA appears red. As explained in section 2.2.5 the wafer was slightly tilted during the measurements. Therefore, not the complete field of view was in the focal plane.
The images in figure 3.14A-C reveal that the Si wafers are completely covered with DPPC. In the presence of HA (fig. 3.14B-C), the coverage with DPPC seems to be less homogeneous than for sole DPPC. The images indicate that HA with $M_W = 1500\ kDa$ has a stronger impact on the lateral distribution of DPPC than HA with $M_W = 10\ kDa$, since more bright spots hinting at a strong accumulation of DPPC can be found in the image for HA with $M_W = 1500\ kDa$ (see fig. 3.14C). The distribution of HA is shown in figure 3.14D-F. Care has to be taken when interpreting these images as even for the image of the sole DPPC layer (fig. 3.14D) a faint red background can be detected even though there were no labels present emitting in the red wavelength spectrum. However, the images of DPPC/HA samples (see fig. 3.14E-F) show a much higher intensity with a clear texture. The signal from labeled HA that has adsorbed to the DPPC layer can be clearly distinguished from the background.The preparation protocol involves a rinsing of the sample with large amounts of NaCl solution. Therefore, it can be concluded that the HA is strongly bound to DPPC and distributed over the whole wafer. However, the distribution is not homogenous, which suggests the HA does not form a compact layer at the bilayer surface. A colocalization of bright red spots, with areas where also the fluorescence from DPPC is enhanced can be detected (see fig. 3.14H-I). This suggests local aggregation of the two components.

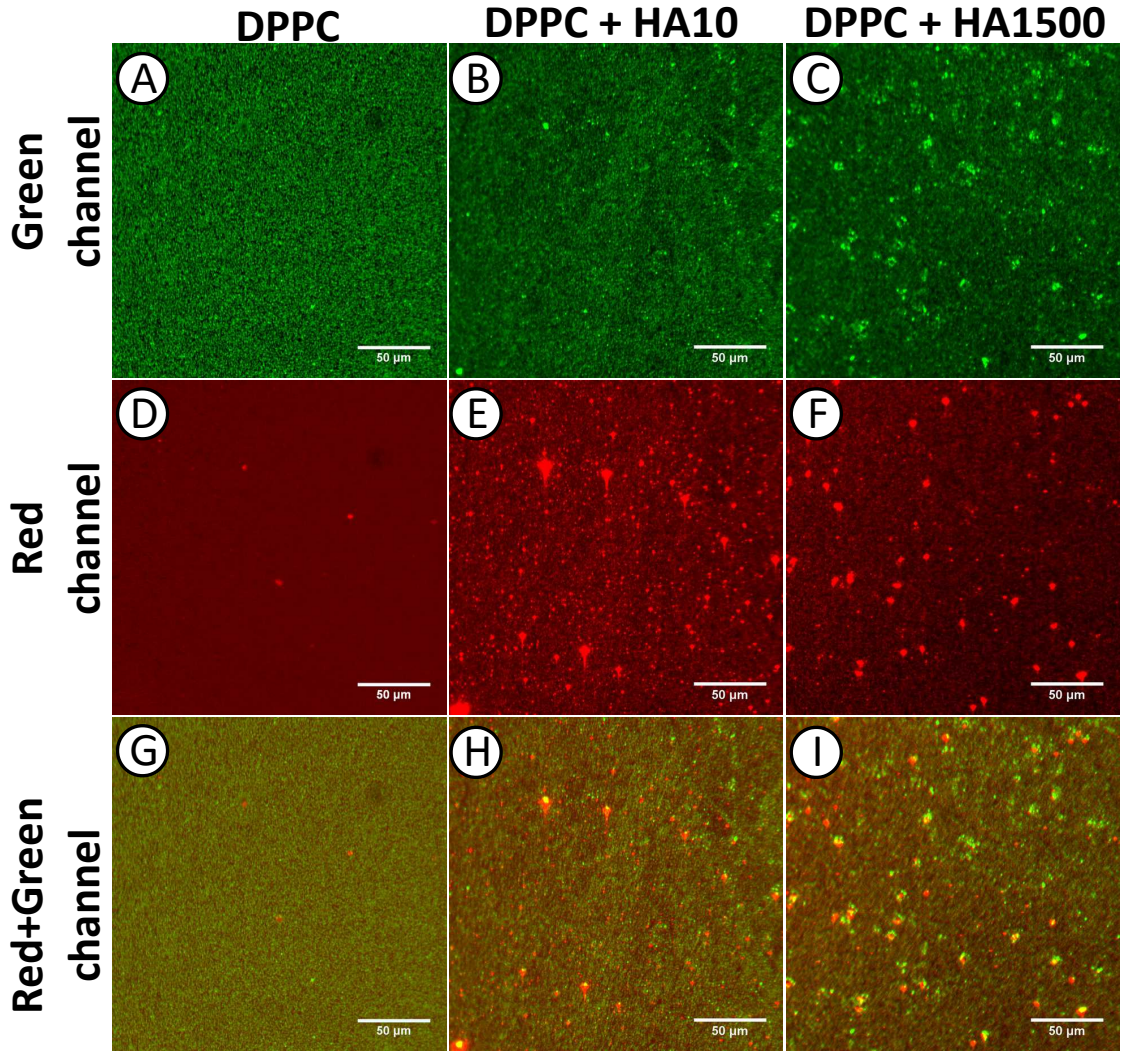

Figure 3.14: *Fluorescence microscopy images of Si supported DPPC and DPPC/HA composites in* 150 *mM NaCl solution. DPPC was labeled with NBD (green channel) and HA was labeled with Rhodamine (red channel)*

3.2.1.2 Structure of DPPC

Before studying the interaction of Si-supported DPPC bilayer and HA the structure of sole Si-supported DPPC bilayers is described. Si-supported DPPC was studied at three different temperatures (25 °C, 39 °C and 55 °C) and different hydrostatic pressures between 60 *bar* and 2000 *bar*. The samples were prepared as described in section 2.1.2. The pressure was first increased stepwise with measurements at 60 *bar*, 100 *bar*, 500 *bar*, 1000 *bar* and 2000 *bar*, and afterwards the pressure was released and a final measurement was performed at 60 *bar* (in the following '60 *bar* D'). Since the structure of the bilayer did not change as function of the pressure for 25 °C and 39 °C only measurements at two pressure points were evaluated (60 *bar*

and 2000 *bar*). As described in section 2.2.4 the measured reflectivity data was fitted with a model electron density for a bilayer consisting of six slabs (see fig. 2.14).

The Fresnel normalized reflectivity curves and the calculated model electron densities of the samples measured at the three different temperatures are shown in figure 3.15 a and b, respectively. Measurement at 60 *bar* and 2000 *bar* are compared with each other, only at 55 °C no model is shown for 2000 *bar*, as no reasonable fit of the reflectivity data was possible. All shown electron density profiles exhibit the shape of a typical bilayer [33]. From left to right the following parts could be identified: a high electron density of the Si-support (pure Si and SiO_2), the DPPC bilayer (head - tail - CH_3 group - tail - head) and water (see fig. 2.14).

At 25 °C the Fresnel normalized reflectivity curves (see fig. 3.15a) show only small differences between 60 *bar* and 2000 *bar*. Mainly the positions of the minima is shifted. The position of the first minimum shifts from $q = 1.66\ nm^{-1}$ to $q = 1.71\ nm^{-1}$ as the pressure is increased from 60 *bar* to 2000 *bar*, indicating a decreased layer thickness. The calculated electron density profiles (see fig. 3.15b) confirm these assumptions. It can be observed that the head-to-head distance decreases from $4.6 \pm 0.1\ nm$ to $4.5 \pm 0.1\ nm$. To calculate the head-to-head distance the center of head group was determined by Gaussian fits. Further it can be observed that the electron density level is increased at 2000 *bar*, compared to 60 *bar*. This effect can be seen for the bilayer itself as well as for the water phase and is attributed to a higher mass density due to the compression of the media induced by increased hydrostatic pressure. From the density profiles it can be told that no strong structural change occur between 60 *bar* and 2000 *bar*. It should be noted, that the roughness of Si support is much lower as the roughnesses of the all other presented samples, which is due to different wafers that were used. The wafer used for DPPC at 25 °C had an exceptional low roughness.

The sample at 39 °C shows the same behavior as the sample at 25 °C. The position of the first minimum of the fresnel normalized reflectivity curves (see fig. 3.15a) shifts from $q = 1.66\ nm^{-1}$ to $q = 1.69\ nm^{-1}$ as the pressure is increased from 60 *bar* to 2000 *bar*, which indicates a decrease of the layer thickness. This is confirmed by the electron density profiles (see fig. 3.15b), showing a decrease of the head-to-head distance from $4.8 \pm 0.2\ nm$ to $4.7 \pm 0.3\ nm$. Further, at 2000 *bar* a generally increased electron density can be observed, which is caused by an higher mass density due to the increased hydrostatic pressure. No strong structural change occurs between 60 *bar* and 2000 *bar*.

Fresnel normalized reflectivity curves of DPPC at 55 °C, measured at different pres-

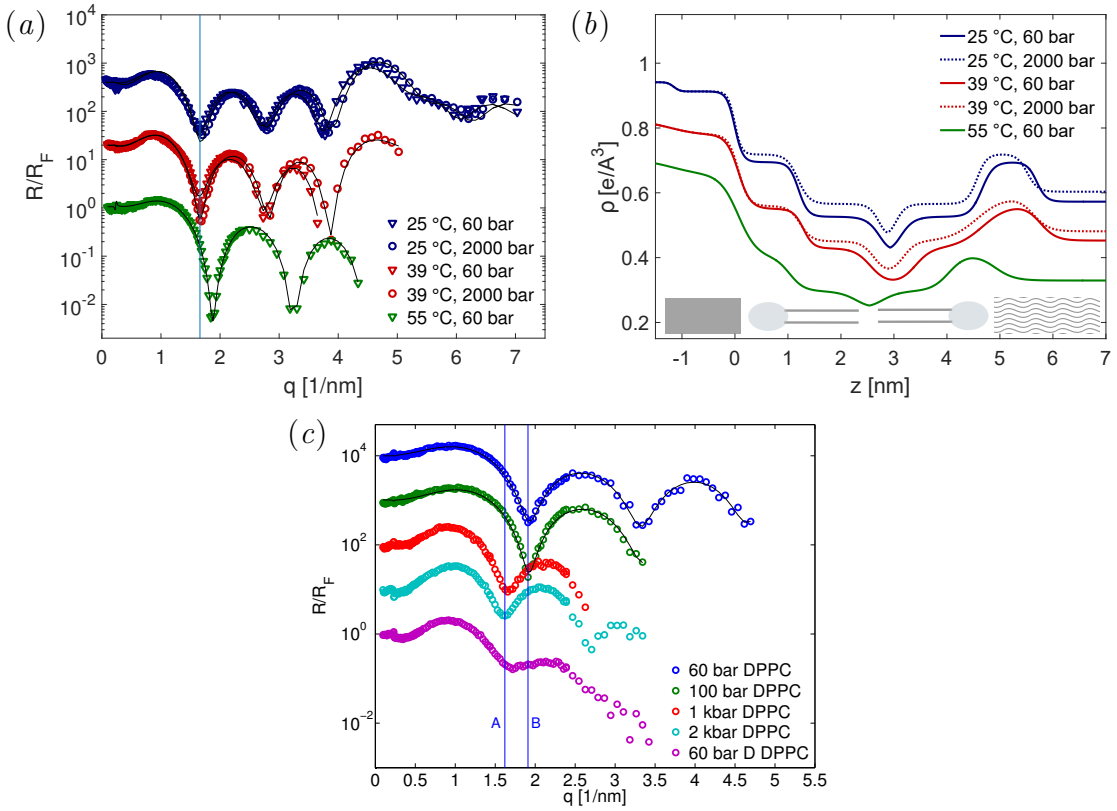

Figure 3.15: *(a) Fresnel normalized reflectivity curves of DPPC samples at different temperatures and two pressures. Black lines indicate fits of the curves and the vertical offset between the different temperatures is for clarity. (b) Calculated electron density profiles. The vertical offset between the different temperatures is for clarity and the sketch below the curves illustrates the Si-supported bilayer. (c)Fresnel normalized reflectivity curves of DPPC at 55 °C at all pressure steps. Black lines indicate fits of the curves and the vertical offset is for clarity.*

sure steps between 60 *bar* and 2000 *bar*, are shown in figure 3.15c. The position of the first minimum is the same at 60 and 100 bar, but at a pressure of 1000 *bar* it is shifted to lower q-values (from position B at $q = 1.92$ *nm* to A at $q = 1.66$ *nm*). From the shift it can be deduced that high pressure induces a structural change, which results in an increased layer thickness. Further the intensity at high q is very low at pressures above 1000 *bar*, indicating a very high roughness of the sample. No significant change in the reflectivity profile is observed when further increasing the pressure to 2000 *bar*. After decreasing the pressure from 2000 *bar* back to 60 *bar* (60 *bar* D) the reflectivity curve changes its shape again, but it does not look identical to the curve measured in the beginning of the pressure cycle (measurements of an other DPPC sample showed similar results). Especially the position of the first minimum does not return to its original position and the oscillations at high q disappear. It was not possible to fit the last three curves (1000 *bar*, 2000 *bar*,

60 *bar* D) with a reasonable bilayer model, therefore, only the measurements at 60 *bar* and 100 bar were fitted. The corresponding profile for 60 *bar* can be found in figure 3.15b. It shows a head-to-head distance of 3.8 ± 0.1 *nm*, which is considerably lower than the values for bilayers at 25 °C and 39 °C. Compared to the structure of the electron density profiles of samples at 25 °C and 39 °C the profile of the sample at 55 °C has a more indistinct structure.

3.2.1.3 Structure of DPPC with hyaluronan at different temperatures

XRR measurements of DPPC and HA were performed at 60 *bar* and three different temperatures: 25 °C, 39 °C and 55 °C. For the experiments HA of two different molecular weights was used. Low molecular weight HA with $M_W = 10$ *kDa* and high molecular weight HA with $M_W = 1500$ *kDa*. However mainly results from samples with HA with $M_W = 1500$ *kDa* will be shown, as HA with a molecular weight of $M_W = 10$ *kDa* show qualitatively the same effects. The samples were prepared as described in section 2.1.2 and the measured reflectivity curves were fitted with model electron density build up of six to seven slabs as described in section 2.2.4.

Fresnel normalized reflectivity curves of measurements of DPPC and HA with a molecular weight of $M_W = 1500$ *kDa* at 60 *bar* and three different temperatures, 25 °C, 39 °C and 55 °C are shown in figure 3.16a along with to the reflectivity curves of sole DPPC for comparison. The shape of the curves gives a first hint about the effect of HA on the layer structure. DPPC/HA layers seem to show a higher roughness compared to layers composed of pure DPPC. This can be concluded from the stronger decrease of the intensity of the reflectivity curves of DPPC/HA at 25 °C in the higher q region. The effect is only weak for measurements at 55 °C and 39 °C, but at these temperatures the oscillations, which were more pronounced for pure DPPC hint at the same direction. The disagreement of the fit with the last two data points for DPPC/HA at 25 °C is due to a high background intensity for this measurement.

The electron density profiles of DPPC/HA are shown in figure 3.16b and are compared to the profiles of sole DPPC. They show typical bilayer structures. At 25 °C and 39 °C the head-to-head distance is determined to be 4.7 ± 0.2 *nm* and 4.5 ± 0.2 *nm*, respectively, while it was considerably smaller at 55 °C: 3.8 ± 0.1 *nm*. The electron density profiles of DPPC and DPPC with HA of a molecular weight of $M_W = 1500$ *kDa* at 25 °C show significant differences. This is especially obvious for the head group region that is oriented towards the water phase, which is

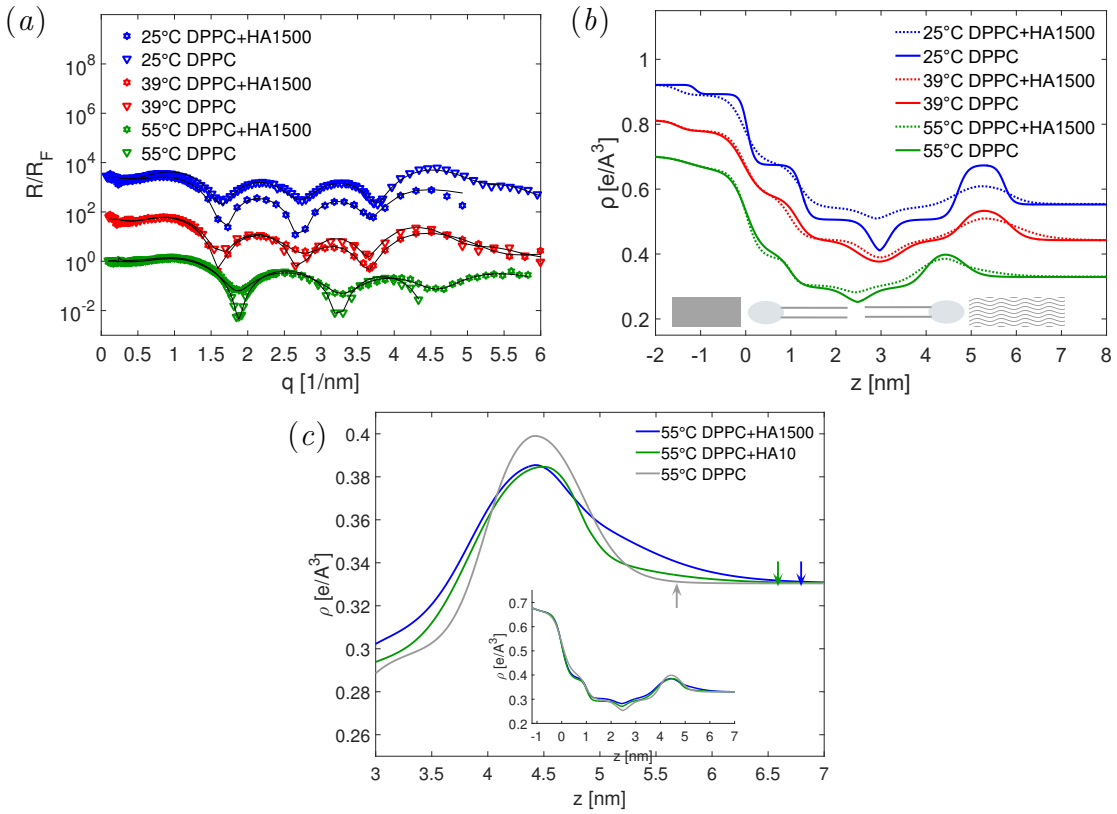

Figure 3.16: *(a) Fresnel normalized scattering curves of DPPC and DPPC/HA, recorded at* 60 *bar and* 25 °*C* , 39 °*C and* 55 °*C. Solid black lines indicate the fits. (b) Electron density profiles of DPPC and DPPC/HA, recorded at* 60 *bar and* 25 °*C* , 39 °*C and* 55 °*C. The curves of a and b are shifted vertically for clarity and the sketch below the curves illustrates the Si-supported bilayer. (c) Magnification of the electron density of the head group region for DPPC, DPPC with HA1500 and DPPC with HA10, measured at* 55 °*C and* 60 *bar.*

very distinct with a low roughness for pure DPPC. DPPC with HA in contrast has a much broader electron density distribution, i.e. the roughness is much higher. Additionally, the electron density of the head group is smaller for DPPC with HA compared to sole DPPC and the electron density in the tail group region is increased in the presence of HA. The samples measured at 39 °C and 55 °C show the same trend, with a lower electron density and a higher width of the head group region of the upper leaflet for DPPC with HA compared to sole DPPC. However the differences are not as pronounced as for the measurements at 25 °C, where sole DPPC shows much lower roughness as sole DPPC at 39 °C and 55 °C. The increase of the roughness as a function of the temperature for sole DPPC samples is probably due to larger thermal fluctuation at higher temperatures and a different phase of the lipids.

The molecular weight of HA causes slight structural differences at the interface

between the layer and the liquid phase. This can be seen in figure 3.16c, where a magnification of the electron density profiles of the head group region of the upper leaflet of the DPPC bilayers with HA is shown. From the profiles it can be concluded, that HA1500 has a stronger effect on the broadening of the head group of DPPC that is oriented towards the water phase than HA10. The broadening results in a higher overall layer thickness (the thickness from the top of the Si-support until the beginning of the water phase) of DPPC/HA samples compared to sole DPPC samples. This is indicated by the arrows in figure 3.16c. However, the head-to-head distance does not seem to be significantly effected by HA.

3.2.1.4 Structure of DPPC with hyaluronan at high hydrostatic pressures

To elucidate how samples composed of DPPC and HA ($M_W = 10\ kDa$ and $M_W = 1500\ kDa$) adapt to high pressures, XRR measurements were performed at pressures up to 2000 *bar* (200 MPa). The samples were prepared as described in section 2.1.2 and probed with a pressure cycle at three different temperatures (25 °C, 39 °C and 55 °C). The pressure was first increased in steps (60 *bar* 100 *bar*, 500 *bar*, 1000 *bar*, 2000 *bar* and a final reflectivity curve was measured at low pressures (1 *bar* or 60 *bar*) to determine if the potential pressure-induced structural changes were reversible. As described in section 2.2.4 the measured reflectivity data was fitted with a model electron density for a bilayer consisting of six to seven slabs (see fig. 2.14). For 25 °C and 39 °C only the results from 60 *bar* and 2000 *bar* are presented, as no considerable structural change took place during the pressure cycle. Further, due to limited beamtime, for 25 °C and 39 °C measurements were performed only for HA of a molecular weight of $M_W = 1500\ kDa$.
The Fresnel normalized reflectivity curves and electron density profiles of DPPC with HA at two pressures (2000 *bar* and 60 *bar*) and two temperatures, 25 °C and 39 °C, are presented in figures 3.17 and 3.18, respectively. At both temperatures only small differences between the electron density profiles at 60 *bar* and 2000 *bar* can be observed. The increase of the electronic density can be attributed to the increased mass density at high hydrostatic pressures. The increase of the electron density of water, due to the high pressure, is in good agreement with theoretically calculated values. Compared to the electron density profiles of sole DPPC it can be seen that the electron density of samples composed of DPPC and HA have much higher roughness. The head-to-head distances of the samples are collected in fig. 3.20. They are in same range for all samples at 25 °C and 39 °C. However, we

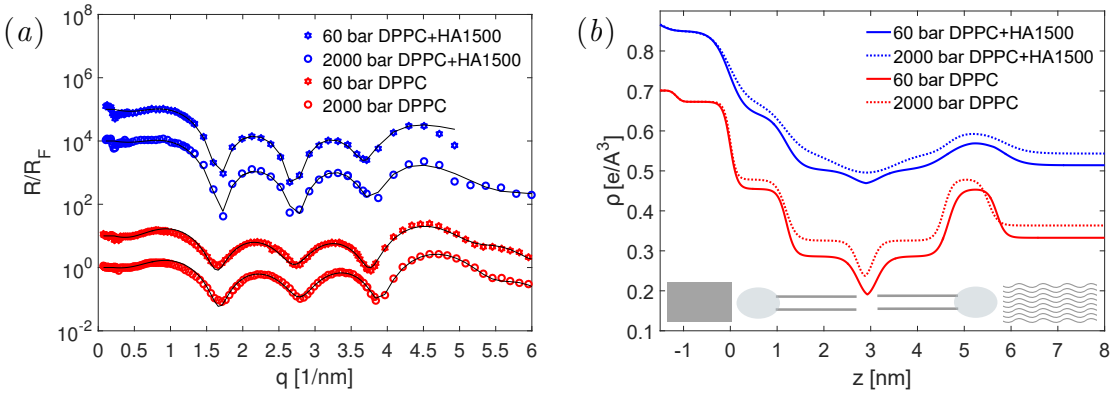

Figure 3.17: *(a) Fresnel normalized scattering profiles of DPPC/HA1500, recorded at various pressures between 60 bar and 2000 bar and 25 °C. Solid black lines indicate the fits. (b) Resulting electron density profiles. The curves are shifted vertically for clarity and the sketch below the curves illustrates the Si-supported bilayer.*

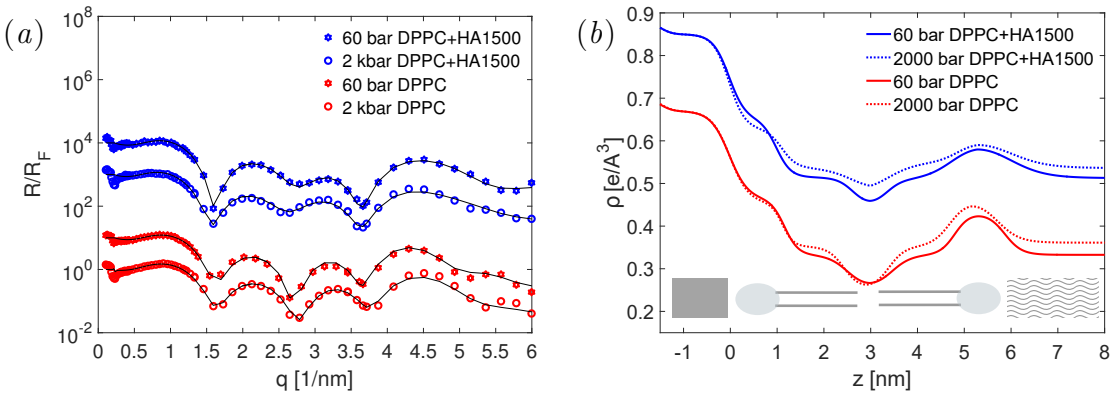

Figure 3.18: *(a) Fresnel normalized scattering profiles of DPPC/HA1500, recorded at various pressures between 60 bar and 2000 bar and 39 °C. Solid black lines indicate the fits. (b) Resulting electron density profiles. The curves are shifted vertically for clarity and the sketch below the curves illustrates the Si-supported bilayer.*

note that the head-to-head distance of pure DPPC bilayers at 25 °C and 39 °C decreases at high pressure (2000 *bar*), whereas the head-to-head distance of samples composed of DPPC with HA seems to stay constant or even increase slightly (see fig. 3.20).

In figure 3.19a and b the Fresnel normalized reflectivity curves and the calculated electron density profiles of DPPC with HA1500 at 55 °C are shown, respectively. The curves and profiles for DPPC with HA with $M_W = 10\ kDa$ (see appendix fig. A.5 a and b) show similar structural changes as those obtained for DPPC with HA with a molecular weight of $M_W = 1500\ kDa$. As for pure DPPC a significant structural difference can be recognized as the pressure is increased from 100 *bar* to

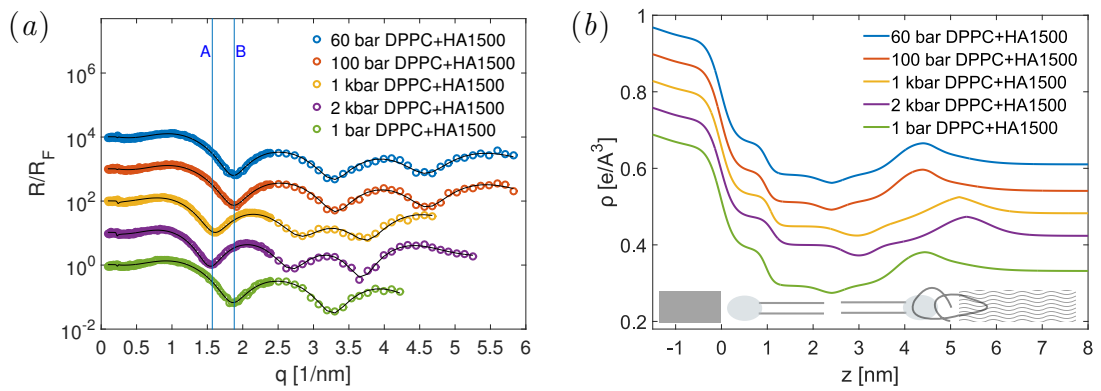

Figure 3.19: *(a) Fresnel normalized scattering profiles of DPPC/HA1500, recorded at various pressures between* 60 *bar and* 2000 *bar and* 55 °*C. Solid black lines indicate the fits. (b) Resulting electron density profiles. The curves are shifted vertically for clarity and the sketch below the curves illustrates the Si-supported bilayer.*

1000 *bar*. The head-to-head distance determined from the electron density profiles at pressures $\leq$ 100 *bar* is 3.8 ± 0.1 *nm*, whereas it increased to 4.7 ± 0.2 *nm* at pressures $\geq$ 1000 *bar*. The head-to-head distance obtained from the reflectivity curves determined at high pressures and 55 °C is comparable to the head-to-head distance measured at 39 °C and 25 °C at low pressures, i.e. with DPPC in the gel state. Especially for DPPC with HA of a molecular weight of $M_W = 1500$ *kDa*

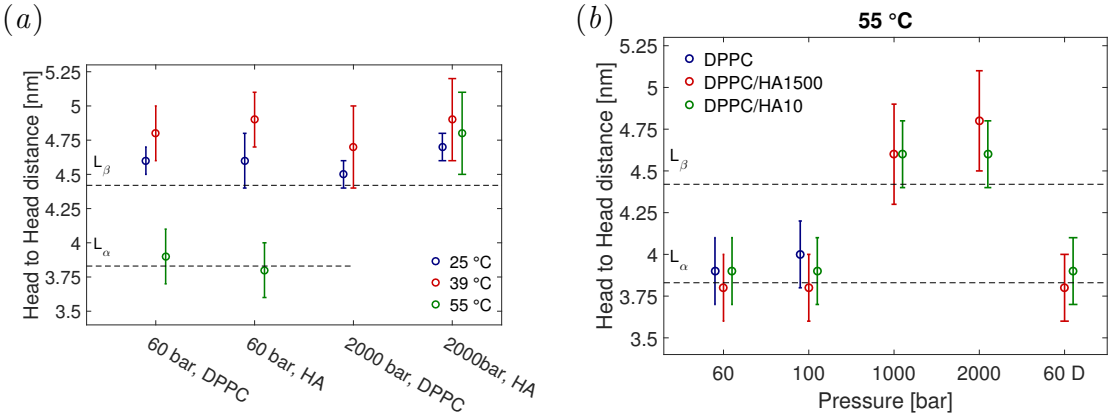

Figure 3.20: *(a) Head-to-head distances of the electron density profiles of DPPC and DPPC with HA at different temperatures and pressures. (b) Head-to-head distances for DPPC and DPPC with HA of different molecular weights different pressure steps and* 55 °*C. The black broken line show the head-to-head distance of for the* $L_{\beta'}$ *phase* ($\approx$ 4.4 *nm*) *and the* L_α *phase* ($\approx$ 3.8 *nm*) *[33].*

it seems that there is a slight further increase of the head-to-head distance while increasing the pressure from 1000 *bar* to 2000 *bar*. It has to be stressed that in contrast to the pure DPPC measurements the pressure induced structural changes

of the sample system composed of DPPC with HA are reversible and the layer returns to its initial structure as the pressure is decreased to 1 bar. The structures exhibit stable transitions in both cases for DPPC with HA with $M_W = 1500\ kDa$ and DPPC with HA with $M_W = 10\ kDa$.

3.2.1.5 Discussion

In the following the results obtained from fluorescent microscopy and XRR will be discussed. First the lateral structure of DPPC and DPPC with HA considered. Afterwards the vertical structures will be discussed, followed by a section about the influence of HA on the vertical structure of DPPC and a section about the influence of HA on the phase behavior of DPPC.

Lateral structure of DPPC/HA

From the fluorescent microscopy images information about the lateral structure and organization on the micrometer scale of Si supported DPPC and DPPC/HA can be obtained. The images show red structures, indicating an adsorption of HA (labeled with a red marker) to the DPPC bilayer. This is in line with the results from experiments on DPPC vesicles with HA, which also indicated an adsorption of HA to DPPC bilayers. Findings from other studies which have used QCM [16] or electron microscopy [99] also support the results. Further the images show that DPPC and HA are distributed over the whole wafer, and that the distribution of HA is not homogeneous. It can be also seen that the distribution of DPPC became less homogenous in the presence of HA as more bright green spots can be observed. This is consistent with AFM images of DPPC-HA layers on Si-wafers as they have been recorded and shown by Wang et al. 2013 [28]. It could also be shown that the molecular weight of HA influences the interaction of DPPC and HA, as the the distribution of DPPC is less homogenous in the presence of HA with $M_W = 1500\ kDa$, compared to HA with$M_W = 10\ kDa$. This is also claimed by Pasquali-Ronchetti et al. 1997 [99] ,who saw different structures for the supramolecular arrangement of DPPC and HA, depending on the molecular weight of HA, and most recently by Wieland et al. 2015 [98]. Wieland et al. 2016 studied the interaction of a DPPC monolayers with a water subphase containing HA at the air water interface using Brewster angle microscopy, GID and XRR. They saw a stronger effect of low molecular weight ($M_W = 10\ kDa$) HA on the DPPC monolayer, which is in contrast to the here presented results suggesting a stronger impact of HA1500 to the lateral structure. This can be attributed to the differences in the sample preparation. Wieland et al. studied a monolayer of DPPC

at the air-water interface, where the monolayer formed on a subphase containing HA. In contrast the herein studied sample system was an already formed bilayer, which came in contact with HA. Therefore some of the interaction mechanisms described by Wieland et al. 2015 may not fully apply here (e.g. the interaction of hydrophobic patches of the HA with the chains of single DPPC molecules).

Vertical structure of DPPC

Before discussing the influence of HA on the vertical structure and the phase behavior of DPPC it is necessary to consider the phase behavior (as a result of temperature and pressure) of Si supported DPPC bilayers. DPPC in contact with excess water in bulk can be present in three different phases: L_α , $P_{\beta'}$ and $L_{\beta'}$ phase. At ambient pressure the transition from $L_{\beta'}$ phase to $P_{\beta'}$ phase occurs at around 35 °C and the transition from $P_{\beta'}$ to L_α phase (also called the 'main transition') can be observed at around 41 °C [30]. Each phase has a characteristic chain configuration. This results in different bilayer thicknesses. The bilayer thickness, and with that the head to head distance, for the fluid phase is lower as compared to the gel phase [30, 32, 33]. This is also observed for our samples. The head to head distance is found to be either $3.7 - 3.9\ nm$ or $4.6 - 4.8\ nm$, depending on the actual pressure and temperature (see fig. 3.20). Thus, at 55 °C and 60 *bar* DPPC bilayers are in the fluid phase and at 25 °C and 60 *bar* the lipids are in the $L_{\beta'}$ phase, which has a stretched chain conformation and, therefore, a higher head to head distance [33]. At 39 °C DPPC in bulk solution is in the $P_{\beta'}$ phase [30, 32]. However, different studies on solid supported bilayer systems show that, due to the constraints induced by the solid support, no $P_{\beta'}$ phase can be observed [35] [36]. This is supported by our measurements as the shape of the electron density at 39 °C is similar to the shape of the electron density for DPPC in the $L_{\beta'}$ phase (25 °C). We note that the shape of the electron density profile of a single solid supported ripple phase bilayer would differ significantly from that of a bilayer in the gel phase. Either would the bilayer partly disassociate from the Si wafer (see. fig. A.6) or the layer should become asymmetric, if only the upper leaflet is in the $P_{\beta'}$ phase. Hence, we conclude that at 39 °C the DPPC bilayer on the Si support is in the $L_{\beta'}$ phase.

At 55 °C a drastic change of the head to head distance of sole DPPC can be observed when the pressure is increased above 1000 *bar*. The head to head distance increases from $3.9 \pm 0.2\ nm$ to $4.6 \pm 0.2\ nm$ from the thickness of a fluid phase bilayer to the thickness of a gel phase bilayer. Such a pressure-induced transition from fluid to gel state has been observed for DPPC in bulk solution at 55 °C and is

well described [102] [103]. It has been reported that the temperature of the main transition shifts to higher values with increasing pressure, at a rate of 20 $K/kbar$ [32], which is consistent with our data. In contrast to what has been found in literature for multilamellar vesicles, the Si supported DPPC bilayers are destabilized at high pressures. An explanation might be found in the area occupied by a DPPC-molecule, as it is larger in the L_α phase compared to the $L_{\beta'}$ phase [33]. Thus, in addition to rearrangements in the vertical structure of the single DPPC chains, the fluid to gel phase transition might result in a patchy structure of the bilayer, as the lipids "move closer together" (e.g. the formation of water filled voids or cracks). It seems also likely that the constraints of the solid support induces strains (e.g. due carbon chains exposed to water), which inhibit the rearrangement of the lipids after a phase transition. As a result, the structural changes the bilayer undergoes at high pressure at 55 °C are not reversible. At 25 °C and 39 °C an increase in pressure does not result in significant changes of the head to head distance or the shape of the electron density profiles. This was expected for DPPC at 25 °C as it should be in the $L_{\beta'}$ phase at all pressures [32]. At 39 °C in bulk a phase transition from the $P_{\beta'}$ phase to the $L_{\beta'}$ phase would be expected [32]. No such transition is observed, underlining that the supported bilayer is in the gel phase at all pressures investigated at 39 °C.

Influence of HA on the vertical structure of DPPC

The electron density profiles of DPPC bilayers with and without HA show many similarities. In particular the bilayer structure remains unchanged in presence of HA, and the head to head distance is not much affected. However, there are some differences. The increase of roughness and gradient at the head group region - water interface (broadening of the head group region), demonstrates adsorption of HA, consistent with the fluorescence microscopy images in figure 3.14. The less distinct electron density profile in presence of HA can be modeled with a high roughness, suggesting that HA does not form a compact layer. This is schematically illustrated in figure 3.21b. Additional, agglomeration seen in the microscopy images (figure 3.14), could contribute to a smearing of the electron density. The results from SAXS measurements show very similar structures with a faint additional layer, which could also be interpreted as a high roughness. Slight difference in the structure of DPPC/HA1500 and DPPC/HA10 composite layers can be ascribed to the different chain length as HA1500 is more prone to form extended structures.
Further, the electron density of the layers composed of DPPC with HA show a higher roughness of the single slabs, than for sole DPPC. Therefore the profile of

DPPC with HA appears more smeared out and less distinct. A lower electron density in the head group region and a higher density in the tail group region hints at a changed packing of the molecules in the upper leaflet of the DPPC/HA composites. This might be induced by HA chains adsorbing at the surface of the bilayer and in particular, among the lipid head groups. This assumption is also supported by DSC measurements of DPPC vesicles with HA. The measurements show the formation of a shoulder on the lower temperature side of the main transition, which can be attributed to an adsorption of HA between the head groups. Results from SAXS measurements can not be used to support or weaken the assumption as the parameters for the bilayer structure were kept fixed for DPPC vesicles and DPPC vesicles with HA. Thus, the changed electron density is most likely the result of a changed

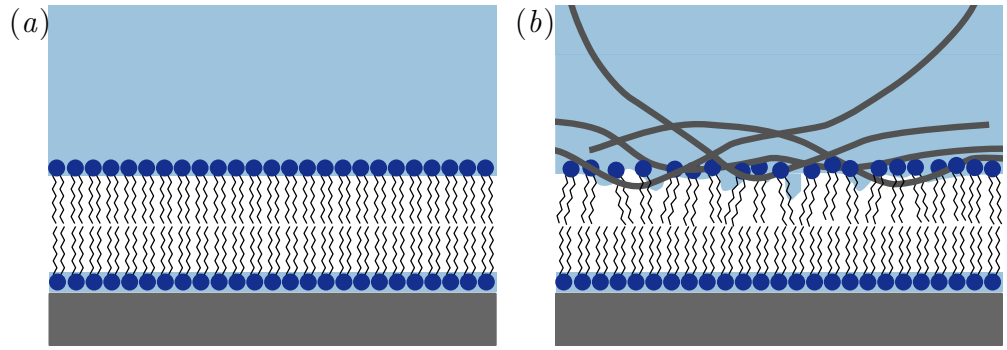

Figure 3.21: *(a) Sketch of a supported bilayer composed of DPPC only. (b) Sketch of a supported DPPC/HA layer.*

packing organization of the lipid molecules and the adsorption of HA between the head groups. Also a partial penetration of HA between the tail group region might be possible. The situation is schematically shown in fig. 3.21b. An infiltration of the tail group region by the HA chains might be facilitated by the hydrophobic patches present along the HA chains [42] [46] [104]. It seems likely that electrostatic attractions between positively charged NH_3^+ groups in the DPPC head groups and the negatively charged carboxyl groups of HA facilitates the adsorption, further may hydrophobic interactions between the non-polar patches along the HA chain and the alkyl chains of DPPC contribute. Association between phospholipids and hyaluronan in biological systems, not at least in the synovial joint area, is well documented (see e.g. [99] [105]) and adsorption of HA to DPPC bilayers is consistent with previous findings [16] [28].

Influence of HA on the phase behavior of DPPC

The measurements show that the phase behavior of composites of DPPC and

HA composites is very similar to the phase behavior of pure DPPC (see fig. 3.20). No transition can be observed at 25 °C and 39 °C as the pressure is increased up to 2000 *bar*, i.e. DPPC is in the gel phase at all pressures investigated. At 55 °C the head to head distance of the layer increases from 3.8 *nm* to 4.6 *nm* when the pressure is increased to 1000 *bar*, signifying a fluid to gel phase transition of the supported lipid bilayer. A striking difference between bilayers of DPPC with HA and pure DPPC bilayers is the reversible phase change observed upon decompression for the system composed of DPPC with HA. This means that the composite layer of DPPC and HA has a higher robustness against high pressures than sole DPPC bilayers. One reason could be that the DPPC bilayer with HA has a higher rigidity, caused by HA adsorbed to the lipid head groups. Friction-force measurements indicated a lower load bearing capacity of DPPC with HA compared to sole DPPC [28] [16], which was suggested to be due to a higher rigidity/lower flexibility of the layer. [106] Other studies also claim a higher robustness of DPPC/HA multilayers as compared to DPPC multilayers against high temperatures [97], which is complementary to our results.

Some further differences between sole DPPC and DPPC/HA with respect to pressure-induced changes in the $L_{\beta'}$ phase are observed. The head to head distance for pure DPPC bilayers shrinks up to 0.2 *nm* as the pressure is raised to 2000 *bar*, which is in the range of what has been reported previously for multilamellar DPPC systems [107]. In contrast, for composite DPPC/HA layers we could not observe any decrease of the layer thickness. The electron density profiles rather indicate that the head to head distance of the layers remains constant or even increases slightly at high pressures (1000 *bar* and 2000 *bar*). Such behavior has only been reported for the so called Gel III phase of multilamellar DPPC vesicles which has been observed at pressures above 2kbar [107]. This indicates a changed phase behavior of the supported bilayer due to the interaction with HA. A reason for this might be that the HA induced changes of the packing organization make a compression of the bilayer parallel to the Si surface more favorable.

3.2.2 Silicon supported DPPC with hyaluronan in sodium chloride solution with calcium chloride

After the sample system of Si supported DPPC/HA composite layers was extensively studied in a solution containing a physiological concentration of sodium chloride the salt composition was slightly changed. Besides monovalent ions also divalent ions can be found in the synovial fluid. To study their impact on the samples structure a small amount of $CaCl_2$ was added. Divalent ions can act as bridging agents [108] and DPPC is known to bind Ca^{2+} [86]. Therefore $CaCl_2$ might influence the interaction of HA and lipids and, thereby, change the properties of the system, which was also shown in chapter 3.1.2. To investigate this effect calcium chloride ($c_{CaCl_2} = 10\ mM$) was used and the system was studied under similar conditions as the system without calcium ions present. The lateral organization was studied using fluorescent microscopy, while the vertical structure of the DPPC and DPPC/HA layers was studied using X-ray reflectivity. Reflectivity measurements have been performed at 55 °C and 39 °C. Due to a limited time at the synchrotron beamlines no measurements were performed at 25 °C. The sample was probed at different pressures up to 2 *kbar*. Measurements were preferably done at 60 *bar* instead of 1 *bar* to avoid air bubbles in the XRR sample cell and it has been shown before (see appendix fig. A.4) that the sample did not change between 1 *bar* and 60 *bar*. The samples were measured at the ID15 beamline, ESRF, Grenoble (for details see sec. 2.2.4).
In the following, first the result obtained from fluorescent microscopy are presented. Afterwards the results from XRR measurements are shown, starting with the results of sole DPPC samples in a solution containing NaCl and $CaCl_2$ at different temperatures and pressures. After DPPC as reference system is described results for samples composed of DPPC with HA in NaCl/$CaCl_2$-solution are shown, to evaluate the influence of HA on DPPC layers in the presence of $CaCl_2$.

3.2.2.1 Lateral structure on the micro meter scale

Images of Si supported DPPC and DPPC/HA samples in 150 mM NaCl with 10 mM $CaCl_2$ were recorded with a fluorescence microscope are shown in figure 3.22 together with images of samples in 150 mM NaCl (left half of the images). Full images of the samples in NaCl/ $CaCl_2$ solution can be found in the appendix (A.7). The samples were prepared as described in section 2.1.2 and according to the used fluorescent labels DPPC appears green in the microscope images and HA appears red. As explained in section 2.2.5 the wafer was slightly tilted during the

measurements. Therefore not the complete field of view was in the focal plane. Images A-C in figure 3.22 show that the wafers are completely covered with DPPC and in the presence of HA (images B and C) the coverage appears less homogenous as for sole DPPC (images A). It also seems that HA1500 (image C) had a stronger

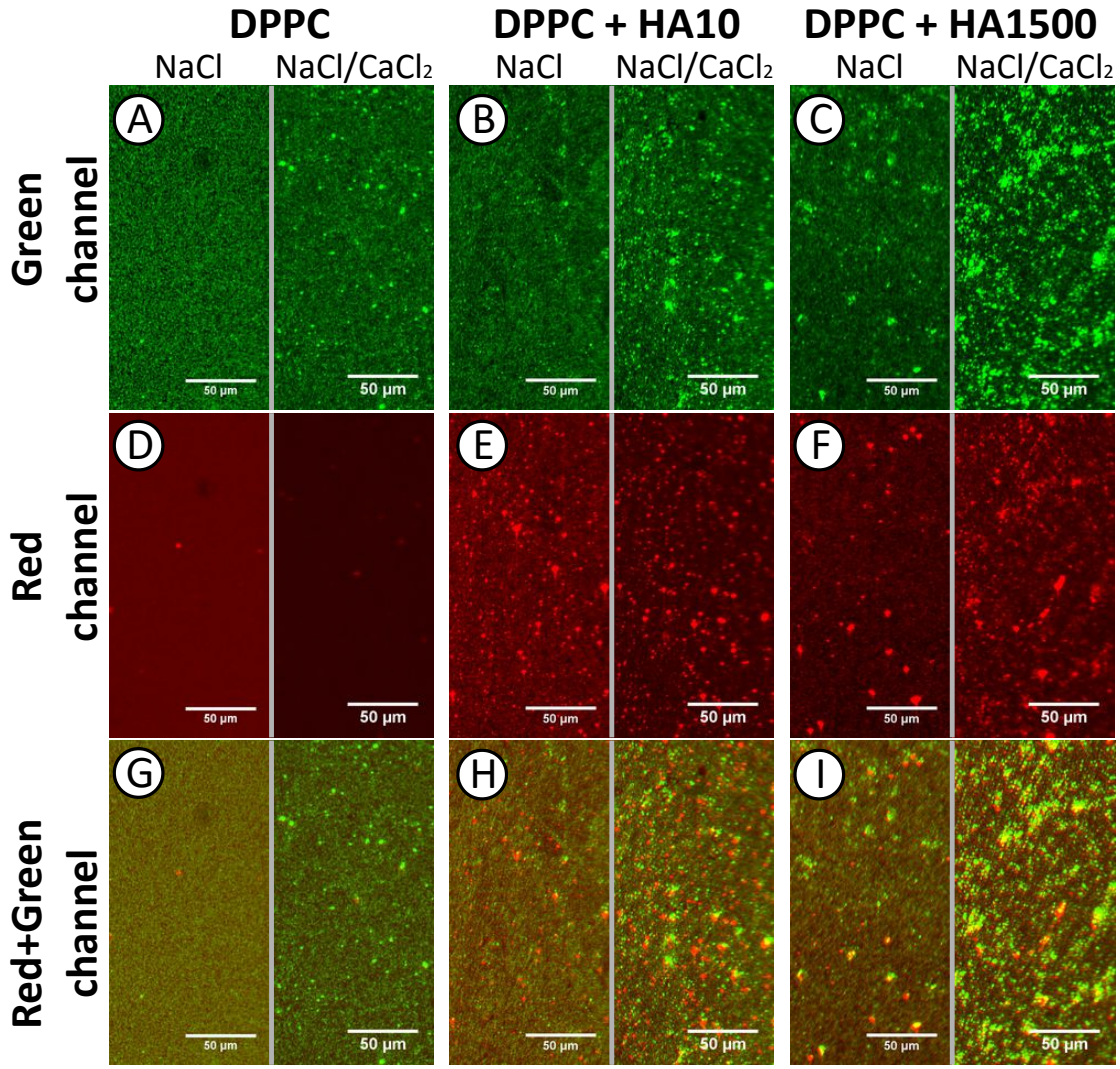

Figure 3.22: *Fluorescence microscopy images of Si supported DPPC and DPPC/HA composites in two different solutions:* 150 *mM NaCl (left)* 150 *mM NaCl with* 10 *mM* $CaCl_2$ *(right). DPPC was labeled with NBD (green channel) and HA was labeled with Rhodamine (red channel)*

impact on the coverage of the DPPC bilayer than HA10 (image B). These finding are valid for samples in both solution.

Images of sole DPPC in 150 *mM* NaCl with 10 *mM* $CaCl_2$ solution show a slight red background (image D in fig. 3.22). Since this background differs significantly from the structures seen for DPPC/HA samples (images E and F) it can be concluded that the signal seen for DPPC/HA stems from the labeled HA that had adsorbed

to the DPPC bilayer. The coverage of HA is very inhomogeneous, which can be concluded from the striking bright red spots hinting at accumulations of HA at certain places. These spots are usually colocalized with bright green spots (accumulations of DPPC) as it can be seen in the images H and I in figure 3.22). The images of DPPC and DPPC/HA in a NaCl/ $CaCl_2$ solution show similar trend as the images of the samples in sole NaCl solution (fig. 3.22). However, the DPPC/HA samples in NaCl/$CaCl_2$ solution show less homogenous coverage of DPPC, with more and larger areas showing a strong accumulation of DPPC (bright green spots), than in sole NaCl solution. This effect is illustrated in figure

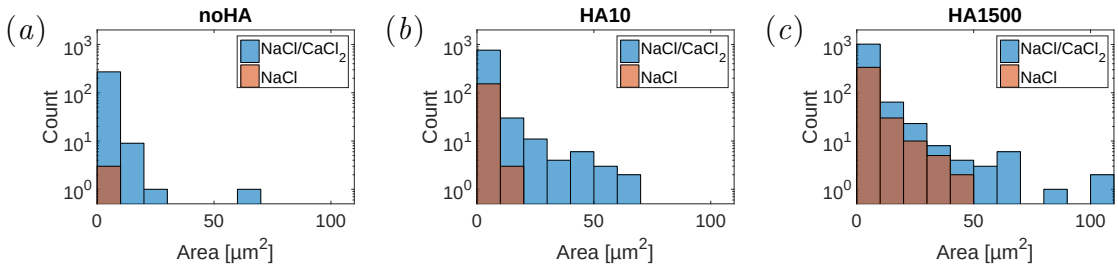

Figure 3.23: *Histograms illustrating the size and count of spots with an increased accumulation of DPPC. Full versions of the images found in figure 3.22 were evaluated. (a) DPPC (b) DPPC with HA10 (c) DPPC with HA1500.*

3.23 where histograms showing the size and number of these spots of samples in NaCl and NaCl/ $CaCl_2$ are compared. The spot size as well as the number of the spots is larger for samples in a solution with 150 mM NaCl and 10 mM $CaCl_2$. These figures show that $CaCl_2$ has a strong impact on the distribution of DPPC and that it also amplifies the effect of HA on the DPPC bilayer.

3.2.2.2 Structure of DPPC in a calcium chloride solution

First the influence of $CaCl_2$ on the interaction of solid supported sole DPPC bilayers will be studied. The influence on DPPC/HA samples will be shown in the next section. Solid supported DPPC bilayers were studied at two different temperatures (39 °C and 55 °C) and different hydrostatic pressures between 60 *bar* and 2000 *bar* in a solution with 150 mM NaCl and 10 mM $CaCl_2$. The samples were prepared

as described in section 2.1.2. The pressure was first increased stepwise with measurements at 60 *bar*, 100 *bar*, 500 *bar*, 1000 *bar* and 2000 *bar*, and afterwards the pressure was released and a final measurement was been performed at 60 *bar* (in the following 60 *bar* D). As described in section 2.2.4 the measured reflectivity data was fitted with a model electron density for a bilayer consisting of six slabs (see fig. 2.14). Fresnel normalized reflectivity curves of the complete pressure cycle together with the fits and the model electron densities are shown in the appendix in figure A.9 and A.10, for 39 °C and 55 °C, respectively.
Model electron densities for the measurements at four pressure steps at 39 °C are shown in figure 3.24a. The electron densities show the typical shape of a solid

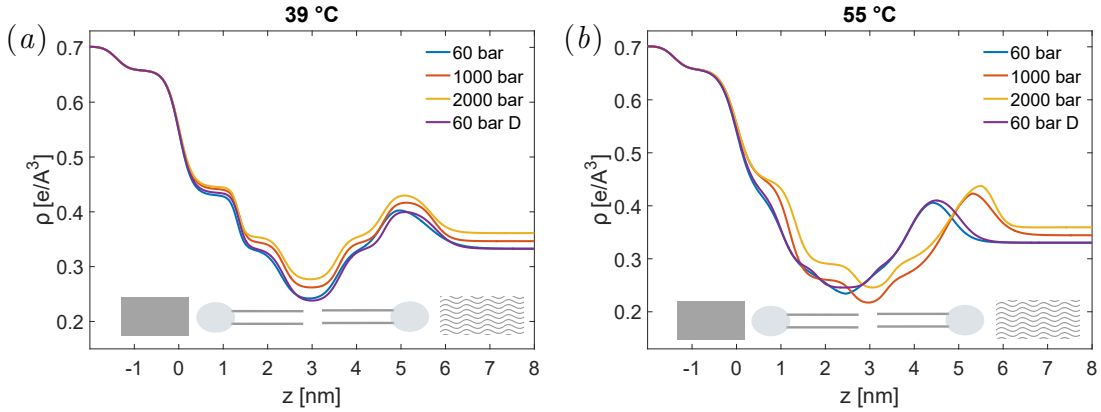

Figure 3.24: *Electron density profiles of DPPC samples at* 39 °*C and* 55 °*C and different pressures in* 150 *mM NaCl with* 10 *mM* $CaCl_2$. *(a) DPPC sample at* 55 °*C. (b) DPPC sample at* 55 °*C.*

supported bilayer. Starting left with a very high electron density of the Si-support (pure Si and SiO_2), followed by a slab for the head group of the lower leaflet, the tail group of the lower leaflet, a slab for the CH_3 group of both leaflets, the tail group of the upper leaflet, the head group of the upper leaflet and finally the water phase. Lower and upper leaflet are very symmetric and show a low roughness. The model for the DPPC sample shows only small changes due to the increased hydrostatic pressures, like the general level of the electron density, which rises as a function of the hydrostatic pressure. Also the electron density of the water phase increases. The layer thickness does not change strongly. It looks a as if the layer at 60 *bar* has a slightly decreased width, but the calculated head-to-head distances in figure 3.25 show only minor differences: 4.4 *nm* for DPPC at 60 *bar* and 4.5 *nm* at 1000 *bar*. This small difference of 0.1 *nm* is within the error for the head-to-head distance.
Electron density profiles for DPPC samples at four different pressures at 55 °C are

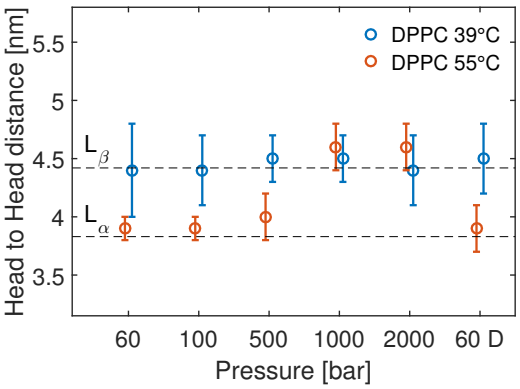

Figure 3.25: *Head-to-head distances of DPPC in* 150 *mM NaCl with* 10 *mM* $CaCl_2$ *for all pressure steps at* 39 °*C and* 55 °*C. The black broken line show the head-to-head distance of for the* $L_{\beta'}$ *phase* ($\approx$ 4.4 *nm*) *and the* L_α *phase* ($\approx$ 3.8 *nm*) *[33].*

shown in figure 3.24b. The profiles show also typical symmetric bilayer structures. A clear structural difference of the structure can be observed between the profiles for 60 *bar* and pressures $\geq$ 1000 *bar* (the transition occurred between 500 and 1000 *bar*, see appendix fig. A.10). At 60 *bar* the bilayer has a lower thickness than at pressures $\geq$ 1000 *bar*. For 60 *bar* a head-to-head distance of 3.9 *nm* was found while it was 4.6 *nm* at 1000 *bar*, which is comparable to the values found for DPPC at 39 °C (see fig. 3.25). From 1000 *bar* to 2000 *bar* a further, very small increase of the thickness can be observed in the electron density profiles in figure 3.29a. However, these differences are in the range of the uncertainties ($\approx 0.1 - 0.2$ *nm*) and the head-to-head distance stays constant. Besides having different thicknesses the two different states (at low and high pressure) differ in the shape of the electron density. At 60 *bar* the bilayer is very symmetric and has a high overall roughness. At pressures $\geq$ 1000 *bar* the roughness of the lower leaflet decreases, while the upper leaflet still shows a high roughness. The structural transition, occurring between 60 *bar* and 1000 *bar*, is almost completely reversible. Only small differences in the head group region of the upper leaflet can be observed, which also lead to different (in the range of the uncertainties) head-to-head distances.

3.2.2.3 Structure of DPPC with hyaluronan in a calcium chloride solution at different temperatures

XRR measurements of DPPC and HA were performed at 60 *bar* and two different temperatures: 39 °C and 55 °C. For the experiments HA of two different molecular weights was used. Low molecular weight HA with $M_W = 10$ *kDa* and high molecular weight HA with $M_W = 1500$ *kDa*. The samples were prepared as described in

section 2.1.2 and the measured reflectivity curves were fitted with model electron density build up of six slabs as described in section 2.2.4.
The Fresnel normalized reflectivity curves and fits of all sample are shown in figure 3.26a along with to the curves of sole DPPC. The electron density profiles calculated from these curves are shown in figure 3.26b and they are not deviating much from the shape for Si supported lipid bilayers. First structural differences between

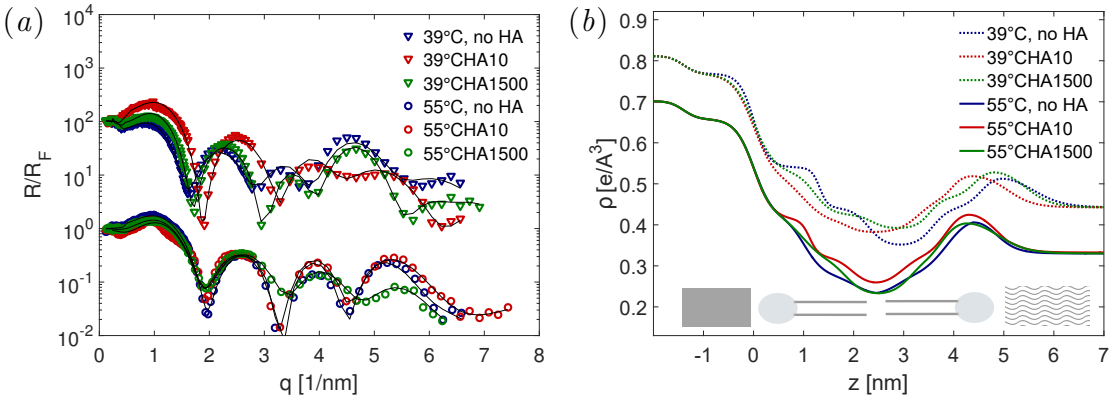

Figure 3.26: *(a) Fresnel normalized scattering curves with fits of DPPC and DPPC with HA (M_W = 10 kDa and M_W = 1500 kDa), recorded at* 60 *bar and* 39 °*C and* 55 °*C in a solution containing* 10 mM $CaCl_2$. *(b) Calculated electron density profiles. The offset between* 39 °*C and* 55 °*C is for clarity.*

samples studied at 39 °C can be directly derived from these Fresnel normalized reflectivity curves without further analysis. The position of the first minimum indicates that he layer composed of sole DPPC has the highest thickness, as the minimum can be found at the lowest q-value: $q_{min} = 1.64 \pm 0.03\ nm^{-1}$. From the calculated electron density profiles (see fig. 3.26b) the head-to-head distance was determined to be $4.4 \pm 0.2\ nm$ for DPPC at 39 °C (see tab. 3.6). In contrast the sample composed of DPPC and low molecular weight HA ($M_W = 10\ kDa$) has the lowest thickness of the three samples, as the minimum can be found at the highest q-value: $q_{min} = 1.90 \pm 0.03\ nm^{-1}$. The corresponding head-to-head distance (determined from the electron density profiles) is $4.0 \pm 0.2\ nm$. This value is comparable to the thickness of sole DPPC at 55 °C. DPPC with HA1500 has a head-to-head distance which is only 0.1 nm lower than for sole DPPC which is also reflected in the fact that the Fresnel normalized scattering curves of these two samples are very similar. DPPC/HA composite samples show a much higher overall roughness than the samples of sole DPPC, especially the sample with low molecular weight HA. Further, they show an asymmetry between the upper and lower leaflet. The electron density of the tail group region of the upper leaflet is strongly increased and considerably higher than the electron density of the lower

leaflet. In general the structure of the lower leaflet is not as pronounced as the structure of the upper leaflet, i.e. the roughnesses of the single slabs is higher in the lower leaflet. In contrast, the electron density profile of sole DPPC sample is very symmetric. However, all profiles show a high roughness at the composite layer-water interface.
The shape of the Fresnel normalized reflectivity curves of the DPPC and DPPC/HA samples measured at 55 °C differs considerably from the curves of the samples measured at 39 °C, as it can be seen in figure 3.26a. The position of the first minimum of the samples measured at 55 °C can be found at higher q-values than the position of the samples measured at 39 °C, which hints at lower layer thicknesses. Consequently the head-to-head distance of the samples at 55 °C, determined from the electron density profiles (see fig. 3.26a), is around 0.5 nm smaller than for samples at 39 °C. Almost no differences of the positions of the minimum and therefore also just very small differences of the thickness (see tab. 3.6) can be found between samples of pure DPPC and DPPC/ HA composite layers measured at 55 °C. The

Table 3.6: *head-to-head distance of DPPC and DPPC/HA layers at two different temperatures and* 60 *bar*.

	no HA	HA10	HA1500
39 °C	$4.4 \pm 0.2\ nm$	$4.0 \pm 0.2\ nm$	$4.3 \pm 0.2\ nm$
55 °C	$3.9 \pm 0.2\ nm$	$3.8 \pm 0.2\ nm$	$3.8 \pm 0.2\ nm$

shape of the Fresnel normalized curves of the DPPC sample and the sample composed of DPPC and low molecular weight HA show in general a very similar shape. In contrast the curve of DPPC with high molecular weight HA has a slightly different shape, which results in large differences of the electron density profiles. While the profile for the DPPC/HA1500 layer shows a very high roughnesses between the different slabs, which can already be deduced from low oscillations of the Fresnel normalized curves at high q, the DPPC/HA10 profile is very pronounced with a generally higher electron density. The head group of the DPPC/HA composite layer is broader than the head group of sole DPPC and the electron density of the tail groups is lower for sole DPPC. In contrast to the electron density profiles of the samples measured at 55 °C (see fig. 3.26b), the profiles from 39 °C are quite symmetric.

3.2.2.4 Structure of DPPC with hyaluronan at high hydrostatic pressures

Measurements of samples composed of DPPC with HA were performed at high hydrostatic pressures up to 2000 *bar* at two different temperatures (39 °C and 55 °C). Again, HA of two molecular weights, $M_W = 10\ kDa$ and $M_W = 1500\ kDa$, was used for the experiments. The samples were prepared as described in section 2.1.2. All samples were probed with the same pressure cycle. The pressure was first increased stepwise from 60 *bar* to 2000 *bar*, with a measurement at 60 *bar*, 100 *bar*, 500 *bar*, 1000 *bar* and 2000 *bar*, and afterwards the pressures was released and a final measurement was performed at 60 *bar*. In the following this pressure step will be denoted as 60 *bar* D, as it was measured after decreasing the pressure. The collected reflectivity curves were fitted with model electron density, as described in section 2.2.4. Fresnel normalized reflectivity curves with fits and electron density profiles can be found in the appendix in figure A.11 - A.13.
In figure 3.27 the electron density profiles obtained for samples composed of DPPC and HA measured at 39 °C in 150 mM NaCl and 10 mM $CaCl_2$ are shown. Comparing the profiles of sole DPPC samples (see fig. 3.24a and b), the profiles of the sample composed of DPPC and HA with a low molecular weight of 10 kDa (see fig. 3.27a) a strong modification of the structure and a different response to high hydrostatic pressures is obvious. As already described in the chapter before, the bilayer of the DPPC/ HA10 sample is in general very asymmetric. Further, a strongly differing structural transition can be observed within the pressure cycle. The structural changes are also not reversible. At 60 *bar* the lower leaflet of the bilayer is very smeared out with a high roughness between the head group and the tail group as it was observed for sole DPPC at 55 °C. An increase of the pressure lead to a structural transition between 100 *bar* and 500 *bar* as it can be concluded from figure A.11 in the appendix, where the electron density profiles for all pressures are shown. At pressures of 500 *bar* and above the head-to-head distance of is increased to 4.4 nm − 4.5 nm, as illustrated in figure 3.28. At lower pressures the value is 4.0 nm. The increase of the head-to-head distance is mainly caused by a structural change of the lower leaflet. For pressures $\geq$ 500 *bar* the structure of the lower leaflet became similar to the structure of sole DPPC, well defined interface between the head group region and the tail group region and a strong increase of the electron density. But also the upper leaflet changes, especially the head group region. Its width increases massively. In general the bilayer does not become symmetric, also the electron density of the tail group region of the upper

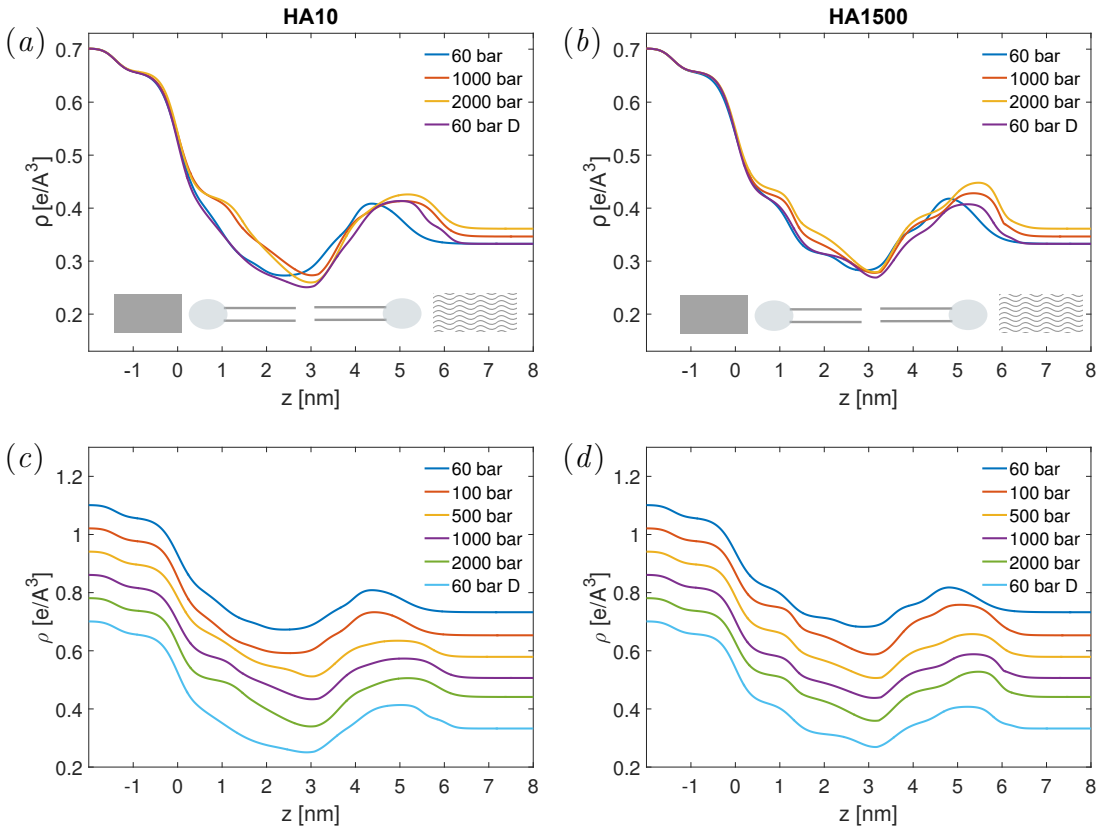

Figure 3.27: *Electron density profiles of DPPC/HA composite samples at* 39 °*C and different pressures. (a) Sample composed of DPPC and HA with* $M_W = 10$ *kDa at four pressures. (b) Sample composed of DPPC and HA with* $M_W = 1500$ *kDa at four pressures. (c) Profiles of DPPC/HA10 at all pressures. Offset for clarity. (d) Profiles of DPPC/HA1500 at all pressures. Offset for clarity.*

and lower leaflet have considerably different levels (with a higher density of the upper leaflet). After the pressure was decreased to 60 *bar* D a further structural change can be observed. The lower leaflet rearranges into its original structure, while the structure of the upper leaflet keeps the shape it has at high pressures. Consequently the head-to-head distance of the bilayer is 4.2 *nm*. This value is in between the observed head-to-head distance of the layer at 60 *bar* and 2000 *bar*.
The profiles of the sample composed of DPPC and HA with a molecular weight of $M_W = 1500$ *kDa* are shown in figures 3.27b and d. This sample show overall the same behavior as the sample with low molecular weight HA ($M_W = 10$ *kDa*). Around 100 *bar* a transition of the structure can be observed (see fig. 3.27d). At all pressures the layer is asymmetric with a higher electron density in the tail group region of the upper leaflet than in the tail group region of the lower leaflet. Increasing the pressure from 60 *bar* to 1000 *bar* lead to an increase of the head-to-head distance from 4.3 *nm* to 4.7 *nm* (see fig. 3.28) and an alteration of the bilayer

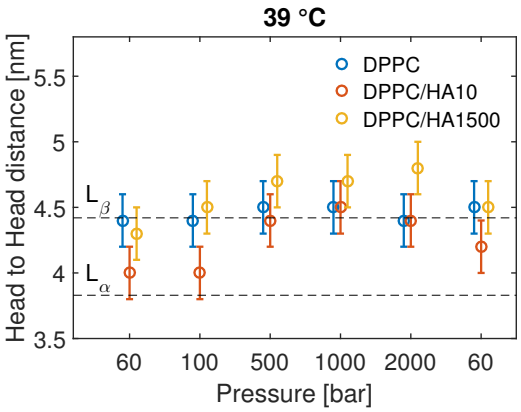

Figure 3.28: *Head-to-head distance of the samples measured at* 39 °*C as function of the hydrostatic pressure. The black broken line show the head-to-head distance of for the* $L_{\beta'}$ *phase* ($\approx$ 4.4 *nm*) *and the* L_α *phase* ($\approx$ 3.8 *nm*) *[33].*

shape can be observed. Especially for the lower leaflet an increase of the electron density and a decrease of the roughness can be detected. A further increase of the hydrostatic pressure to 2000 *bar* causes mainly a higher electron density. Decreasing the pressure back to 60 *bar* has a similar effect as for the low molecular weight HA. While the original shape of the lower leaflet is mainly restored, the upper leaflet kept roughly the shape of the bilayer from high hydrostatic pressures ($\geq$ 1000 *bar*). Thus, the head-to-head distance of the bilayer at 60 *bar* D has a value of 4.5 *nm*.

In figure 3.29a and c the electron density profiles of a sample composed of DPPC and HA with a molecular weight of $M_W = 10\ kDa$ are shown, which were measured at 55 °C. Like the profiles of sole DPPC (see fig. 3.24b) a clear bilayer structure can be seen, with a structural transition that occurs between 500 *bar* and 1000 *bar* (see fig. 3.27c). At low pressures ($\leq$ 500 *bar*) the bilayer structure is symmetric, only the roughness of the lower leaflet is a little bit lower. At high pressures ($\geq$ 1000 *bar*) the bilayer is not symmetric anymore. The upper leaflet shows a significantly higher electron density compared to the lower leaflet. Interestingly the asymmetry is mainly caused by a change of the upper leaflet. The lower leaflet shows only a changed thickness (especially of the the tail group region) of $\approx$ 0.6 *nm*. The upper leaflet in contrast changes its shape considerably. An increase of the pressure to 2000 *bar* lead to a strong overall increase of the electron density. After decreasing the pressure to 60 *bar* D the original shape of the bilayer structure is nearly restored. The head-to-head distance of the bilayer increases as function of the hydrostatic pressure (from $\leq$ 500 *bar* to $\geq$ 1000 *bar*) from 4.0 *nm* to 4.5 *nm*, which can be seen in figure 3.30. A further increase from 1000 *bar* to 2000 *bar*

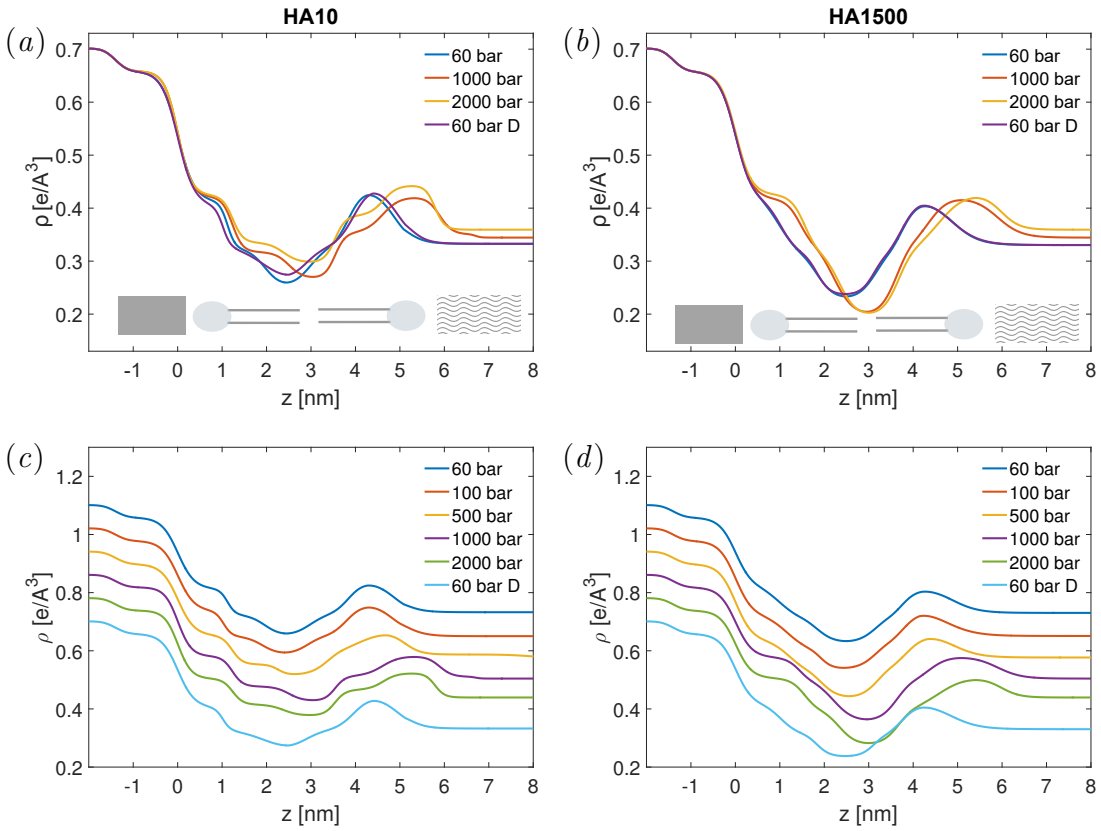

Figure 3.29: *Electron density profiles of DPPC/HA composite samples at 55 °C and different pressures. (a) Sample composed of DPPC and HA with $M_W = 10$ kDa at four pressures. (b) Sample composed of DPPC and HA with $M_W = 1500$ kDa at four pressures. (c) Profiles of DPPC/HA10 at all pressures. Offset for clarity. (d) Profiles of DPPC/HA1500 at all pressures. Offset for clarity.*

leads to a small decrease (0.1 *nm*) of the head-to-head distance, which is within the uncertainties.

The electron density profiles of samples composed of DPPC and HA with a molecular weight of $M_W = 1500$ *kDa*, which were measured at 55 °C, are presented in figure 3.29b and d. They show as well as the profiles of samples composed of sole DPPC and DPPC with low molecular weight HA a bilayer shape and a structural transition between 500 *bar* and 1000 *bar* (see fig. 3.29d). A very dominating CH_3 group region could be detected (see fig. 3.29b). At low pressures ($\leq$ 500 *bar*) the bilayer is symmetric and shows a very high roughness. Increasing the pressure above 1000 *bar* lead to slight changes of the bilayer shape, as it can be seen in figure 3.29b. The bilayer becomes slightly asymmetric with a higher electron density of tail group region for the upper leaflet compared to the lower leaflet. Further, the CH_3 group region is also at high pressures very dominant and the roughness between the CH_3 group region and the tail group region is very high. A further

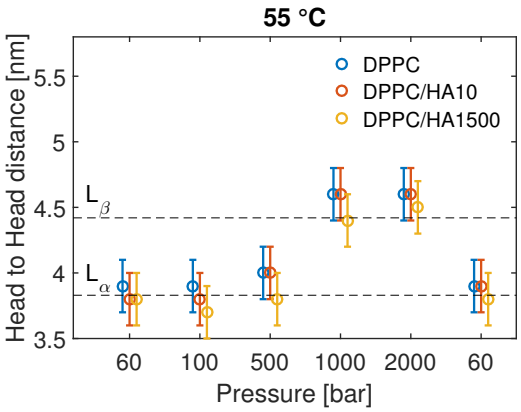

Figure 3.30: *Head-to-head distance of the samples measured at* 55 °*C as function of the hydrostatic pressure. The black broken line show the head-to-head distance of for the* $L_{\beta'}$ *phase* ($\approx$ 4.4 *nm*) *and the* L_α *phase* ($\approx$ 3.8 *nm*) *[33].*

increase of the hydrostatic pressure to 2000 *bar* causes only a slight increase of the bilayer thickness (0.1 *nm*). After decreasing the pressure back to 60 *bar* D the original structure of the bilayer is completely restored. The structural transition between 500 *bar* and 1000 *bar* leads also to different head-to-head distances: 3.8 *nm* for pressures $\leq$ 500 *bar* and 4.4 *nm* for pressures $\geq$ 1000 *bar*, as shown in figure 3.30.

3.2.2.5 Discussion

In the following the results obtained from the measurements of Si supported DPPC bilayers and DPPC/HA in a solution containing NaCl and $CaCl_2$ will be discussed. First the influence of $CaCl_2$ on the structure of DPPC and DPPC with HA will be discussed, followed by a discussion on the influence of $CaCl_2$ on the phase behavior of DPPC (in the absence and presence of HA) at high hydrostatic pressures. Finally the results from Si supported samples will be compared to the results from vesicles samples.

The effect of Calcium on the structure of DPPC and DPPC/HA at low pressure

From the fluorescent microscopy images conclusions about the lateral structure and organization on the micrometer scale of Si supported DPPC and DPPC/HA layers can be drawn. The images show in general similar trends as the images from samples in sole NaCl solution. DPPC and HA are distributed over the whole wafer. HA shows a non homogenous distribution of HA and many bright red spots

indicate a accumulation of HA. Therefore, the existence of a compact HA layer can be excluded. Further, the DPPC coverage looks less homogenous in the presence of HA. The number and size of spots with strong accumulation of DPPC is much higher in the presence of HA, as it can be seen in the histogram figure (fig. 3.23). This is consistent with the results from samples in sole NaCl solution and AFM images by Wang et al 2013 [28]. Again, it could seen that HA with a higher molecular weight seems to have a stronger effect (more and larger areas of DPPC accumulation) on the lateral structure of the sample than HA with low molecular weight. However, comparing the images from samples in sole NaCl solution with samples in NaCl/ $CaCl_2$ solution it can be observed that $CaCl_2$ induces a stronger inhomogeneity of the DPPC bilayer especially for DPPC/ HA composite samples. This can be explained by a stronger interaction between DPPC and HA due to the presence of divalent Ca^{2+} ions, acting as bridging agents, as it was already proposed for the interaction of DPPC vesicles and HA in the presence of Ca^{2+}. Wieland et al. 2016 [98], who recently studied the interaction of DPPC monolayer at the air liquid interface on a subphase containing HA, report on a quite similar effect. Brewster angle microscopy images of the DPPC layer at the air liquid interface show a strong alteration of the structures on the micrometer scale when $CaCl_2$ was added to the solution. Especially for HA with a molecular weight of $M_W = 1500\ kDa$ the structures also became very inhomogeneous. The changes of the structures are claimed to be due to an increased interaction of DPPC and HA, caused by divalent Ca^{2+} ions. Besides increasing the interaction of DPPC and HA, Ca^{2+} could also facilitate a stronger interaction between the Si support and DPPC or between the Si support and HA, which could also lead to a higher inhomogeneity of the DPPC bilayer. It is already reported that Ca^{2+} ions do strongly change the interactions at the Si-water interface, as the ions could enable a bridging between the negatively charged Si surface and negatively charged molecules like HA or between the Si surface and DPPC [53, 108]. This would also explain why even the sole DPPC bilayer in the NaCl/ $CaCl_2$ solution shows a lower homogeneity than a DPPC bilayer sole NaCl.

Results from XRR experiments, performed at 60 *bar*, provide information about the vertical structure of the samples. XRR measurements with $CaCl_2$ were performed at 39 °C and 55 °C, corresponding to the $P_{\beta'}$ and the L_α phase in bulk, respectively (see DSC results in sec. 3.1.2) [30]. However, as discussed for the DPPC samples in sole NaCl solution it is very likely that the $P_{\beta'}$ phase is suppressed for DPPC bilayers on solid support and that the DPPC bilayer is instead in the $L_{\beta'}$ phase at 39 °C [35, 36]. The shape of the electron density profiles of sole

DPPC as well as the values found for the head-to-head distances (see fig. 3.25) are comparable to the results from supported DPPC in sole NaCl solution and to the results from SAXS measurements on bulk solution (see sec. 3.1.2.3). They confirm that the bilayer is in $L_{\beta'}$ phase at 39 °C and in L_α phase at 55 °C [30, 33, 87, 95]. After the effect of $CaCl_2$ on Si supported sole DPPC layers has been discussed the effect on DPPC HA composite layers will be discussed now. The profiles of DPPC with HA in a solution containing NaCl and $CaCl_2$ are asymmetric. The electron density of the tailgroup of the upper leaflet is slightly higher than the electron density of the tailgroup of the lower leaflet (see fig. 3.26b). As such a strong asymmetry is not observed in sole NaCl solution, it can be concluded that it is facilitated by divalent Ca^{2+} ions. The asymmetry is probably caused by changed packing of the lipids in the upper leaflet, due to a stronger interaction between HA and DPPC. It is known that Ca^{2+} ions are enriched in the plane of lipid head groups [86] and as Ca^{2+} can lead to charge inversion of the negatively charged phosphate group it is very reasonable that the negatively charged HA can accumulate easily between the head groups. Much better than for samples in sole NaCl were it gets repulsed by the phosphate groups. The asymmetry can also be interpreted as a decoupling of the two leaflets. A decoupling was already claimed for mica supported DMPC and DPPC bilayers studied with AFM [109–111] and is facilitated by a $CaCl_2$ induced strengthened binding between the lipids and Si substrates [53]. The two leaflets therefore are in contact with two very different environments, that both strongly interact with the DPPC molecules. At 55 °C the asymmetry is weaker than at 39 °C. Here, the lipid tails are more flexible and the molecules have a higher mobility. This higher flexibility is probably the reason for lower asymmetry.
Further, the head-to-head distance of the samples composed of DPPC and HA in a solution containing NaCl and $CaCl_2$ shows a very interesting effect. In general, the head-to-head distance is the same as for sole DPPC samples (see tab. 3.6), within the the range of the uncertainties. This was also observed for samples in sole NaCl solution. Only for the sample containing HA with a molecular weight of $M_W = 10\ kDa$ $CaCl_2$ lead to a strong decrease of the head-to-head distance of around 0.4 nm at 39 °C. The thickness of this sample is closer to the thickness of the DPPC sample at 55 °C than to the thickness of the DPPC sample at 39 °C and also the shape of the electron density profiles of this sample show the typical characteristics (high roughness between the single slabs of the bilayer) of a sample at 55 °C. This was not observed for DPPC/ HA10 samples in sole NaCl solution. Therefor it seems that at 39 °C $CaCl_2$ does change the phase of the bilayer from $L_{\beta'}$ to L_α for samples composed of DPPC and HA of a molecular weight of

$M_W = 10\ kDa$. A transition from $L_{\beta'}$ to $P_{\beta'}$ can be excluded as the head-to-head distance of lipid bilayer in these two phases should be almost identical [34, 112]. Since the DSC measurements only revealed a small decrease of the transition temperature in the presence of HA (to 42 °C), HA alone cannot be responsible for this effect. Further, such an effect was not observed for DPPC and HA in solution containing only NaCl. Therefore the origin must be a complex interplay between the Si support, the Ca^{2+} ions and the low molecular weight HA. It can be speculated that the bilayer at 39 °C is in a energetically unfavorable state, due the suppressed ripple phase. This leads in combination with the disturbance of the lipid ordering by HA to a change in the phase behavior. The fact that both leaflets, the lower and the upper leaflet, are disturbed might be explained by the low molecular weight of the HA. HA with a molecular weight of 10 kDa is, in contrast to the coiled structure of high molecular weight HA [45, 93], rod like [113]. Thus it may diffuse through small voids and cracks in the bilayer between the Si surface and DPPC bilayer. The adsorption of HA at the Si surface might can be facilitated by Ca^{2+} ions, as it is known that they can bridge the negative charge of the Si surface and negative charge of molecules [53, 108].

The effect of HA on the phase behavior and structure of DPPC at high pressures

First the behavior of sole DPPC samples at high pressure in NaCl/ $CaCl_2$ solution will be discussed, followed by a discussion of DPPC/ HA composite samples. At 39 °C the DPPC bilayer does not show a structural transition, as for Si supported DPPC in NaCl, and the head-to-head distance correlates with the value for DPPC in the $L_{\beta'}$ phase (see fig. 3.28). At 55 °C the head-to-head distance of the bilayer indicates that the bilayer is in the L_α phase below 500 bar and in the $L_{\beta'}$ phase above 500 bar (see fig. 3.28 and 3.30), which is in accordance with the literature [103, 114]. Thus the measurements DPPC samples at different hydrostatic pressures between 60 bar and 2 $kbar$ at 39 °C and 55 °C show the expected phase behavior [32, 103, 114] with a suppressed rippled phase [35, 36] as for DPPC in sole NaCl. The absence of the $P_{\beta'}$ phase can be for example deduced from the fact that no structural transition was observed at 39 °C. According to Winter et al. 2009 [32], who studied the phase behavior of DPPC vesicles at high hydrostatic pressures, an increased hydrostatic pressure should lead to a phase transition from $P_{\beta'}$ to $L_{\beta'}$ at around 500 bar. This transition should alter the structure of the bilayer (as discussed in section 3.2.1.5). However, at 55 °C a differing behavior of

DPPC in the two solution conditions is revealed. Bilayers in a solution containing NaCl and $CaCl_2$ shows a reversible phase transition (L_α - $L_{\beta'}$ - L_α). For bilayers in sole NaCl solution it was observed that DPPC bilayers at 55 °C get damaged by the phase transition at high pressures. It seems likely that Ca^{2+} ions leads to a stabilization of the bilayer. Several studies already claimed that these ions bind to the negatively charged phosphate groups of the lipid heads [82, 83, 86, 87]. Thereby a bridging between the single lipids occurs (as already discussed in section 3.1.2), that probably inhibits a break down of the bilayer structure. Further, it is known that Ca^{2+} ions do alter the properties of solid supported bilayers as they induce a strong interact of the lipids and the surface [115], which leads to a further stabilization.

After the phase behavior of sole DPPC samples has been discussed, the influence $CaCl_2$ on the samples composed of DPPC and HA can be examined. HA with two different molecular weights was studied to investigate the effect of the molecular weight on the interaction between DPPC and HA. $CaCl_2$ causes strong differences in the phase behavior as well as in the structure of the DPPC/ HA composite layers. Especially at higher pressures new structures form, which do not look like typical bilayers.

HA/DPPC composite samples at 39 °C show an asymmetry at all pressures (see fig. 3.27), with a higher electron density of the tailgroup of the upper leaflet than of the lower leaflet. It has been discussed before that this hints at a strong accumulation of HA between the lipids, due to a stronger interaction between DPPC and HA in the presence of Ca^{2+} ions, as also reported by Wieland 2016 [98]. This increased interaction has the effect that the sample composed of DPPC and low molecular weight HA ($M_W = 10\ kDa$) is in the L_α phase at 60 bar. At increased pressure the electron density profiles show structural changes between 100 bar and 500 bar and between 60 bar and 100 bar, for HA of molecular weight of 10 kDa and 1500 kDa, respectively. This can be seen in figure 3.27c, figure 3.27d and also concluded from the head-to-head distances in figure 3.28. For DPPC with HA10 this change seems to be a sign for a phase transition. Above 100 bar DPPC/ HA10 is in the $L_{\beta'}$ phase while below 100 bar it is seems to be in the L_α phase. DPPC with HA1500 probably remains in the $L_{\beta'}$ phase at all pressures, which means that the structural change is not associated with a phase transition. The structural modification and especially the phase transition were not expected, as such a behavior is neither observed for sole DPPC in NaCl/ $CaCl_2$ solution nor for DPPC and DPPC/HA in sole NaCl solution. After the modification the shape of the electron density profiles of the DPPC/HA samples is strongly altered and the asymmetry iss even

more increased. Especially the electron density level of the tail group of the upper leaflet is further increased. This might be due to a reordering at high pressures, as exemplary illustrated in figure 3.31 for DPPC with HA10. At high pressures after

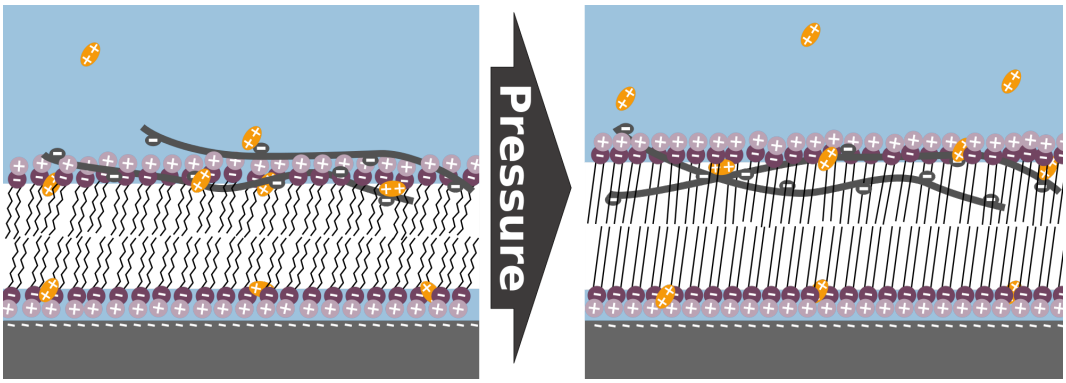

Figure 3.31: *Sketch of the structure of Si supported DPPC/HA samples at low (left) and high (right) pressure.*

the transition HA gets squeezed into tail group region and increases thereby the electron density. It is well known that hydrophobic interaction gets weaker at high hydrostatic pressure [116], which could facilitate an adsorption of HA in the tail group region. After releasing the pressure the electron density profiles show that the upper leaflet of the DPPC/HA samples does not restore its original structure (see fig. 3.27a and b), which means that the HA chains remain within the tail group region. In contrast, the transition of lower leaflet, where no HA is incorporated, is fully reversible. It should be noted that the two bilayer leaflets of the DPPC/ HA10 composite sample seem to be completely decoupled with the lower leaflet being in the L_α phase and the upper leaflet in the $L_{\beta'}$ phase.
At 55 °C the head-to-head distances (see fig. 3.30) at different pressures indicate that the phase behavior of the sample is similar to sole DPPC and also to DPPC with HA in sole NaCl solution and in accordance with the literature [30, 32, 103]. Below 500 *bar* the head-to-head distance of the bilayer corresponds very well to a DPPC bilayer in the L_α phase and above 500 *bar* it corresponds to a DPPC bilayer in the $L_{\beta'}$ phase [33]. At least no differences for the measured pressures and temperatures could be observed. However, the exact phase behavior was not in the scope of this thesis as other techniques like e.g. DSC are more appropriate to explore the phase behavior as a function of pressure or temperature. Here the focus is set on the structure of the composite layers. As long as the DPPC/HA samples are in the L_α phase their electron density profiles do not show a considerable asymmetry (fig.3.26). However, after the transition to the $L_{\beta'}$ phase the structure shows an asymmetry, which was not observed for DPPC/HA samples in

sole NaCl solution. Again samples composed of DPPC and HA with a molecular weight of $M_W = 10\ kDa$ shows a stronger effect, very likely due to its rod like conformation. Another explanation might be that there are more HA molecules of the low molecular weight HA, as always the same mass concentration of HA was used. As the asymmetry occurs after the transition to the $L_{\beta'}$ phase, it is very likely that the strong intercalation of the HA chains is correlated with the $L_{\beta'}$ phase. Lipids in the $L_{\beta'}$ phase occupy a lower area per molecule than in L_α phase [31, 33]. Thus it is very likely that Si supported bilayers in the $L_{\beta'}$ phase, which were prepared at 55 °C, show an increased number of defects, which are probably very suitable interaction sights for HA. After releasing the pressure the electron density profiles restore their original shape and the structural transitions are completely reversible. This was not observed for the measurements at 39 °C. A reason might be that the lipids at 55 °C in the L_α phase show a much higher flexibility and mobility (the lateral diffusion coefficient is reduced up to three orders of magnitude [117] in the $L_{\beta'}$ phase), which enhances a reorganization of the sample.

Comparison of DPPC vesicles with HA and Si supported DPPC bilayer with HA in the presence of $CaCl_2$

Results from both experiments settings, vesicles and solid supported layers, show strong effect of $CaCl_2$ on the structure and properties of DPPC and DPPC/HA. The results from SAXS and DLS revealed a positive net charging of the vesicles which lead to stronger interaction with the HA chains. An increased interaction strength was also observed for Si supported DPPC/HA samples. All methods except, fluorescence microscopy, show a stronger effect for small molecular weight HA. There are different reasons for this. First the results from fluorescence microscopy give information on the lateral structure of the samples on the micrometer scale, while XRR and DSC provide information on the molecular level of the sample and XRR in particular information on the vertical structure of the sample. The difference between results from DLS and microscopy is, that DLS shows an aggregation of vesicles which are not fixed in space, while a bilayer in the case of the Si supported samples for microscopy is fixed to the support. The visible effect of a large molecule is therefore probably much stronger.

By comparing the results from the two experimental designs it could be observed that the phase behavior is significantly influenced by its environment (Si support). DSC results show that HA decreases the main transition temperature slightly (maximum 0.8 K of HA10). However the XRR measurements indicated that the Si supported DPPC/ HA10 composite sample is in the L_α phase at 39 °C (3 K below the

main phase transition temperature). One reason for this might be that the vesicles that were studied in DSC are closed structures without strong defects, while DPPC layer on top of the Si support shows many defects and inhomogeneities as shown by fluorescent microscopy. These defects probably make an interaction of HA and DPPC much easier. Further is the Si supported DPPC layer in an energetically unfavorable state, as the $P_{\beta'}$ is suppressed.

Chapter 4

Summary

Information about the interaction of lipid bilayers and HA is essential for a better understanding of the processes leading to the exceptional good lubrication properties found in the synovial joint. Therefore, the interaction of DPPC (a common lipid in the synovial joint) and HA was studied by means of two different sample systems which are both inspired by the synovial joint: DPPC vesicles with HA in solution (studied using DSC, DLS and SAXS) and solid supported DPPC bilayer with HA (studied using fluorescent microscopy and XRR). These sample systems allowed to investigate aspects of the interaction of unbound structures as they may occur in the synovial fluid and the structures forming on the surface of the cartilage. One main aspect in this thesis is to elucidate how the samples system gets impacted by high pressure, which simulates high loads as they occur in synovial joints during daily motion [8, 9]. Further two solution conditions (150 mM NaCl and 150 mM NaCl with 10 mM $CaCl_2$) have been probed to examine the influence of divalent ions.

The results obtained from the two samples systems strongly indicate that the HA chains interact mainly with the zwitterionic head group region of the DPPC phospholipid. No modifications of the tail group region could be detected for samples consisting of DPPC vesicles and HA. Thus, it is very likely that the interaction is mainly driven by electrostatic forces. Results from measurements in a solution containing divalent Ca^{2+} ions strenghened this hypothesis. The addition of Ca^{2+} ions strongly altered the interaction and allowed HA chains to enter deeper into the bilayer structures. HA chains in sole NaCl solution are attracted by the positively charged part of the head groups. As a result they preferably stay at the surface of the bilayer. On the other hand, divalent Ca^{2+} ions have the ability to bind the negatively charged HA chains to negatively charged deeper parts of the head

group regions. As Ca^{2+} and other positively charged multivalent ions are found in the synovial fluid it can be presumed that the interaction in the synovial joint between HA and DPPC is rather strong. In contrast to the bilayer structure of DPPC vesicles, which only shows minor modification due to interactions with HA, the structure of supported bilayers is strongly affected by HA (especially in the presence of $CaCl_2$). Defects in the structure of the supported bilayers are probably the reason this effect. Such defects can facilitate a stronger accumulation of HA between the head groups of the lipids.

At high pressure it was observed that sole DPPC bilayers are not stable. They broke down after pressure induced phase transitions. The addition of HA or $CaCl_2$ lead to a stabilization of the bilayers at high pressures, so that the bilayer withstands the pressure induced phase transitions. The stabilization might be caused by a fastening of single lipid molecules due to adsorbed HA or Ca^{2+} ions. The integrity of the bilayer, even at high hydrostatic pressure (i.e. at high loads), is of great importance for the lubrication properties, as only intact bilayers provide low friction. This shows that the interaction of different components can have beneficial effects for the joint lubrication. However, if HA is added in combination with $CaCl_2$ the HA chains strongly affect the bilayer structure at high pressure. At temperatures below the phase transition it was observed that the DPPC bilayer structure was strongly changed at high pressures and the original structures was not restored after releasing the pressure, i.e. the structural modification was irreversible. It is questionable if such a irreversibly changed structure is beneficial for the joint lubrication.

HA found in the synovial fluid of patients suffering from arthritis show a decreased molecular weight. Therefore, it was of high interest to explore if the molecular weight of HA has an influence on the interaction with DPPC for biological relevant experimental settings. The results from the experiments presented in this thesis confirm that the molecular weight has an influence on the organization of the DPPC/ HA structure. HA with a low molecular weight has a much stronger effect on the structure of DPPC bilayers than HA with high molecular weight. It is assumed that the different strength of interaction is caused by differences in the global structure of the HA.

Chapter 5

Conclusion

To shed light on the mechanisms leading to low friction in the synovial joints the molecular arrangement of a simple binary model system consisting of the phospholipid DPPC and HA was studied. The results obtained from the here presented experiments underline the complexity of the interaction of the different molecules in the synovial joint. Even for such a simple model system many different parameters can be found which all have strong influences on the interaction. Three parameters have been systematically varied in this study: phase of the DPPC bilayer, solution condition and molecular weight of the HA. It could be demonstrated that these different parameters have a major impact on the assembly and performance of the system under high pressure. The results of this study proved that HA and DPPC interact mainly via electrostatic interactions, which makes it highly sensitive to changed solution conditions (e.g. the addition of $CaCl_2$). Further, it leads to an adsorption of HA to the head group region of DPPC. Most important for the lubrication properties of synovial joints is probably that HA and divalent calcium ions lead to a stabilization of the lipid bilayer against high hydrostatic pressure. It could also be shown that HA with a low molecular weight tends to alter the bilayer structure stronger than high molecular weight HA. This might be another reason why high molecular weight HA is beneficial for the treatment of different joint diseases, besides the well known fact that solutions with high molecular weight HA show a higher viscosity. The ambivalent response of the system to the molecular weight of HA proofs that the interplay between the single components is a key factor for the joint lubrication.

With the here presented results an important contribution was made to get a better insight into the complex molecular interplay enabling the exceptional good lubrication properties of the synovial joint. To further improve the understanding of these

mechanisms it will be necessary to study the interaction of the different components also under other outer conditions (e.g. different shear rates). Also additional constituents of the synovial fluid need to be added to obtain a more realistic model in order to completely understand the molecular mechanisms.

Bibliography

[1] Eric Shirley Jones. Joint lubrication. *The Lancet*, 227(5879):1043–1045, May 1936.

[2] Kenneth Holmberg, Peter Andersson, and Ali Erdemir. Global energy consumption due to friction in passenger cars. *Tribology International*, 47:221–234, Mar 2012.

[3] J Klein. Molecular mechanisms of synovial joint lubrication. *Proceedings of the Institution of Mechanical Engineers, Part J: Journal of Engineering Tribology*, 220(8):691–710, 2006.

[4] I. M. Schwarz and B. A. Hills. Surface-active phospholipid as the lubricating component of lubricin. *Rheumatology*, 37(1):21–26, Jan 1998.

[5] K. C. Morrell, W. A. Hodge, D. E. Krebs, and R. W. Mann. Corroboration of in vivo cartilage pressures with implications for synovial joint tribology and osteoarthritis causation. *Proceedings of the National Academy of Sciences*, 102(41):14819–14824, Oct 2005.

[6] Maria Pia Zamorani and Maura Valle. Bone and joint. In *Ultrasound of the musculoskeletal system*, pages 137–185. Springer, 2007.

[7] Andra Dedinaite. Biomimetic lubrication. *Soft Matter*, 8(2):273–284, 2012.

[8] WA Hodge, RS Fijan, KL Carlson, RG Burgess, WH Harris, and RW Mann. Contact pressures in the human hip joint measured in vivo. *Proceedings of the National Academy of Sciences*, 83(9):2879–2883, 1986.

[9] NY Afoke, PD Byers, and WC Hutton. Contact pressures in the human hip joint. *Journal of Bone & Joint Surgery, British Volume*, 69(4):536–541, 1987.

[10] A. V. Sarma, G. L. Powell, and M. LaBerge. Phospholipid composition of articular cartilage boundary lubricant. *Journal of Orthopaedic Research*, 19(4):671–676, Jul 2001.

[11] Torvard C Laurent, Ulla BG Laurent, and J Robert E Fraser. The structure and function of hyaluronan: An overview. *Immunol Cell Biol*, 74(2):A1–A7, Apr 1996.

[12] E.A. Balazs. *Disorders of the Knee*, chapter The Physical Properties of Synovial Fluid and the Special Role fo Hyaluronic Acid, pages 63–75. J. B. Lippincott Company, 1982.

[13] Subir Ghosh, Dipankar Choudhury, Nabangshu Shekhar Das, and Belinda Pingguan-Murphy. Tribological role of synovial fluid compositions on artificial joints - a systematic review of the last 10 years. *Lubrication Science*, 26(6):387–410, May 2014.

[14] B. A. Hills. Surface-active phospholipid: a pandora's box of clinical applications. part ii. barrier and lubricating properties. *Internal Medicine Journal*, 32(5-6):242–251, May 2002.

[15] BA Hills. Oligolamellar lubrication of joints by surface active phospholipid. *The Journal of Rheumatology*, 16(1):82–91, 1989.

[16] Chao Liu, Min Wang, Junxue An, Esben Thormann, and Andra Dėdinaitė. Hyaluronan and phospholipids in boundary lubrication. *Soft Matter*, 8(40):10241–10244, 2012.

[17] T. Murakami, S. Yarimitsu, K. Nakashima, T. Yamaguchi, Y. Sawae, N. Sakai, and A. Suzuki. Superior lubricity in articular cartilage and artificial hydrogel cartilage. *Proceedings of the Institution of Mechanical Engineers, Part J: Journal of Engineering Tribology*, 228(10):1099–1111, Apr 2014.

[18] D A Swann, F H Silver, H S Slayter, W Stafford, and E Shore. The molecular structure and lubricating activity of lubricin isolated from bovine and human synovial fluids. *Biochemical Journal*, 225(1):195–201, Jan 1985.

[19] M.P. Heuberger, M.R. Widmer, E. Zobeley, R. Glockshuber, and N.D. Spencer. Protein-mediated boundary lubrication in arthroplasty. *Biomaterials*, 26(10):1165–1173, Apr 2005.

[20] Teruo Murakami, Seido Yarimitsu, Kazuhiro Nakashima, Yoshinori Sawae, and Nobuo Sakai. Influence of synovia constituents on tribological behaviors of articular cartilage. *Friction*, 1(2):150–162, Jun 2013.

[21] L B Dahl, I M Dahl, A Engstrom-Laurent, and K Granath. Concentration and molecular weight of sodium hyaluronate in synovial fluid from patients with rheumatoid arthritis and other arthropathies. *Annals of the Rheumatic Diseases*, 44(12):817–822, Dec 1985.

[22] Endke A. Balazs, Donald Watson, Ivan F. Duff, and Saul Roseman. Hyaluronic acid in synovial fluid. i. molecular parameters of hyaluronic acid in normal and arthritic human fluids. *Arthritis & Rheumatism*, 10(4):357–376, Aug 1967.

[23] Dong Woog Lee, Xavier Banquy, Saurabh Das, Nicholas Cadirov, Gregory Jay, and Jacob Israelachvili. Effects of molecular weight of grafted hyaluronic acid on wear initiation. *Acta Biomaterialia*, 10(5):1817–1823, May 2014.

[24] Lorne R Gale, Yi Chen, and Ross Hills, Brian Aand Crawford. Boundary lubrication of joints: Characterization of surface-active phospholipids found on retrieved implants. *Acta Orthopaedica*, 78(3):309–314, Jan 2007.

[25] Debby P. Chang, Nehal I. Abu-Lail, Farshid Guilak, Gregory D. Jay, and Stefan Zauscher. Conformational mechanics, adsorption, and normal force interactions of lubricin and hyaluronic acid on model surfaces. *Langmuir*, 24(4):1183–1193, Feb 2008.

[26] L.M. Grant and F. Tiberg. Normal and lateral forces between lipid covered solids in solution: Correlation with layer packing and structure. *Biophysical Journal*, 82(3):1373–1385, Mar 2002.

[27] Ronit Goldberg, Avi Schroeder, Gilad Silbert, Keren Turjeman, Yechezkel Barenholz, and Jacob Klein. Boundary lubricants with exceptionally low friction coefficients based on 2D close-packed phosphatidylcholine liposomes. *Advanced Materials*, 23(31):3517–3521, Jul 2011.

[28] Min Wang, Chao Liu, Esben Thormann, and Andra Dedinaite. Hyaluronan and phospholipid association in biolubrication. *Biomacromolecules*, 14(12):4198–4206, Dec 2013.

[29] Roger S. Armen, Olivia D. Uitto, and Scott E. Feller. Phospholipid component volumes: Determination and application to bilayer structure calculations. *Biophysical Journal*, 75(2):734–744, Aug 1998.

[30] Rumiana Koynova and Martin Caffrey. Phases and phase transitions of the phosphatidylcholines. *Biochimica et Biophysica Acta (BBA)-Reviews on Biomembranes*, 1376(1):91–145, 1998.

[31] Stephanie Tristram-Nagle and John F. Nagle. Lipid bilayers: thermodynamics, structure, fluctuations, and interactions. *Chemistry and Physics of Lipids*, 127(1):3–14, Jan 2004.

[32] Roland Winter and Christoph Jeworrek. Effect of pressure on membranes. *Soft Matter*, 5(17):3157, 2009.

[33] John F. Nagle and Stephanie Tristram-Nagle. Structure of lipid bilayers. *Biochimica et Biophysica Acta (BBA) - Reviews on Biomembranes*, 1469(3):1591195, Nov 2000.

[34] Kiyotaka Akabori and John F. Nagle. Structure of the dmpc lipid bilayer ripple phase. *Soft Matter*, 11(5):918–926, 2015.

[35] Christoph Naumann, Thomas Brumm, and Thomas M Bayerl. Phase transition behavior of single phosphatidylcholine bilayers on a solid spherical support studied by dsc, nmr and ft-ir. *Biophysical journal*, 63(5):1314–1319, 1992.

[36] SJ Johnson, TM Bayerl, DC McDermott, GW Adam, AR Rennie, RK Thomas, and E Sackmann. Structure of an adsorbed dimyristoylphosphatidylcholine bilayer measured with specular reflection of neutrons. *Biophysical journal*, 59(2):289–294, 1991.

[37] Andrea Alessandrini and Paolo Facci. Phase transitions in supported lipid bilayers studied by afm. *Soft Matter*, 2014.

[38] Frederic Harb, Anne Simon, and Bernard Tinland. Ripple formation in unilamellar-supported lipid bilayer revealed by frapp. *The European Physical Journal E*, 36(12), Dec 2013.

[39] A. Almond. Hyaluronan. *Cell. Mol. Life Sci.*, 64(13):1591–1596, May 2007.

[40] J Necas, L Bartosikova, P Brauner, and J Kolar. Hyaluronic acid (hyaluronan): a review. *Veterinarni medicina*, 53(8):397–411, 2008.

[41] Mary K. Cowman and Shiro Matsuoka. Experimental approaches to hyaluronan structure. *Carbohydrate Research*, 340(5):791–809, Apr 2005.

[42] Michel Milas and Marguerite Rinaudo. *Characterization and Properties of Hyaluronic Acid (Hyaluronan) in: Polysaccharides: Structural Diversity and Functional Versatility*, chapter 22, pages 535–550. 1998.

[43] Struther Arnott, A.K. Mitra, and S. Raghunathan. Hyaluronic acid double helix. *Journal of Molecular Biology*, 169(4):861–872, Oct 1983.

[44] John E Scott, C Cummings, A Brass, and YUAN Chen. Secondary and tertiary structures of hyaluronan in aqueous solution, investigated by rotary shadowing-electron microscopy and computer simulation. hyaluronan is a very efficient network-forming polymer. *Biochem. j*, 274:699–705, 1991.

[45] Andrew Almond, Paul L. DeAngelis, and Charles D. Blundell. Hyaluronan: The local solution conformation determined by nmr and computer modeling is close to a contracted left-handed 4-fold helix. *Journal of Molecular Biology*, 358(5):1256–1269, May 2006.

[46] J. E. Scott and F. Heatley. Hyaluronan forms specific stable tertiary structures in aqueous solution: A 13c nmr study. *Proceedings of the National Academy of Sciences*, 96(9):4850–4855, Apr 1999.

[47] Eric Buhler and Francois Boue. Chain persistence length and structure in hyaluronan solutions: Ionic strength dependence for a model semirigid polyelectrolyte. *Macromolecules*, 37(4):1600–1610, Feb 2004.

[48] G. Ribitsch, J. Schurz, and V. Ribitsch. Investigation of the solution structure of hyaluronic acid by light scattering, saxs, and viscosity measurements. *Colloid and Polymer Science*, 258(12):1322–1334, Dec 1980.

[49] Toshiyuki Kikuchi, Harumoto Yamada, and Masayuki Shimmei. Effect of high molecular weight hyaluronan on cartilage degeneration in a rabbit model of osteoarthritis. *Osteoarthritis and Cartilage*, 4(2):99–110, Jun 1996.

[50] Robert C. MacDonald, Ruby I. MacDonald, Bert Ph.M. Menco, Keizo Takeshita, Nanda K. Subbarao, and Lan rong Hu. Small-volume extrusion apparatus for preparation of large, unilamellar vesicles. *Biochimica et Biophysica Acta (BBA) - Biomembranes*, 1061(2):297 – 303, 1991.

[51] Werner Kern and David A. Puotinen. Cleaning solutions based on hydrogen peroxide for use in silicon semiconductor technology. *RCA Review*, 31:187–206, 1970.

[52] Werner Kern. The evolution of silicon wafer cleaning technology. *Journal of The Electrochemical Society*, 137(6):1887, 1990.

[53] Ralf Richter, Anneke Mukhopadhyay, and Alain Brisson. Pathways of lipid vesicle deposition on solid surfaces: A combined qcm-d and afm study. *Biophysical Journal*, 85(5):3035–3047, Nov 2003.

[54] Tania Kjellerup Lind, Marité Cárdenas, and Hanna Pauliina Wacklin. Formation of supported lipid bilayers by vesicle fusion–effect of deposition temperature. *Langmuir*, 2014.

[55] Jens Als-Nielsen and Des McMorrow. *Elements of modern X-ray physics*. John Wiley & Sons, 2011.

[56] O. Glatter and O. Kratky, editors. *Small-Angle X-ray Scattering*. Academic Press INC. (London) LTD, 1982.

[57] Georg Pabst, Michael Rappolt, Heinz Amenitsch, and Peter Laggner. Structural information from multilamellar liposomes at full hydration: Full q - range fitting with high quality x-ray data. *Phys. Rev. E*, 62:4000–4009, Sep 2000.

[58] Georg Pabst, Richard Koschuch, Beatriz Pozo-Navas, Michael Rappolt, Karl Lohner, and Peter Laggner. Structural analysis of weakly ordered membrane stacks. *Journal of Applied Crystallography*, 36(6):1378–1388, 2003.

[59] Clement E. Blanchet, Alessandro Spilotros, Frank Schwemmer, Melissa A. Graewert, Alexey Kikhney, Cy M. Jeffries, Daniel Franke, Daniel Mark, Roland Zengerle, Florent Cipriani, and et al. Versatile sample environments and automation for biological solution x-ray scattering experiments at the P12 beamline (PETRA III, DESY). *J Appl Crystallogr*, 48(2):431–443, Mar 2015.

[60] Thomas F. Coleman and Yuying Li. On the convergence of interior-reflective Newton methods for nonlinear minimization subject to bounds. *Mathematical Programming*, 67(1-3):189–224, Oct 1994.

[61] Thomas F. Coleman and Yuying Li. An interior trust region approach for nonlinear minimization subject to bounds. *SIAM Journal on Optimization*, 6(2):418–445, May 1996.

[62] Cyrille Rochas and Erik Geissler. Measurement of dynamic light scattering intensity in gels. *Macromolecules*, 47(22):8012–8017, Nov 2014.

[63] R. Pecora. Dynamic light scattering measurement of nanometer particles in liquids. *Journal of Nanoparticle Research*, 2(2):123–131, 2000.

[64] B. Chu. *Soft Matter Characterization*, chapter Dynamic Light Scattering, pages 335–372. Springer Science + Business Media, 2008.

[65] Jeremy Pencer and F. Ross Hallett. Effects of vesicle size and shape on static and dynamic light scattering measurements. *Langmuir*, 19(18):7488–7497, Sep 2003.

[66] Alan Cooper, Margaret A Nutley, and Abdul Wadood. Differential scanning microcalorimetry. *Protein-ligand interactions: Hydrodynamics and calorimetry*, pages 287–318, 2000.

[67] Rodney L Biltonen and Dov Lichtenberg. The use of differential scanning calorimetry as a tool to characterize liposome preparations. *Chemistry and Physics of Lipids*, 64(1):129–142, 1993.

[68] Alex Dopico. *Methods in membrane lipids*, volume 400. Springer Science & Business Media, 2007.

[69] Jens Als-Nielsen, Didier Jacquemain, Kristian Kjaer, Franck Leveiller, Meir Lahav, and Leslie Leiserowitz. Principles and applications of grazing incidence x-ray and neutron scattering from ordered molecular monolayers at the air-water interface. *Physics Reports*, 246(5):251–313, Oct 1994.

[70] Metin Tolan. *X-Ray Scattering from Soft-Matter Thin Films*, volume 148 of *Springer Tracts in Modern Physics*. Springer Berlin Heidelberg, 1999.

[71] Jean Daillant and Alain Gibaud. X-ray and neutron reflectivity. *Lecture Notes in Physics*, 770:133–182, 2009.

[72] L. Parratt. Surface studies of solids by total reflection of x-rays. *Phys. Rev.*, 95(2):359–369, Jul 1954.

[73] Florian J. Wirkert, Michael Paulus, Julia Nase, Johannes Möller, Simon Kujawski, Christian Sternemann, and Metin Tolan. X-ray reflectivity measurements of liquid/solid interfaces under high hydrostatic pressure conditions. *J Synchrotron Radiat*, 21(1):76–81, Nov 2014.

[74] Michael Paulus, Daniela Lietz, Christian Sternemann, Kaveh Shokuie, Florian Evers, Metin Tolan, Claus Czeslik, and Roland Winter. An access to buried interfaces: the x-ray reflectivity set-up of bl9 at delta. *J Synchrotron Radiat*, 15(6):600–605, Oct 2008.

[75] Thomas Arnold, Chris Nicklin, Jonathan Rawle, John Sutter, Trevor Bates, Brian Nutter, Gary McIntyre, and Martin Burt. Implementation of a beam deflection system for studies of liquid interfaces on beamline i07 at diamond. *J Synchrotron Rad*, 19(3):408–416, Mar 2012.

[76] P. R. Willmott, D. Meister, S. J. Leake, M. Lange, A. Bergamaschi, M. Böge, M. Calvi, C. Cancellieri, N. Casati, A. Cervellino, and et al. The materials science beamline upgrade at the swiss light source. *J Synchrotron Radiat*, 20(5):667–682, Sep 2013.

[77] M Tanaka, G Girard, R Davis, A Peuto, and N Bignell. Recommended table for the density of water between 0 °c and 40 °c based on recent experimental reports. *Metrologia*, 38(4):301–309, Aug 2001.

[78] Luís M.S.. Loura, Fábio Fernandes, A.C. Fernandes, and J.P. Prates Ramalho. Effects of fluorescent probe nbd-PC on the structure, dynamics and phase transition of dppc. a molecular dynamics and differential scanning calorimetry study. *Biochimica et Biophysica Acta (BBA) - Biomembranes*, 1778(2):491–501, Feb 2008.

[79] Caroline A Schneider, Wayne S Rasband, and Kevin W Eliceiri. Nih image to imagej: 25 years of image analysis. *Nature Methods*, 9(7):671–675, Jun 2012.

[80] Frank C. Linn and Leon Sokoloff. Movement and composition of interstitial fluid of cartilage. *Arthritis & Rheumatism*, 8(4):481–494, Aug 1965.

[81] Jonathan Black and Garth Hastings, editors. *Handbook of Biomaterial Properties*. Springer US, 1998.

[82] Shuji Aruga, Ryoichi Kataoka, and Shigeki Mitaku. Interaction between ca2+ and dipalmitoylphosphatidylcholine membranes. *Biophysical Chemistry*, 21(3-4):265–275, Mar 1985.

[83] Ryoichi Kataoka, Shuji Aruga, Shigeki Mitaku, Kazuhiko Kinosita, and Akira Ikegami. Interaction between ca2+ and dipalmitoylphosphatidylcholine membranes. *Biophysical Chemistry*, 21(3-4):277–284, Mar 1985.

[84] L. J. Lis, W. T. Lis, V. A. Parsegian, and R. P. Rand. Adsorption of divalent cations to a variety of phosphatidylcholine bilayers. *Biochemistry*, 20(7):1771–1777, Mar 1981.

[85] L. J. Lis, V. A. Parsegian, and R. P. Rand. Binding of divalent cations to dipalmitoylphosphatidylcholine bilayers and its effect on bilayer interaction. *Biochemistry*, 20(7):1761–1770, Mar 1981.

[86] J Seelig. Interaction of phospholipids with ca ions. on the role of the phospholipid head groups. *Cell Biology International Reports*, 14(4):353–360, Apr 1990.

[87] Daniela Uhríková, Norbert Kucerka, José Teixeira, Valentin Gordeliy, and Pavol Balgavý. Structural changes in dipalmitoylphosphatidylcholine bilayer promoted by ca 2+ ions: a small-angle neutron scattering study. *Chemistry and physics of lipids*, 155(2):80–89, 2008.

[88] Ferenc Horkay, Peter J. Basser, David J. Londono, Anne-Marie Hecht, and Erik Geissler. Ions in hyaluronic acid solutions. *J. Chem. Phys.*, 131(18):184902, 2009.

[89] Tannin A. Schmidt, Nicholas S. Gastelum, Quynhhoa T. Nguyen, Barbara L. Schumacher, and Robert L. Sah. Boundary lubrication of articular cartilage: Role of synovial fluid constituents. *Arthritis & Rheumatism*, 56(3):882–891, 2007.

[90] Ronald N. McElhaney. The use of differential scanning calorimetry and differential thermal analysis in studies of model and biological membranes. *Chemistry and Physics of Lipids*, 30(2-3):229–259, May 1982.

[91] Todd P. W. McMullen, Ruthven N. A. H. Lewis, and Ronald N. McElhaney. Differential scanning calorimetric study of the effect of cholesterol on the thermotropic phase behavior of a homologous series of linear saturated phosphatidylcholines. *Biochemistry*, 32(2):516–522, Jan 1993.

[92] B. Klajnert, J. Janiszewska, Z. Urbanczyk-Lipkowska, M. Bryszewska, and R.M. Epand. Dsc studies on interactions between low molecular mass peptide dendrimers and model lipid membranes. *International Journal of Pharmaceutics*, 327(1-2):145–152, Dec 2006.

[93] Raniero Mendichi, Ladislav Soltes, and Alberto Giacometti Schieroni. Evaluation of radius of gyration and intrinsic viscosity molar mass dependence and stiffness of hyaluronan. *Biomacromolecules*, 4(6):1805–1810, Nov 2003.

[94] V. Crescenzi, A. Taglienti, and I. Pasquali-Ronchetti. Supramolecular structures prevailing in aqueous hyaluronic acid and phospholipid vesicles mixtures: an electron microscopy and rheometric study. *Colloids and Surfaces A: Physicochemical and Engineering Aspects*, 245(1-3):133–135, Sep 2004.

[95] J.F. Nagle, R. Zhang, S. Tristram-Nagle, W. Sun, H.I. Petrache, and R.M. Suter. X-ray structure determination of fully hydrated l alpha phase dipalmitoylphosphatidylcholine bilayers. *Biophysical Journal*, 70(3):1419–1431, Mar 1996.

[96] Norbert Kucerka, Jeremy Pencer, Jonathan N. Sachs, John F. Nagle, and John Katsaras. Curvature effect on the structure of phospholipid bilayers. *Langmuir*, 23(3):1292–1299, Jan 2007.

[97] M. Kreuzer, M. Strobl, M. Reinhardt, M.C. Hemmer, T. Hauß, R. Dahint, and R. Steitz. Impact of a model synovial fluid on supported lipid membranes. *Biochimica et Biophysica Acta (BBA) - Biomembranes*, 1818(11):2648–2659, Nov 2012.

[98] Florian Wieland, Patrick Degen, Thomas Zander, Sören Gayer, Akanksha Raj, Junxue An, Andra Dedinaite, Per M Claesson, and Regine Willumeit-Römer. Structure of dppc-hyaluronan interfacial layers - effects of molecular weight and ion composition. *Soft Matter*, 2016.

[99] Ivonne Pasquali-Ronchetti, Daniela Quaglino, Giuseppe Mori, Barbara Bacchelli, and Peter Ghosh. Hyaluronan-phospholipid interactions. *Journal of Structural Biology*, 120(1):1–10, Oct 1997.

[100] Hideko Hayashi, Ken-ichi Tozaki, Chiaki Ikeuchi, and Hideaki Inaba. Phase transitions in dipalmitoylphosphatidylcholine–water and dipalmitoylphosphatidylcholine–cacl 2 aqueous solution system by means of a high resolution and high-sensitive differential scanning calorimeter. *Thermochimica acta*, 431(1):205–211, 2005.

[101] Carlos E. Espinosa, Qiong Guo, Virendra Singh, and Sven H. Behrens. Particle charging and charge screening in nonpolar dispersions with nonionic surfactants. *Langmuir*, 26(22):16941–16948, Nov 2010.

[102] R. Winter and W.-C. Pilgrim. A sans study of high pressure phase transitions in model biomembranes. *Berichte der Bunsengesellschaft für physikalische Chemie*, 93(6):708–717, Jun 1989.

[103] Lellis F Braganza and David L Worcester. Hydrostatic pressure induces hydrocarbon chain interdigitation in single-component phospholipid bilayers. *Biochemistry*, 25(9):2591–2596, 1986.

[104] Peter Ghosh, Nongporn Hutadilok, Naomi Adam, and Aldo Lentini. Interactions of hyaluronan (hyaluronic acid) with phospholipids as determined by gel permeation chromatography, multi-angle laser-light-scattering photometry and 1H-nmr spectroscopy. *International Journal of Biological Macromolecules*, 16(5):237–244, Jan 1994.

[105] D. W. Nitzan. The role of hyaluronic acid in protecting surface-active phospholipids from lysis by exogenous phospholipase a2. *Rheumatology*, 40(3):336–340, Mar 2001.

[106] Min Wang, Thomas Zander, Xiaoyan Liu, Chao Liu, Akanksha Raj, D.C. Florian Wieland, Vasil M. Garamus, Regine Willumeit-Römer, Per Martin Claesson, and Andra Dedinaite. The effect of temperature on supported dipalmitoylphosphatidylcholine (dppc) bilayers: Structure and lubrication performance. *Journal of Colloid and Interface Science*, 445:84–92, May 2015.

[107] C Czeslik, O Reis, R Winter, and G Rapp. Effect of high pressure on the structure of dipalmitoylphosphatidylcholine bilayer membranes: a synchrotron-x-ray diffraction and ft-IR spectroscopy study using the diamond anvil technique. *Chemistry and Physics of Lipids*, 91(2):135–144, Feb 1998.

[108] Bastien Seantier and Bengt Kasemo. Influence of mono- and divalent ions on the formation of supported phospholipid bilayers via vesicle adsorption. *Langmuir*, 25(10):5767–5772, May 2009.

[109] A. Charrier and F. Thibaudau. Main phase transitions in supported lipid single-bilayer. *Biophysical Journal*, 89(2):1094–1101, Aug 2005.

[110] Z. Vivian Feng, Tighe A. Spurlin, and Andrew A. Gewirth. Direct visualization of asymmetric behavior in supported lipid bilayers at the gel-fluid phase transition. *Biophysical Journal*, 88(3):2154–2164, Mar 2005.

[111] Heng-Liang Wu, Yujin Tong, Qiling Peng, Na Li, and Shen Ye. Phase transition behaviors of the supported dppc bilayer investigated by sum frequency generation (sfg) vibrational spectroscopy and atomic force microscopy (afm). *Phys. Chem. Chem. Phys.*, 18(3):1411–1421, 2016.

[112] Stephanie Tristram-Nagle, Yufeng Liu, Justin Legleiter, and John F. Nagle. Structure of gel phase dmpc determined by x-ray diffraction. *Biophysical Journal*, 83(6):3324–3335, Dec 2002.

[113] A. Almond, A. Brass, and J.K. Sheehan. Deducing polymeric structure from aqueous molecular dynamics simulations of oligosaccharides: predictions from simulations of hyaluronan tetrasaccharides compared with hydrodynamic and x-ray fibre diffraction data. *Journal of Molecular Biology*, 284(5):1425–1437, Dec 1998.

[114] A. Landwehr and R. Winter. The t,x,p-phase diagram of binary phospholipid mixtures. *Berichte der Bunsengesellschaft für physikalische Chemie*, 98(12):1585–1589, Dec 1994.

[115] Ralf P. Richter, Rémi Bérat, and Alain R. Brisson. Formation of solid-supported lipid bilayers: an integrated view. *Langmuir*, 22(8):3497–3505, Apr 2006.

[116] Michael Gross and Rainer Jaenicke. Proteins under pressure. the influence of high hydrostatic pressure on structure, function and assembly of proteins and protein complexes. *European Journal of Biochemistry*, 221(2):617–630, Apr 1994.

[117] L.K. Tamm and H.M. McConnell. Supported phospholipid bilayers. *Biophysical Journal*, 47(1):105–113, Jan 1985.

Acknowledgment

Foremost I would like to thank my supervisors Regine Willumeit-Römer and Andreas Schreyer for providing the opportunity to work on this very interesting subject and particularly for their advice and support.

I would especially like to thank Florian Wieland for his support during the last 3.5 years. Whenever I needed help or a good advice I could rely on him and I could not think of a better workmate to be with during all the long and stressful beamtimes we had. Further, and probably most important, it was always a lot of fun to spend time with him.

I also want to express my thanks to Vasyl Haramus for helpful discussions and for his help during data evaluation and paper writing.

Many thanks to the great colleagues from the KTH in Stockholm: Per Claesson, Andra Dedinaite, Akanksha Raj and Min Wang. It was always a big pleasure to work and discuss with them.

Besides the colleagues from the KTH I want to thank Christian Sternemann, Michael Paulus and Florian Wirkert from the TU-Dortmund for lending their high pressure XRR-cell to me which was of essential importance for my work.

Numerous people helped me during the dark hours at different beamtimes and I really appreciated their invaluable support. Therefore, thanks to: Akanksha Raj, Benedikt Nowak, Christina Krywka, Florian Wieland, Min Wang, Paul Salmen, Philipp Layer and Susanne Dogan. Also many thanks to the beamline scientists: Jonathan Rawle (Diamond Light Source, UK), Nicola Casati (Swiss Light Source, Switzerland), Veijo Honkimäki (ESRF, France), Christian Sternemann and Michael Paulus (both DELTA, Germany).

But also the lab experiments wouldn't have been such a success without some help. Special thanks to Dorothee Scharfenberg for advising me with the fluorescent microscope and thanks to Markus Perbandt for giving me access to the DLS-machine. Also many thanks for their help in the chemistry labs to Brit Heilmann, Lena Frenzel and Milena Lippmann.

I also want to thank all my colleagues from the HZG. It was a big pleasure to work with them.

Last but not least I want to thank my girlfriend Anja Wechler for her encouragement, especially during the final stage of writing, and my family for their support.

Appendix A

Appendix

Small angle scattering

150mM NaCl

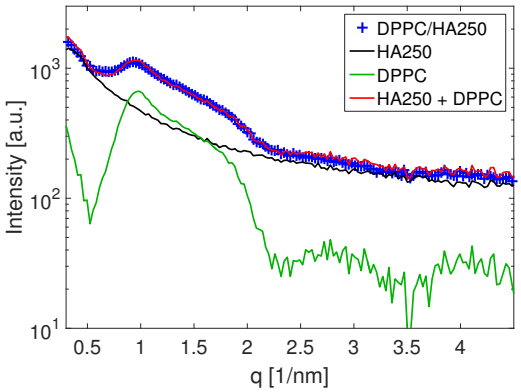

Figure A.1: *Scattering curves of measured at 25 °C. The concentration of DPPC and HA250 was 4 mg/mL, respectively. For 'HA250 + DPPC' the curves from DPPC and HA250 were summed up.*

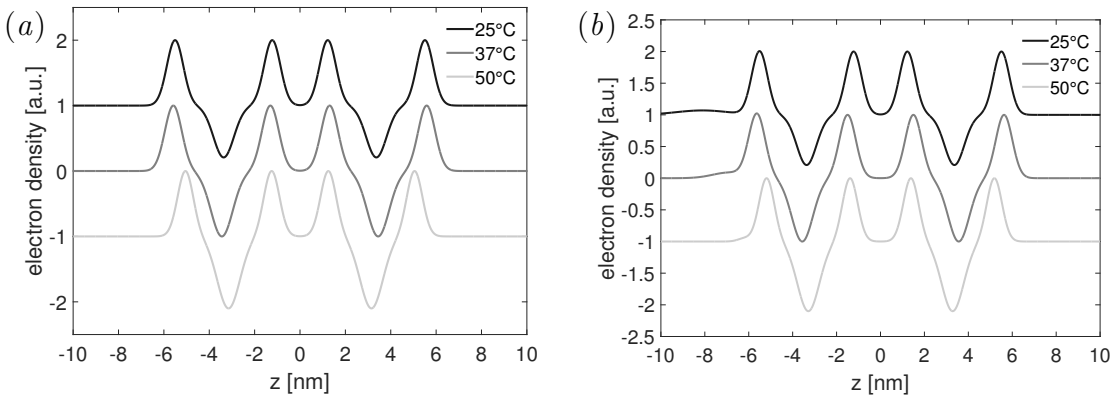

Figure A.2: *Relative electron density profiles of a double layered vesicle at the three temperatures in NaCl, calculated from fits of the scattering curves. (a) DPPC (b) DPPC with HA* $M_W = 250$.

150mM NaCl + 10mM $CaCl_2$

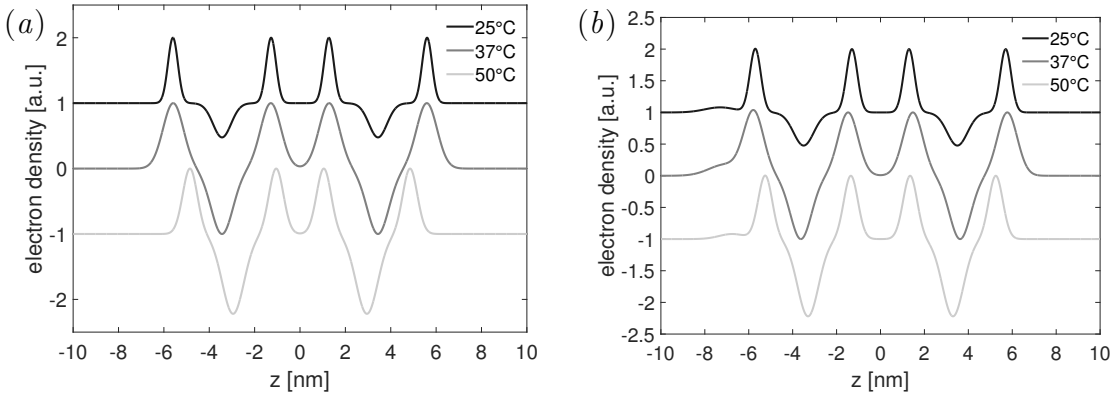

Figure A.3: *Relative electron density profiles of a double layered vesicle at the three temperatures in NaCl with* $CaCl_2$*, calculated from fits of the scattering curves. (a) DPPC (b) DPPC with HA* $M_W = 250$.

X-ray reflectivity

150mM NaCl

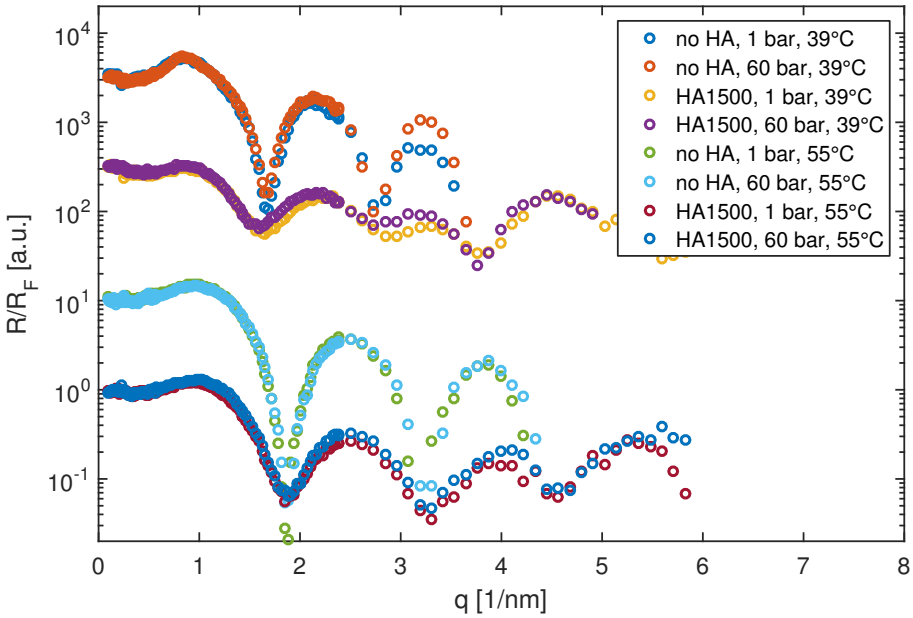

Figure A.4: *Fresnel normalized reflectivity curves of several samples measured at* 1 *bar and* 60 *bar.*

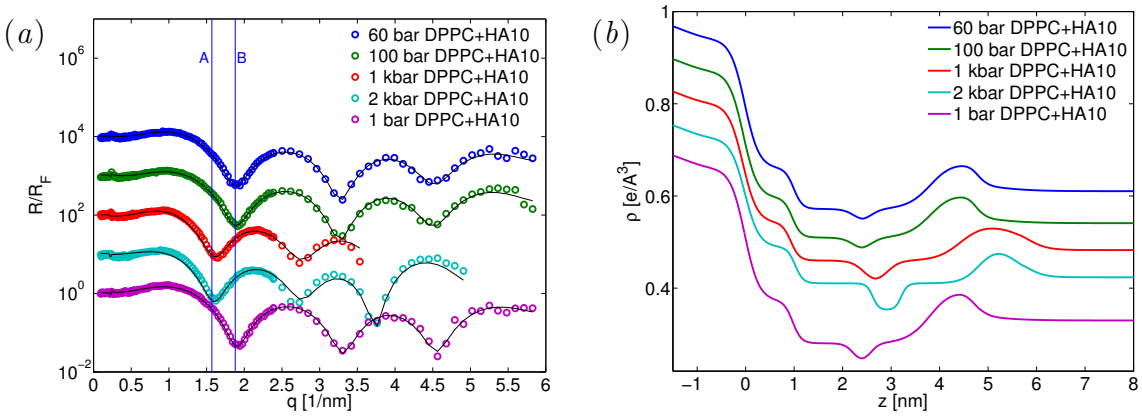

Figure A.5: *(a) Fresnel normalized scattering profiles of DPPC/HA10, recorded at various pressures between* 60 *bar and* 2 *kbar and* 55 °*C. Solid black lines indicate the fits. (b) Resulting electron density profiles. The curves are shifted vertically for clarity.*

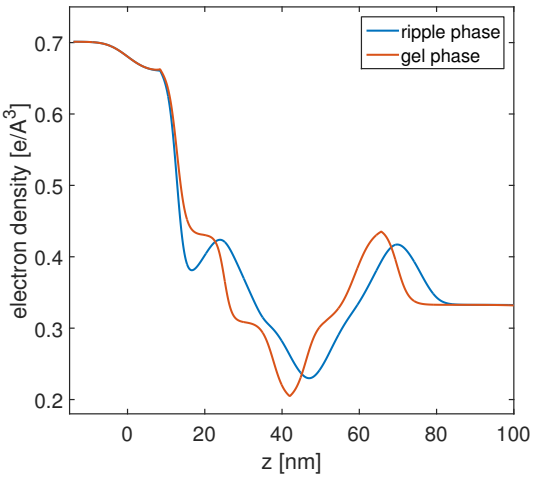

Figure A.6: *Comparison of simulated electron density profiles of a Si supported bilayer in the $L_{\beta'}$ phase and in the $P_{\beta'}$ phase.*

150mM NaCl + 10mM $CaCl_2$

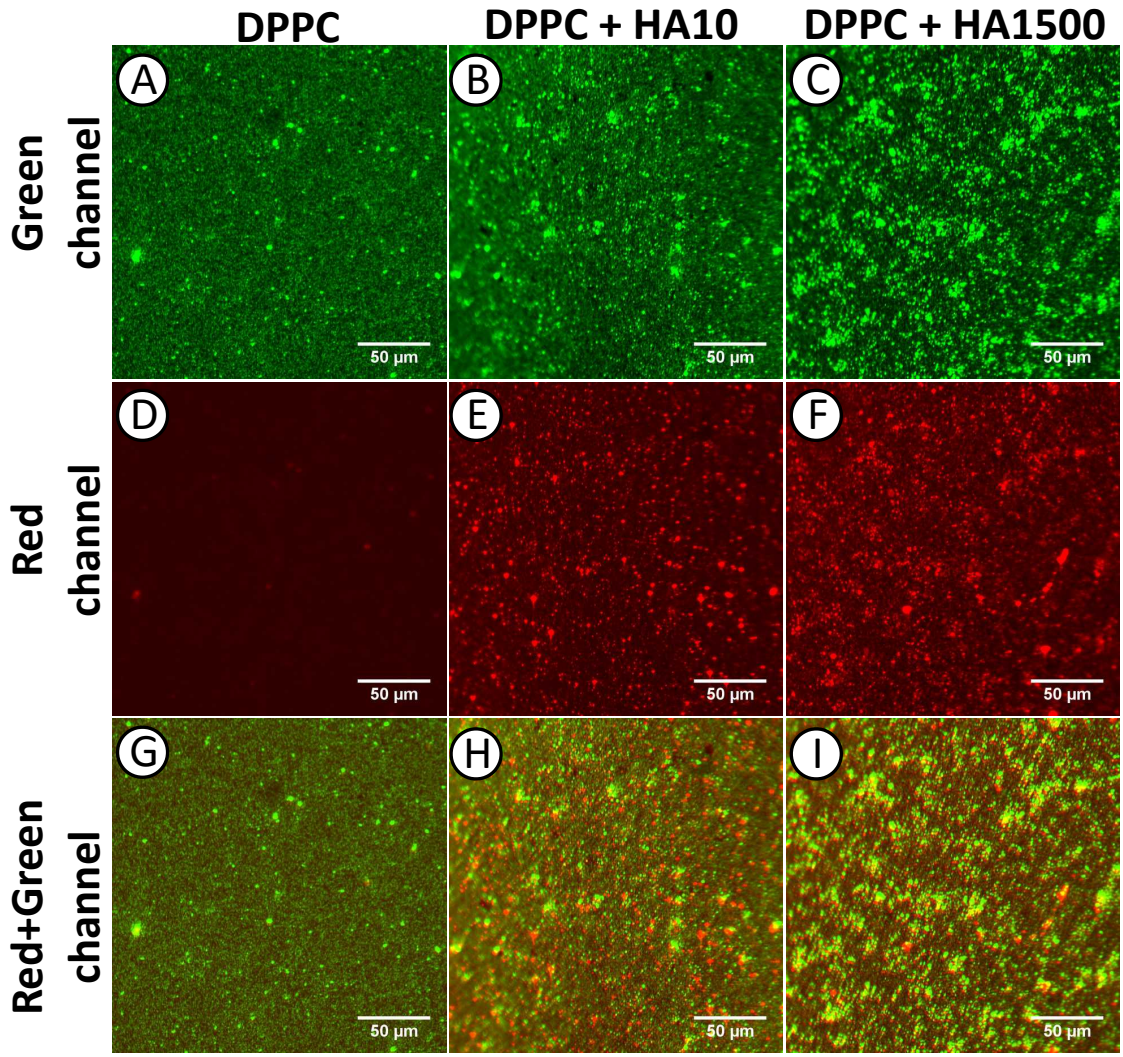

Figure A.7: *Fluorescence microscopy images of Si supported DPPC and DPPC/HA composites in two different solutions:* 150 *mM NaCl (left)* 150 *mM NaCl with* 10 *mM* $CaCl_2$ *(right). DPPC was labeled with NBD (green channel) and HA was labeled with Rhodamine (red channel)*

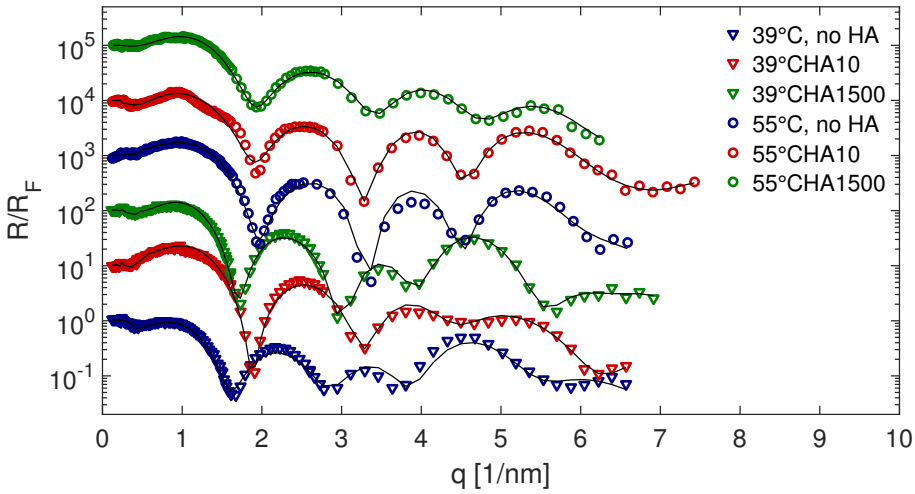

Figure A.8: *Fresnel normalized scattering curves of DPPC and DPPC with HA (two molecular weights). Black lines indicate fits of the data and the offset is for clarity.*

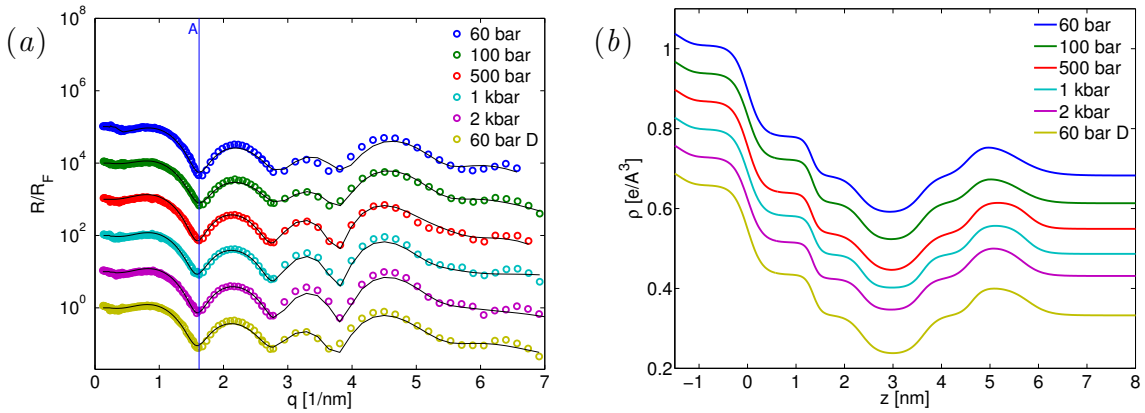

Figure A.9: *(a) Fresnel normalized scattering profiles of DPPC, recorded at various pressures between 60 bar and 2 kbar and 39 °C. Solid black lines indicate the fits. (b) Resulting electron density profiles. The curves are shifted vertically for clarity.*

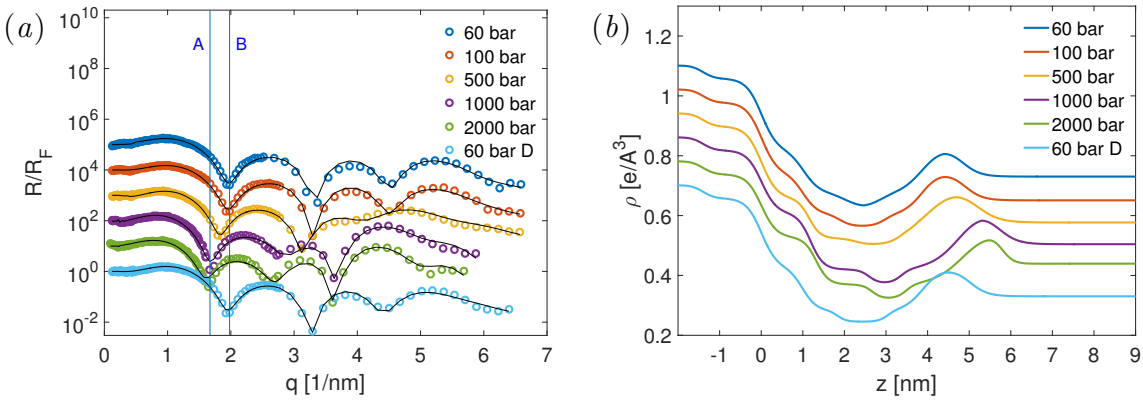

Figure A.10: *(a) Fresnel normalized scattering profiles of DPPC, recorded at various pressures between* 60 *bar and* 2 *kbar and* 55 °*C. Solid black lines indicate the fits. (b) Resulting electron density profiles. The curves are shifted vertically for clarity.*

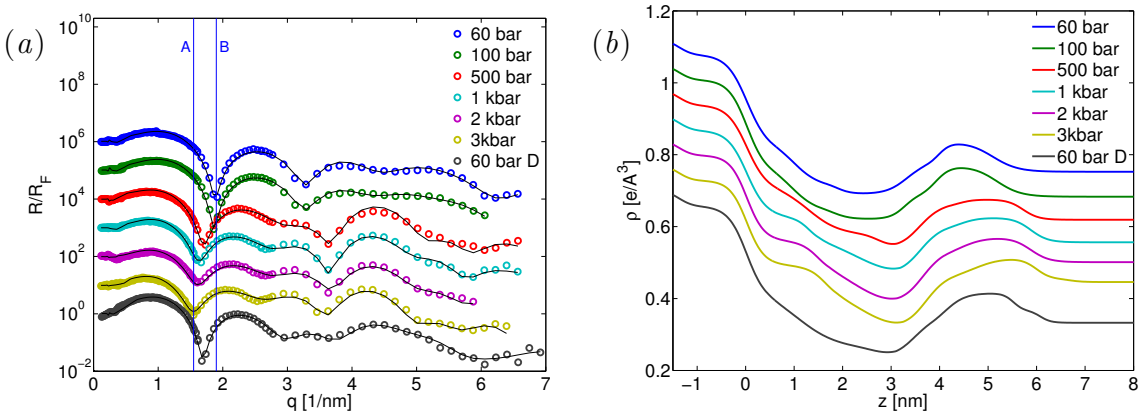

Figure A.11: *(a) Fresnel normalized scattering profiles of DPPC/HA10, recorded at various pressures between* 60 *bar and* 3 *kbar and* 39 °*C. Solid black lines indicate the fits. (b) Resulting electron density profiles. The curves are shifted vertically for clarity.*

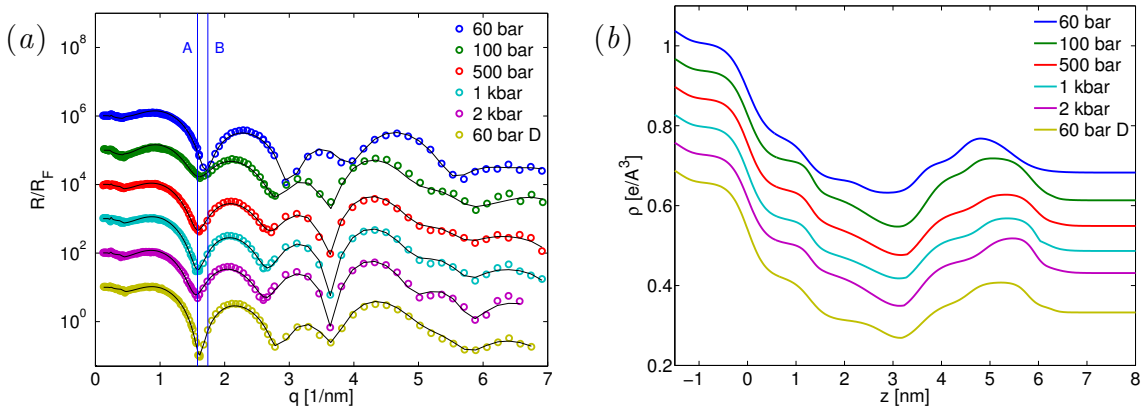

Figure A.12: *(a) Fresnel normalized scattering profiles of DPPC/HA1500, recorded at various pressures between 60 bar and 2 kbar and 39 °C. Solid black lines indicate the fits. (b) Resulting electron density profiles. Curves are shifted vertically for clarity.*

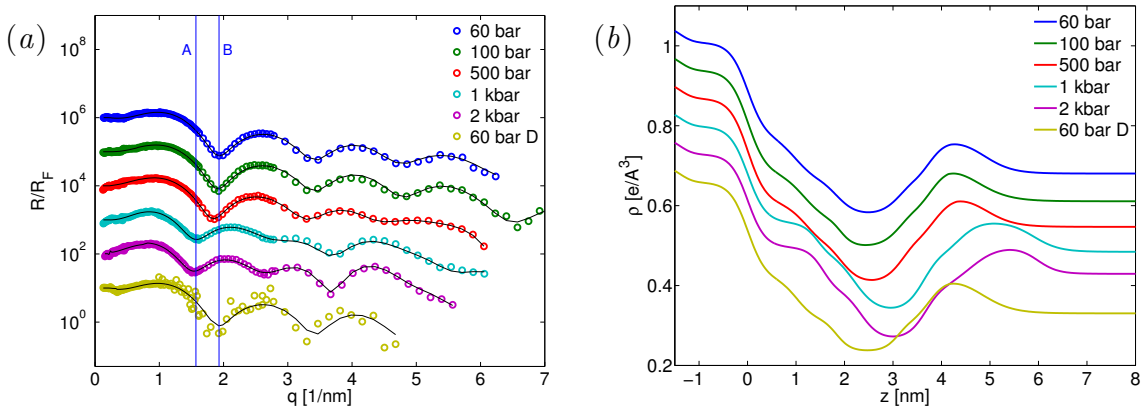

Figure A.13: *(a) Fresnel normalized scattering profiles of DPPC/HA1500, recorded at various pressures between 60 bar and 2 kbar and 55 °C. Solid black lines indicate the fits. (b) Resulting electron density profiles. The curves are shifted vertically for clarity.*

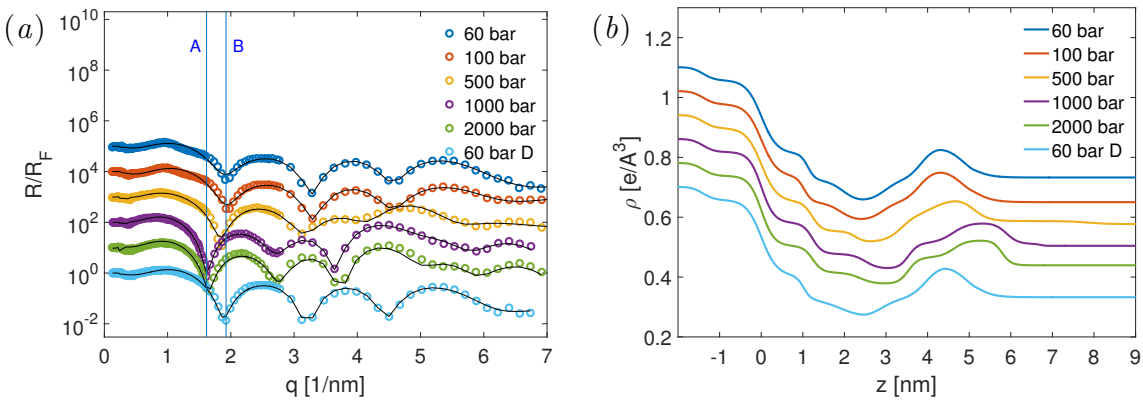

Figure A.14: *(a) Fresnel normalized scattering profiles of DPPC/HA10, recorded at various pressures between* 60 *bar and* 3 *kbar and* 55 °*C. Solid black lines indicate the fits. (b) Resulting electron density profiles. The curves are shifted vertically for clarity.*